MAX - PLANCK - INSTITUT FÜR QUANTENOPTIK

Interacting Feshbach Molecules

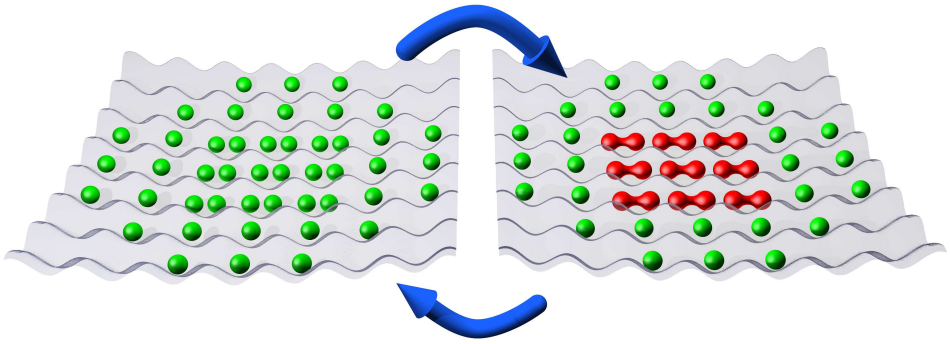

Niels Syassen

MPQ 319 January 2008

Cover illustration: Coherent atom-molecule oscillations with ultracold bosons in an optical lattice. Left: Atomic Mott insulator state consisting of a core of doubly occupied lattice sites and a shell of singly occupied sites. Right: A magnetically-tunable Feshbach resonance is used to associate molecules on doubly occupied lattice sites. A fast jump of the magnetic field to the Feshbach resonance leads to atom-molecule oscillations. This experiment is described in Chapter 5.

Abstract

This thesis reports on experiments with ultracold atomic and molecular quantum gases. A Bose-Einstein condensate of ^{87}Rb atoms serves as a starting point for the experiments. Magnetically tunable Feshbach resonances are used to associate diatomic molecules that are as cold as the atoms.

A frequently used method for the formation of ultracold molecules relies on a slow ramp of the magnetic field across the Feshbach resonance. This converts pairs of atoms into molecules in an adiabatic rapid passage. In this thesis, an alternative method for molecule association is studied in a three-dimensional optical lattice. A sudden jump of the magnetic field to the Feshbach resonance is applied. The jump induces coherent atom-molecule oscillations with large amplitude. These weakly damped oscillations are experimentally resolved up to the 29^{th} cycle. The observed amplitude and frequency of the oscillations depend on magnetic field and atomic density in a way that is well described by an analytic model.

Another central part of this thesis is the realization of a dissipative analog of the Tonks-Girardeau gas. Here the Feshbach molecules are confined to one spatial dimension by applying a two-dimensional optical lattice. Inelastic collisions between the molecules lead to particle loss. This interaction between the molecules is so strong that the system reaches the strongly correlated regime and the molecules, which are bosons, are forced to behave much like fermions. The strong correlations suppress the molecule loss rate by one order of magnitude. The loss is further suppressed by two orders of magnitude by applying a weak optical lattice in the third direction. New theory is developed that agrees with the experimental observations.

Finally, measurements on various loss-rate coefficients near Feshbach resonances are presented. In one experiment, the loss-rate coefficients due to inelastic collisions of a Feshbach molecule with another atom or molecule are determined. Another experiment studies three-body recombination. An enhancement of the three-body loss-rate coefficient by four orders of magnitude as a function of the magnetic field is observed, in good agreement with theory.

Zusammenfassung

Die vorliegende Arbeit berichtet über Experimente mit ultrakalten atomaren und molekularen Quantengasen. Ein Bose-Einstein-Kondensat aus ^{87}Rb Atomen dient als Ausgangspunkt für die Experimente. Magnetisch-induzierte Feshbach-Resonanzen werden zur Erzeugung von zweiatomigen Molekülen benutzt. Diese sind so kalt wie die Atome.

Eine weit verbreitete Methode zur Erzeugung ultrakalter Moleküle basiert auf einer langsamen Magnetfeldrampe über eine Feshbach-Resonanz hinweg. Dadurch werden Atompaare in einer adiabatischen Passage in Moleküle überführt. In dieser Arbeit wird eine alternative Methode für die Erzeugung ultrakalter Moleküle in einem dreidimensionalen optischen Gitter untersucht. Diese Methode beruht auf einem abrupten Sprung des Magnetfeldes auf die Resonanz. Der Sprung verursacht kohärente Atom-Molekül-Oszillationen mit großer Amplitude. Diese schwach gedämpften Oszillationen werden experimentell bis zur 29. Periode aufgelöst. Die Abhängigkeit der beobachteten Amplitude und Frequenz der Oszillationen von Magnetfeld und atomarer Dichte wird gut durch ein analytisches Modell beschrieben.

Ein weiterer zentraler Teil dieser Arbeit ist die Realisierung eines dissipativen Analogons des Tonks-Girardeau-Gases. Die Feshbach-Moleküle werden zunächst durch ein zweidimensionales optisches Gitter auf eine räumliche Dimension eingeschränkt. Inelastische Stöße zwischen den Molekülen führen zu Teilchenverlust. Diese Wechselwirkung zwischen den Molekülen ist so stark, dass das System das stark korrelierte Regime erreicht, und die Moleküle, welche Bosonen sind, gezwungen werden, sich ähnlich wie Fermionen zu verhalten. Die starken Korrelationen unterdrücken die Molekülzerfallsrate um eine Größenordnung. Der Verlust wird um zwei weitere Größenordnungen unterdrückt, indem ein schwaches optisches Gitter entlang der dritten Richtung angelegt wird. Es wird ein Modell entwickelt, das mit den experimentellen Daten überein stimmt.

Schließlich werden verschiedene Verlustratenkoeffizienten in der Nähe von Feshbach-Resonanzen gemessen. In einem Experiment werden Verluste durch inelastische Stöße von Feshbach-Molekülen mit anderen Atomen oder Molekülen bestimmt. Ein anderes Experiment untersucht atomare Dreikörper-Rekombination. In der Nähe einer Feshbach-Resonanz wird eine Erhöhung des Verlustkoeffizienten um vier Größenordnungen beobachtet, in guter Übereinstimmung mit der Theorie.

Contents

1 Introduction

Since the first realization of a Bose-Einstein condensate (BEC) in 1995, the field of quantum gases has seen enormous progress, and research is still advancing at a high pace. Two physical concepts that have attracted considerable attention are Feshbach resonances [Köh06] which led to the association of ultracold molecules and optical lattices [Blo05]. This thesis is concerned with the experimental investigation of Feshbach resonances and ultracold molecules. Most of the experiments are performed in an optical lattice. In the following, the basic concepts that are relevant for this thesis work are introduced. An attempt is made to highlight important developments during recent years before an outline of the present work is given.

1.1 Bose-Einstein Condensation

Bose-Einstein condensation is a quantum-statistical effect that occurs in an ideal three-dimensional gas of indistinguishable bosons. It was predicted in 1925 by A. Einstein based on the work of S.N. Bose [Bos24, Ein24, Ein25]. A Bose-Einstein condensate (BEC) forms when the thermal de-Broglie wavelength of the particles becomes comparable to the inter-particle distance. In this regime the particles' wave functions begin to overlap and a macroscopic number of particles occupies the single-particle ground state of the system.

Dilute gases are well-suited for studies of a BEC. The interactions between the particles are so weak that they can be described in a perturbative approach, and quantitative modeling of this many-body system becomes possible. However, reaching Bose-Einstein condensation with a dilute gas is an experimental challenge. The low densities of typically $\sim 10^{14}\,\mathrm{cm}^{-3}$ require temperatures of the order of $\sim 500\,\mathrm{nK}$. Luckily, the experimental realization of a BEC can build on powerful laser-cooling and trapping techniques. Laser cooling relies on the repeated absorption and emission of photons. It turned out that alkali atoms are particularly suitable for laser cooling because their optical transitions can be excited by available lasers, and because of the favorable structure of their internal energy levels. Since laser cooling alone cannot reach the required temperatures and densities yet, evaporative cooling is used in a second step to further reduce the temperature. Evaporative cooling relies on the selective removal of particles with the highest energy. Elastic collisions rethermalize the sample so that the temperature of the remaining particles

drops. Further details on cooling, trapping, and the creation of a BEC are presented in Refs. [Met99, Pet02, Pit03].

In 1995, seventy years after its prediction, BEC was achieved in dilute vapors of ^{87}Rb, ^{7}Li and ^{23}Na [And95, Bra95, Dav95]. This was a real breakthrough that marked the beginning of the new field of quantum-degenerate gases.

The cooling and trapping schemes were subsequently adapted to gases of fermionic atoms, and quantum degeneracy for fermions was first reached in 1999 for ^{40}K [DeM99]. Today, close to a hundred experiments have reached the quantum degenerate regime for atoms of 13 different bosonic and 4 different fermionic species [Dan].

1.2 Feshbach Resonances

Interparticle interactions play an important role in ultracold quantum gases. They determine many properties of the system such as the lifetime of the gas, the stability of a BEC, the thermalization rate during evaporative cooling, fundamental and collective excitations, and correlations between particles. The control of these interactions therefore is of great interest. Microscopically the interparticle interactions are caused by elastic and inelastic collisions. Since the gas is dilute, two-body collisions dominate.

During a collision, two particles can temporarily form a molecule. This requires that the two particles can couple to a molecular bound state. If the collision energy of the two particles is resonant with the energy of the molecular state, a Feshbach resonance occurs. The resonantly enhanced population of the bound state during the collision leads to a dramatic change of the scattering properties. Feshbach resonances were originally introduced in the context of nuclear physics [Fes58, Fes62].

In ultracold gases, the collision energy is fixed, and the bound-state energy can be tuned into resonance with the collision energy by applying external electromagnetic fields. A resonant change of the collisional properties as a function of a static magnetic field was first discussed in terms of inelastic collisions leading to loss of particles [Stw76, Tie92]. Later, it was proposed to magnetically tune the elastic scattering properties [Tie93].

The first experimental observations of Feshbach resonances were reported in 1998 for the bosonic species ^{23}Na, ^{85}Rb, and ^{133}Cs [Ino98, Cou98, Rob98, Vul99]. These experiments demonstrated the desired change in the elastic scattering length as well as an enhancement of inelastic collisions leading to particle loss. The latter was considered to be a serious limitation for future experiments, and several groups abandoned the subject.

The interest in the field was renewed when the Wieman group presented several beautiful results employing a Feshbach resonance in ^{85}Rb: the creation of a stable BEC of ^{85}Rb [Cor00], the observation of a controlled collapse of

the condensate [Don01], and the coherent coupling of the free atomic state to the molecular bound state causing the Feshbach resonance [Don02]. The last experiment was an important step towards the creation of a BEC of molecules as proposed in Ref. [Tim99a]. The interest in Feshbach resonances was further intensified by two proposals [Tim01, Hol01], suggesting that Feshbach resonances could be used in ultracold Fermi gases to obtain Cooper pairing and Bardeen-Cooper-Schrieffer (BCS) superfluidity.

In 2002, Feshbach resonances were also observed in fermionic ^{40}K [Lof02], and ^{6}Li [O'H02, Die02, Joc02] as well as in bosonic ^{7}Li [Kha02, Str02] and ^{87}Rb [Mar02]. By now, Feshbach resonances are routinely used to control the scattering properties of ultracold quantum gases. Alternative methods for tuning the scattering properties with electric fields [Mar98] or with laser light [Fed96a, Fat00, The04] have not been used much yet.

1.3 Ultracold Molecules

The realization of quantum degenerate gases of atoms made beautiful experiments possible. The question arises naturally whether molecules can also be prepared in a quantum degenerate gas. Compared to atoms, molecules offer additional degrees of freedom such as rotation and vibration and, for polar molecules, a permanent electric dipole moment. Molecular quantum gases would make studies of new quantum phases [Büc07] and quantum interfaces [And06] possible. In addition, they could be applied in high-precision measurements [Hud05] and matter-wave interferometers.

In 2003, several groups associated ultracold dimer molecules from atomic ^{40}K [Reg03], ^{133}Cs [Her03], ^{87}Rb [Dür04a], ^{6}Li [Cub03, Str03] and ^{23}Na [Xu03] using Feshbach resonances. In most of these experiments a technique proposed in 2000 [Mie00] was employed. A magnetic-field ramp across the Feshbach resonance transferred population from the atomic-pair state into the molecular state. This association technique constitutes a form of "super-chemistry". The temporal evolution of the chemical reaction is under complete experimental control and the reaction is fully reversible. No latent heat is released and the molecules ideally have the same temperature as the atoms before association.

Molecules created using Feshbach resonances are in highly excited rovibrational states. Hence, inelastic collisions can lead to rovibrational deexcitation and the released binding energy is converted into kinetic energy of the colliding particles. Since the kinetic energy is typically much larger than the trapping potential, the colliding particles are lost. Soon it turned out that the lifetime of molecules associated from *bosonic* atoms differ largely from the lifetime observed for molecules associated from *fermionic* atoms. Measurements in bosonic systems, ^{23}Na and ^{133}Cs, revealed two-body loss-rate coefficients of typically $5 \times 10^{-11}\,\mathrm{cm}^3/\mathrm{s}$ [Muk04, Chi05]. In fermionic systems, like ^{6}Li and

^{40}K, the loss-rate coefficients far away from the Feshbach resonance are similar, but the loss can be suppressed by orders of magnitude for magnetic fields close to the Feshbach resonance [Cub03, Reg04a]. An explanation based on the Pauli exclusion principle for fermions was put forward [Pet04b]. Recently, the molecule lifetime in the *bosonic* systems was increased considerably in an optical lattice [Tha06, Vol06].

At the end of 2003, the long lifetimes in the fermionic systems were exploited to produce the first molecular BECs [Joc03, Gre03, Zwi03]. Only a few months later, the same groups observed condensation of fermionic pairs on the Fermi-side of the Feshbach resonance [Reg04b, Bar04, Zwi04]. A proof for superfluidity of these pairs was given in 2005, based on the creation of vortices on the Fermi-side of the BEC-BCS crossover [Zwi05].

Experiments with molecules associated from bosonic atoms were comparatively difficult because of the short lifetimes. This made it impossible so far to create molecular BECs. Experiments concentrated on the systematic investigation of the association [Mar05, Hod05] and dissociation process [Muk04, Dür04b, Vol05] as well as on one- and two-body decay [Muk04, Tho05a, Chi05, Sya06]. Experiments on coherent molecular optics were performed [AS05], and an alternative method for the production of molecules was shown by applying a radio-frequency field near a Feshbach resonance [Tho05b]. Recently, heteronuclear Feshbach molecules were associated from a Bose-Bose mixture of ^{85}Rb and ^{87}Rb [Pap06] as well as from a Bose-Fermi mixture of ^{40}K and ^{87}Rb [Osp06].

1.4 Optical Lattices

Optical lattices are periodic potentials created by standing-wave light fields. Ultracold atoms and molecules stored in optical lattices resemble solid-state systems. But optical lattices offer the advantage that parameters, such as the potential depth, can be adjusted in real time. The combination of optical lattices with Feshbach resonances offers additional control parameters, and a variety of experiments based on this combination have been performed in this thesis work as well as by other groups, see e.g. [Rom04, Wid04, Köh05, Mor05, Chi06b, Osp06, Win06, Win07, Lan08, Wid07]. Two previous experiments with optical lattices were of particular importance for the experiments carried out in this thesis, namely the creation of a Mott insulator [Gre02] and the realization of a Tonks-Girardeau gas [Par04, Kin04]. These two topics are briefly introduced in the following.

The concept of the Mott insulator was originally proposed in the context of solid-state physics. The proposal aimed to explain the low conductivity observed in transition metal compounds at low temperature. In metals the electrical conductivity involves the motion of electrons within the periodic crystal

potential. In 1937, N.F. Mott suggested that "...[even] if the transparency of the potential barriers is low, it is quite possible that the electrostatic interaction between the electrons prevents them from moving at all ..." [Mot37]. As the insulating effect is a result of interactions, not of quantum statistics, a Mott insulator can also be realized with bosons as pointed out in Ref. [Fis89]. An experiment with ultracold bosonic atoms in an optical lattice was carried out in 2002 [Gre02] based on a proposal in Ref. [Jak98]. In addition to the observation of a Mott insulator, that experiment also induced a quantum phase transition between the Mott insulator and a superfluid by changing the depth of the optical lattice potential. Because the interaction dominates over the kinetic energy of the particles, the same number of atoms is found on each lattice site and the particles cannot move. This many-body state is an example of a strongly correlated system.

Strongly correlated systems were also studied in lower dimensions. In 1936, L. Tonks studied the equation of state for a one-dimensional (1D) classical gas consisting of hard elastic spheres theoretically [Ton36]. In 1960, M. Girardeau [Gir60] showed that bosons with infinitely strong elastic interactions confined to 1D are described by a many-body wave function that is almost the same as the one describing a system of identical fermions. Girardeau's model was generalized by Lieb and Liniger [Lie63] to the case of finite repulsive interactions. Today, a 1D gas of strongly interacting bosons is known as a Tonks-Girardeau gas. The strong repulsions dominate the dynamics and the bosons are forced to behave much like fermions. In 2004, the first experimental realization of such a system was demonstrated [Par04, Kin04]. The Tonks-Girardeau gas was created by confining repulsively interacting bosons to 1D using an optical lattice.

1.5 This Thesis

This thesis begins with an introduction into the relevant theoretical concepts in **Chapter 2**. It covers the basic theory of Feshbach resonances, the association of ultracold molecules, the description of bosons in optical lattices, and the theory of inelastic scattering in the ultracold limit.

The experiments were carried out in an apparatus that had already been built and used for similar experiments. In particular, ultracold molecules had been created with this setup using slow magnetic-field ramps across a Feshbach resonance [Dür04a]. During this PhD work, the apparatus was extended by an improved optical dipole trap that enables the creation of Bose-Einstein condensates with small particle number and good reproducibility. Moreover, a three-dimensional optical lattice setup was implemented. At that point, the experiment-control and data-analysis system was re-designed. A new system was implemented in order to control the large number of experimental param-

eters. The experimental setup is described in **Chapter 3**.

This dissertation covers only part of the studies performed during my PhD work. After I joined the team, we demonstrated experimentally that the dissociation of Feshbach molecules can populate a d wave although the incoming flux in the association is only in the s wave. The two outgoing partial waves create an interference pattern that is observed in time of flight images [Vol05]. We developed a theory that describes the dissociation in terms of a half collision. The theory agrees with our experimental findings [Dür05]. In a second experiment, we created a state with exactly one molecule at each site of an optical lattice. We started from an atomic Mott insulator with exactly two atoms per lattice site and associated molecules in a deep optical lattice. The spatial distribution of the atoms before association is then mapped to the spatial distribution of molecules. The resulting state is a Mott-like state of molecules [Vol06, Dür06]. The experiments discussed so far have already been reported in the PhD thesis of T. Volz [Vol07] and will not be discussed in this thesis.

Collisional decay limits the lifetime of ultracold gases. Loss measurements in the vicinity of a Feshbach resonance are presented in **Chapter 4**. We measured the loss-rate coefficients for atomic three-body recombination [Smi07] and for inelastic two-body collisions of Feshbach molecules with each other or with other atoms [Sya06].

Chapter 5 describes an alternative technique for associating Feshbach molecules. Instead of a linear ramp, we use coherent atom-molecule oscillations when jumping the magnetic field quickly to the Feshbach resonance. These experiments were performed in a deep optical lattice to prevent molecule loss due to inelastic collisions. We study the dependence of the amplitude and frequency of the oscillation on atomic density and magnetic field and find good agreement with the theoretical expectation [Sya07].

In **Chapter 6**, the attention is directed to many-body states in an optical lattice and to the investigation of strongly interacting molecules in 1D. By observing molecule loss, it is shown for the first time that dissipation due to inelastic molecule-molecule collisions leads to a strongly correlated many-body system. This is the dissipative analog of a Tonks-Girardeau gas [Sya08] where the bosonic molecules are forced to behave much like fermions. In order to model the data, we developed new theory that agrees with the experimental observations.

The results of this thesis work offer prospects for future experiments. This is illustrated in the outlook in **Chapter 7**.

2 Theoretical Background

This chapter reviews the theoretical background of this thesis work. It begins with a discussion on the influence of magnetically tunable Feshbach resonances on elastic and inelastic binary collisions in Sec. 2.1 and shows how these resonances can be used for the association and dissociation of ultracold molecules. Section 2.2 presents the Bose-Hubbard model describing bosons in optical lattices and discusses the quantum phase transition between a superfluid and a Mott insulator. Finally, Sec. 2.3 analyzes inelastic scattering of bosons within multichannel scattering theory. Inelastic scattering typically leads to loss of the colliding particles from the trap. The corresponding loss rates are derived including pair-correlations.

2.1 Feshbach Resonances and Molecules

The collisional properties of two colliding particles can strongly be modified by the presence of scattering resonances. In the field of ultracold gases, these scattering resonances, known as Feshbach resonances, are now commonly used to tune elastic as well as inelastic scattering properties. Furthermore, Feshbach resonances are a useful tool for the association of ultracold diatomic molecules from ultracold atoms.

After a short summary of ultracold collisions in Sec. 2.1.1, the principle of a Feshbach resonance is illustrated in Sec. 2.1.2 before the focus is shifted to magnetically tunable Feshbach resonances in Sec. 2.1.3. Eventually, the principle of association of molecules is briefly discussed in Sec. 2.1.4. For a recent review, the reader is referred to Ref. [Köh06]. Previous work on this subject performed in our experimental setup is described in Refs. [Mar03, Vol07].

2.1.1 Ultracold Collisions

In ultracold gases, the scattering of particles can be reduced to the problem of binary collisions, since the mean inter-particle distance is much larger than the typical range of the interaction potential. For ultracold gases the limit of vanishing energy of the incoming wave is important and scattering of particles can be described in terms of partial waves. For sufficiently low energies the centrifugal barrier prevents partial waves with angular momentum quantum

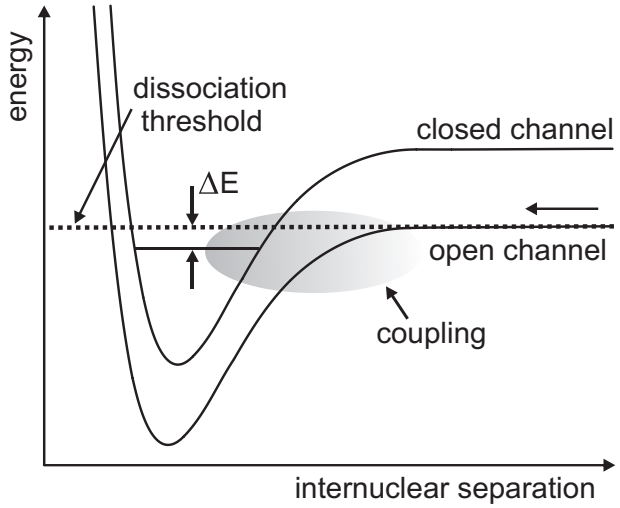

Figure 2.1: Principle of a Feshbach resonance. Atoms enter in the open channel with kinetic energy close to the dissociation threshold. This channel is coupled to an energetically closed channel which supports a bound state. For $\Delta E \rightarrow 0$, the population of the bound state is resonantly enhanced and a Feshbach resonance occurs.

number $l \neq 0$ from penetrating into the central region of the scattering potential. The higher partial waves do not probe the actual scattering potential and the lowest partial wave ($l = 0$) dominates over all other partial waves. This defines the s-wave limit. In this limit, the scattering phase δ_0 modulo π is proportional to the wave vector of the relative motion k of the two colliding particles. The scattering can be fully described by the scattering length

$$a = -\lim_{k \to 0} \frac{\tan \delta_0}{k} \, . \tag{2.1}$$

Elastic scattering is described by the real part of a and inelastic scattering is described by the imaginary part of a.

2.1.2 Principle of a Feshbach Resonance

Feshbach resonances are scattering resonances that occur for particles with an internal degree of freedom such as spin. Figure 2.1 schematically shows the two-atom scattering potentials for two different spin states. Each potential is referred to as a scattering channel. The incoming atoms have very low kinetic energy and we assume that they enter in the open channel close to the dissociation threshold. They cannot separate in the upper channel due to energy conservation. The upper channel is therefore energetically closed. If the closed channel supports a bound state with an energy that is close to the energy of the incoming atoms, this bound state can temporarily be populated

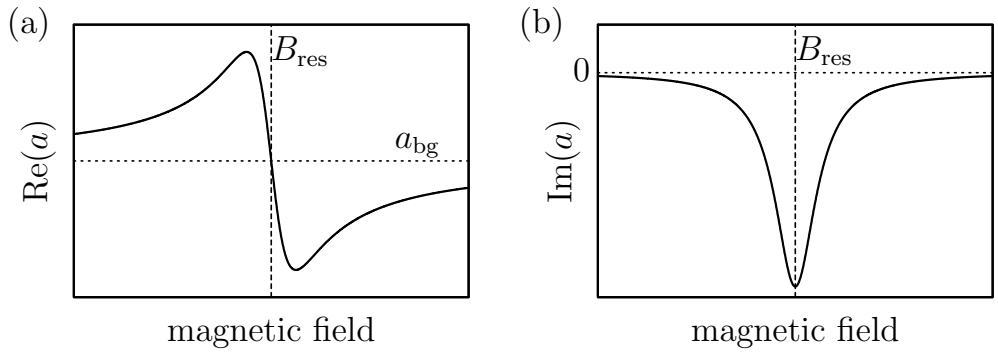

Figure 2.2: Magnetically tunable Feshbach resonance. (a) The real part of the scattering length shows a dispersive behavior close to the Feshbach resonance at B_{res}. Far away from the resonance the scattering length reaches the background value a_{bg}. (b) The imaginary part of the scattering length is described by a Lorentzian centered B_{res}. It represents inelastic collisions, which are strongest on resonance. Here, $a_{\mathrm{bg}} > 0$, $\Delta B > 0$ and $\Gamma > 0$.

during the scattering process provided that the Hamiltonian can flip spins. The energy difference between the bound state and the open-channel dissociation-threshold is denoted by ΔE. If $\Delta E \to 0$, the population of the bound state is resonantly enhanced and a Feshbach resonance occurs.

2.1.3 Magnetically Tunable Feshbach Resonances

The scattering channels typically have different spins and, therefore, they also have different magnetic moments. Thus, the Zeeman effect can be used to tune ΔE by applying a magnetic field. Close to $\Delta E = 0$ a linear approximation holds

$$\Delta E \;=\; \Delta\mu\,(B - B_{\mathrm{res}}) \;. \tag{2.2}$$

Here, $\Delta\mu = \mu_m - 2\mu_a$ denotes the difference in magnetic moment between the bound state μ_m and two atoms $2\mu_a$ and B_{res} is the magnetic field value where $\Delta E = 0$.

Close to resonance, the coupling of the free atom-pair state to the bound state strongly modifies the scattering properties of the free atoms. In the case of s-wave scattering, the magnetic-field dependence of the scattering length is given by [Hut07, Die07]

$$a(B) \;=\; a_{\mathrm{bg}}\left(1 - \frac{\Delta B}{B - B_{\mathrm{res}} + i\frac{\hbar\Gamma}{2\Delta\mu}}\right) \;. \tag{2.3}$$

Far away from the resonance, the scattering length approaches its background value a_{bg} which we assume to be real. The magnetic field width of the resonance is denoted by ΔB which is also real. The total decay rate of the

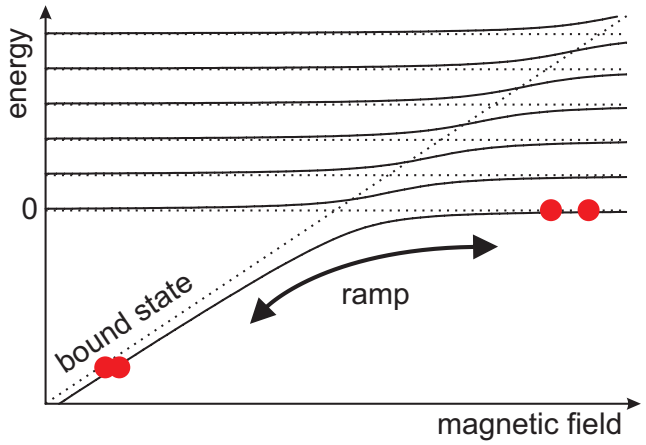

Figure 2.3: Molecule association and dissociation. The energy eigenstates of two atoms in a harmonic trap are sketched as a function of the magnetic field close to the Feshbach resonance with $\mu_a = 0$. Solid (dashed) lines represent the eigenstates in the presence (absence) of coupling between open and closed channel. An adiabatic magnetic field ramp across the Feshbach resonance (arrow) transfers population between the atomic-pair state and the bound state and vice versa. A ramp from high to low magnetic field associates molecules while a ramp in the reverse direction dissociates them.

population in the bound state into all open channels is Γ. For $\Gamma \neq 0$, the real part $\mathrm{Re}(a)$ is displayed in Fig. 2.2(a). It shows a dispersive behavior with an inflection point at B_{res}. The imaginary part $\mathrm{Im}(a)$, shown in Fig. 2.2(b), is described by a Lorentzian centered at B_{res} with full-width at half-maximum (FWHM) of $\hbar\Gamma/\Delta\mu$. Inelastic collisions are thus strongest on resonance. In the special case $\Gamma = 0$ [Moe95], $\mathrm{Im}(a)$ vanishes and the real part has a pole at $B = B_{\mathrm{res}}$. In this case, ΔB corresponds to the difference between the zero crossing and the pole of a.

2.1.4 Feshbach Molecules

Feshbach resonances have proved to be an efficient tool for the association of molecules from ultracold atoms [Köh06]. Most of the work presented in this thesis relies on a magnetic field ramp across the Feshbach resonance [Mie00, Reg03]. In order to illustrate the physical concept, we consider two atoms in a harmonic trap. In this case, the continuum of open-channel atom-pair states above threshold is replaced by a ladder of discrete trap states as depicted in Fig. 2.3. The coupling between the bound state and the open-channel trap-state leads to a series of avoided crossings. If the corresponding matrix element (see Appendix B) is small compared to the energy spacing of the trap states, the crossing between the lowest trap state and the bound state can be described as a two-level system close to the Feshbach resonance.

To associate molecules, two atoms are first prepared at a magnetic field above the Feshbach resonance in the lowest trap state. A subsequent ramp of the magnetic field across the Feshbach resonance transfers population into the bound state by adiabatically following the lower branch of the avoided crossing as indicated by the arrow in Fig. 2.3. The magnetic field value at the end of the ramp determines the binding energy. For slow ramps, the association efficiency approaches 100%.

After association of molecules, a reverse magnetic field ramp can be used to dissociate the molecules. If the ramp speed is slow compared to the timescale associated with the atom-molecule coupling, the population will follow the lower branch of the avoided crossing adiabatically and the dissociated atoms end up in the lowest trap state with the same energy as before association. In this case, molecule association and subsequent dissociation is a fully reversible process, whereas if the ramp speed is fast compared to the atom-molecule coupling, the bound-state population will be diabatically transferred across the avoided crossing. The final energy of the bound-state population is controlled by the magnetic field at the end of the ramp. If the final energy is detuned from the energy of a higher trap state, the dissociation of the bound state into atom pairs is strongly suppressed. If the final energy is close to the energy of a higher trap state, the bound state dissociates into atom pairs (see also Sec. 5.4).

Molecule association was also demonstrated in ultracold clouds containing many atoms. A detailed theoretical description must consider the complex many-body nature of the system. If the energy spacing of the open-channel trap-states is smaller than or comparable to the coupling matrix element, the simultaneous coupling of the bound state to more than one open-channel trap-state has to be included. The ultimate limit is the case of free space where the bound state is coupled to the continuum of open-channel states.

The molecule association efficiency is predicted to reach high values in the many-body case [Köh06]. For fermions, high association efficiencies were demonstrated experimentally [Reg03]. For bosons, on the other hand, the association efficiency in free space is low. Atoms disappear during the association ramp and only few molecules are observed. Since the associated molecules are in a highly-excited rovibrational state, they can decay to a lower-lying vibrational state during an inelastic collision with atoms or other molecules. The difference in binding energy is released as kinetic energy in the relative motion of the collision partners. The released energy is typically larger than the trap depth and both particles are lost from the trap. As demonstrated in recent experiments, high association efficiencies can be reached by using an optical lattice to suppress inelastic collisions [Tha06, Vol06].

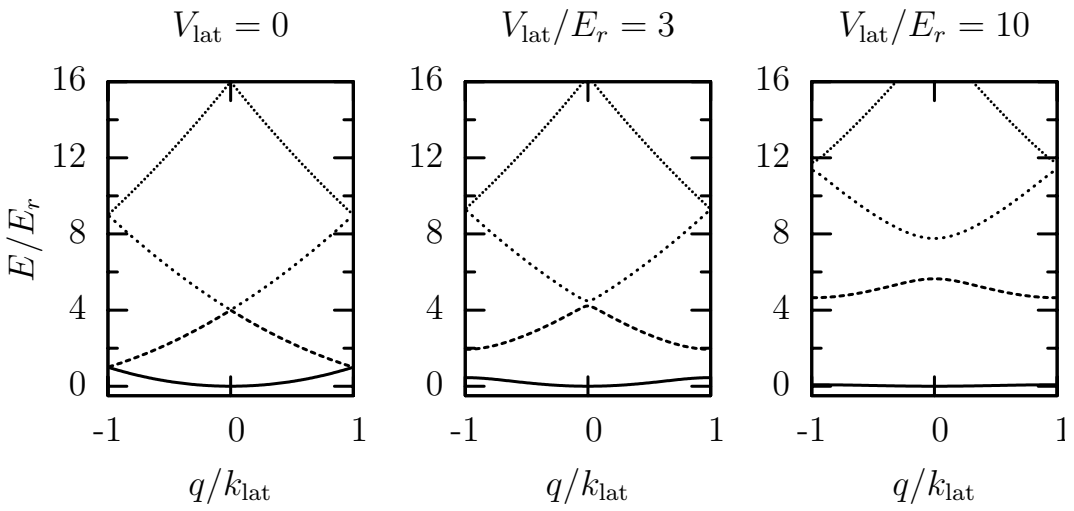

Figure 2.4: One-dimensional single-particle band structure. The lowest bands created by a sinusoidal potential are shown as a function of quasi-momentum q. With increasing potential depth $V_{\rm lat}$, the band gaps increase and the bands flatten. The energy is plotted in units of the recoil energy E_r. $E = 0$ is chosen at the minimum of the lowest band.

2.2 Bosons in Optical Lattices

Optical lattices created by far-detuned standing-wave light fields are a commonly used tool for confining atoms or molecules in periodic potentials or configurations of reduced dimensionality. In Sec. 2.2.1 we briefly review the single-particle band structure in a periodic potential. A bosonic many-particle system in a lattice is described by the Bose-Hubbard model which is presented in Sec. 2.2.2. A discussion of the phase transition from a superfluid state to a Mott-insulator state follows in Sec. 2.2.3. Finally, the case of an inhomogeneous Mott insulator is addressed in Sec. 2.2.4. For a recent review of this field see Ref. [Blo07].

2.2.1 Band Structure

Standing wave light fields can be used to create periodic potentials for ultracold atoms or molecules. As in solid state systems, a periodic potential $V(\mathbf{r})$ leads to a band structure of the energy levels. According to Bloch's theorem, the solution to the time-independent Schrödinger equation can be obtained using the ansatz

$$\psi_{\mathbf{q}}^{(n)}(\mathbf{r}) \;=\; e^{i\mathbf{q}\mathbf{r}}\, u_{\mathbf{q}}^{(n)}(\mathbf{r}) \;, \tag{2.4}$$

where $\mathbf{q}$ is the quasi-momentum and n is the index corresponding to different energy bands. Equation (2.4) represents a product of a plane wave $e^{i\mathbf{q}\mathbf{r}}$ and a periodic function $u_{\mathbf{q}}^{(n)}(\mathbf{r})$ which has the same period as the potential $V(\mathbf{r})$

[Ash76]. We only consider the case of a simple cubic, sinusoidal lattice

$$V(\mathbf{r}) \;=\; -V_x \cos^2(k_{\mathrm{lat}} x) - V_y \cos^2(k_{\mathrm{lat}} y) - V_z \cos^2(k_{\mathrm{lat}} z)\;, \tag{2.5}$$

where $\lambda_{\mathrm{lat}} = 2\pi/k_{\mathrm{lat}}$ is the wavelength of the lattice light. The problem is separable so that it is sufficient to solve the 1D Schrödinger equation. For $V_x = V_y = V_z$ we denote this value as V_{lat}. Figure 2.4 shows the single-particle band structure for different potential depths. It is convenient to express the energies in the system in terms of the recoil energy defined as

$$E_r \;=\; \frac{\hbar^2 k_{\mathrm{lat}}^2}{2m}\,, \tag{2.6}$$

where m is the particle mass.

2.2.2 Bose-Hubbard Model

For a single atom, the energy eigenstates for a periodic potential are Bloch wave functions (2.4) which are delocalized across the whole lattice. An alternative single-particle basis are the Wannier functions $w^{(n)}(\mathbf{r}-\mathbf{r}_j)$ that can be expressed as a superposition of Bloch functions by

$$w^{(n)}(\mathbf{r}-\mathbf{r}_j) \;=\; \frac{1}{\sqrt{\mathcal{N}}} \sum_{\mathbf{q}} e^{-i\mathbf{q}\cdot\mathbf{r}_j} \psi_{\mathbf{q}}^{(n)}\;, \tag{2.7}$$

where $\mathcal{N}$ is a normalization constant. The Wannier functions are centered at the individual lattice sites $\mathbf{r}_j$. For all bands n and all sites $\mathbf{r}_j$ they form an orthonormal basis. If the energies involved in the dynamics of the system are much smaller than the band gap between the two lowest bands, it suffices to consider only the lowest band ($n = 0$). Thus, the bosonic field operator $\hat{\Psi}(\mathbf{r})$ can be expanded as

$$\hat{\Psi}(\mathbf{r}) \;=\; \sum_j \hat{a}_j w(\mathbf{r}-\mathbf{r}_j)\;, \tag{2.8}$$

where $w(\mathbf{r}-\mathbf{r}_j) = w^{(0)}(\mathbf{r}-\mathbf{r}_j)$ and $\hat{a}_j$ is the bosonic annihilation operator for a particle at site j.

Many-body states of interacting bosons which are subject to an optical lattice potential $V_{\mathrm{lat}}(\mathbf{r})$ and an additional slowly varying trapping potential $V_{\mathrm{trap}}(\mathbf{r})$ can be described by the Bose-Hubbard Hamiltonian[1] [Fis89, Jak98]

$$\hat{H} \;=\; -J \sum_{\langle i,j\rangle} \hat{a}_i^\dagger \hat{a}_j + \frac{\mathrm{Re}(U)}{2} \sum_i \hat{n}_i(\hat{n}_i - 1) + \sum_i (\epsilon_i - \mu)\hat{n}_i\;. \tag{2.9}$$

[1] To derive the Bose-Hubbard Hamiltonian, one starts with the Hamiltonian Eq. (2.42) with $V(\mathbf{r}) = V_{\mathrm{lat}}(\mathbf{r}) + V_{\mathrm{trap}}(\mathbf{r})$ describing a many-body system of identical bosons with two-body interactions modeled by a contact potential. Inserting Eq. (2.8) and assuming that the overlap of Wannier functions at different lattice sites is small, only terms describing on-site and nearest-neighbor interaction are relevant. This yields Eq. (2.9)

Here, $\hat{n}_i = \hat{a}_i^\dagger \hat{a}_i$ is the particle number operator for the lattice site i and $\langle i, j \rangle$ denotes the sum over nearest neighboring sites.

The first term describes the tunneling of particles between adjacent lattice sites. The tunneling amplitude J can be calculated from

$$J = -\int \mathrm{d}^3 r \; w^*(\mathbf{r} - \mathbf{r}_i) \left(-\frac{\hbar^2}{2m}\nabla^2 + V_{\mathrm{lat}}(\mathbf{r}) \right) w(\mathbf{r} - \mathbf{r}_j) \; . \tag{2.10}$$

The second term in Eq. (2.9) describes the interaction of atoms on the same site (on-site interaction) due to elastic scattering. The interaction strength is given by

$$U = g \int \mathrm{d}^3 r \; |w(\mathbf{r})|^4 \; . \tag{2.11}$$

It is proportional to the complex valued interaction coefficient

$$g = \frac{4\pi\hbar^2}{m} a \; , \tag{2.12}$$

characterized by the s-wave scattering length a. The real and imaginary part of g describe elastic and inelastic scattering, respectively. Inelastic scattering typically leads to loss of both colliding particles from the trapping potentials. Loss of particles can be included in the Bose-Hubbard model using a master equation approach as described in Sec. 2.3.5.

The third term in Eq. (2.9) includes the chemical potential μ and the energy offset ϵ_i at lattice site i. The offset $\epsilon_i \approx E_0 + \frac{m}{2}\omega \mathbf{r}_i^2$ is created by the zero-point energy E_0 of a particle confined at one lattice site and by the external harmonic confinement $V_{\mathrm{trap}}(\mathbf{r})$ characterized by the angular frequency ω.

Fig. 2.5 shows the dependence of the tunneling amplitude J and the on-site interaction energy $\mathrm{Re}(U)$ on the lattice depth for repulsive interaction ($a > 0$). When V_{lat} is increased, the tunneling-barrier height is increased and J drops approximately exponentially. At the same time $\mathrm{Re}(U)$ increases slightly due to the increased confinement at the lattice site.

2.2.3 Mott-Insulator Phase Transition

In this section we neglect the external confinement so that ϵ_i is independent of i. We can set all ϵ_i to zero by resetting the zero point of the energy. We assume that there is no loss, i.e. $\mathrm{Im}(U) = 0$. The Bose-Hubbard model describes the competition between tunneling where the particles lower their kinetic energy by delocalizing over the lattice sites and the repulsive on-site interaction which disfavors having more than one particle at a given site. In the limit $U/J \ll 1$, the tunneling term Eq. (2.9) dominates the Bose-Hubbard Hamiltonian. As a result, the particles tend to delocalize across the lattice to minimize the

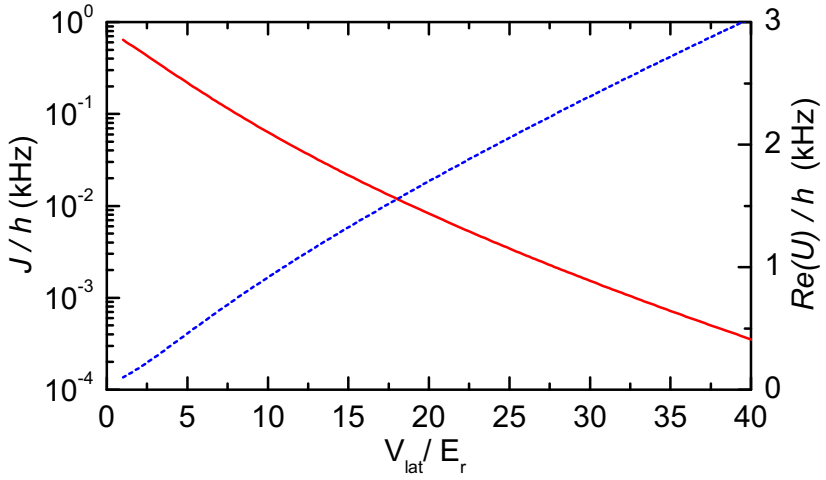

Figure 2.5: Parameters for the Bose-Hubbard model. The tunneling amplitude J (solid line) decreases approximately exponentially with lattice depth V_{lat} while the on-site interaction energy $\mathrm{Re}(U)$ (dashed line), shown for repulsive interactions, grows only slowly. Consequently, the ratio $\mathrm{Re}(U)/J$ can be tuned over several orders of magnitude by adjusting the lattice depth V_{lat}. The curves are obtained from a band structure calculation for ^{87}Rb atoms and $\lambda_{\mathrm{lat}} = 830\,\mathrm{nm}$.

tunneling energy. The many-body wave function for N bosons occupying M lattice sites is a product of identical delocalized single-particle states

$$|\Psi_{\mathrm{SF}}\rangle \overset{U\to 0}{=} \left(\frac{1}{\sqrt{M}}\sum_{i=1}^{M}\hat{a}_i^{\dagger}\right)^{N}|0\rangle \ . \tag{2.13}$$

Here, $|0\rangle$ denotes the vacuum state. In this limit, the ground state of the Bose-Hubbard Hamiltonian is a BEC. Therefore, there is a well-defined phase across the lattice. For each lattice site the many-body state is a superposition of different atom-number states. A measurement of the particle number for each site will yield random results according to a Poissonian number distribution as schematically shown in Fig. 2.6.

In the opposite limit, $U/J \gg 1$, the interaction term in Eq. (2.9) dominates the Bose-Hubbard Hamiltonian. The interaction energy is minimized if there is exactly the same number of particles on each lattice site. Any fluctuation of the particle number or inhomogeneity in the particle distribution would increase the interaction energy. The minimal energy cost to move a particle to an adjacent site is U. As a consequence, transport of particles between lattice sites is inhibited as long as excitations are smaller than U. The ground state of the multi-particle system is a Mott insulator. For n particles per site the

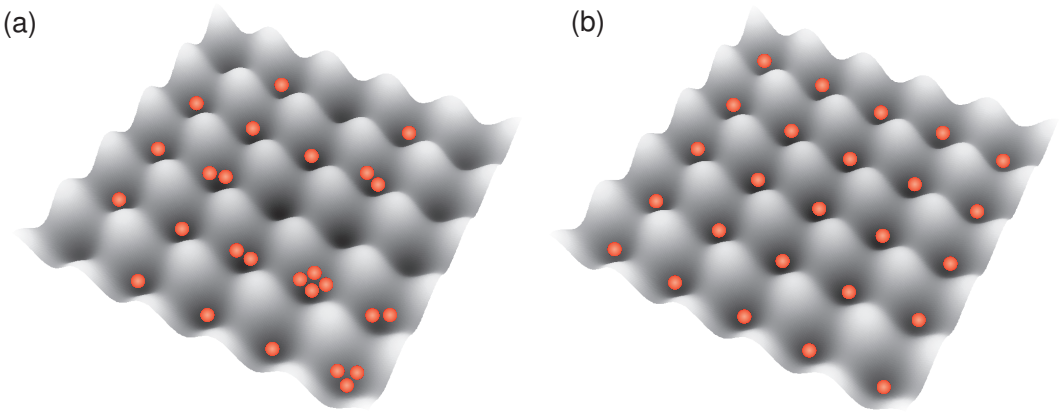

Figure 2.6: Superfluid and Mott insulator phase for the Bose-Hubbard model. (a) In the superfluid regime ($U \ll J$), the particles are delocalized across the lattice. Thus the particle number for each lattice site is random. (b) In the Mott insulator state ($U \gg J$), the on-site interaction dominates and the energy is minimized if all sites contain exactly the same number of particles.

ground-state wave function is a product of local Fock states

$$|\Psi_{\mathrm{MI}}\rangle \overset{J\to 0}{=} \left(\prod_{i=1}^{M} \frac{1}{\sqrt{n!}} \hat{a}_i^{\dagger n} \right) |0\rangle \ . \tag{2.14}$$

The well-defined particle number results in a maximum uncertainty in the phase. Consequently, the system shows no macroscopic phase coherence. Note that in the Mott insulating state, the particle dynamics is dominated by the particle-particle interaction and cannot be described by mean-field theory.

The ground state properties of the Bose-Hubbard Hamiltonian are determined by the ratio U/J. The superfluid regime $U/J \ll 1$ and the Mott-insulator regime $U/J \gg 1$ are connected by a quantum phase transition. In a 3D simple cubic lattice with $\bar{n} = 1$ the phase transition occurs for $(U/J)_{\mathrm{crit}} \approx 29$ [CS07]. This value corresponds to a lattice depth of $V_{\mathrm{lat,crit}} \approx 12.3 E_r$ for $\lambda_{\mathrm{lat}} = 830\,\mathrm{nm}$ in the case of atomic ^{87}Rb. A sweep of V_{lat} across $V_{\mathrm{lat,crit}}$ must be adiabatic to avoid single-particle excitations as well as excitations of the many-body state. The superfluid-to-Mott-insulator phase transition was first demonstrated experimentally in Ref. [Gre02].

2.2.4 Inhomogeneous Mott Insulator

In the experiment, there is a harmonic confinement in addition to the lattice potential. This is partly due to the dipole trap and partly due to the Gaussian shape of the lattice beams. In a deep lattice where $J \to 0$, the confinement leads to a position dependent atom distribution. In 3D, shells of Mott insulator regions with constant n will form. For given U, μ and ϵ_i, steps in the lattice

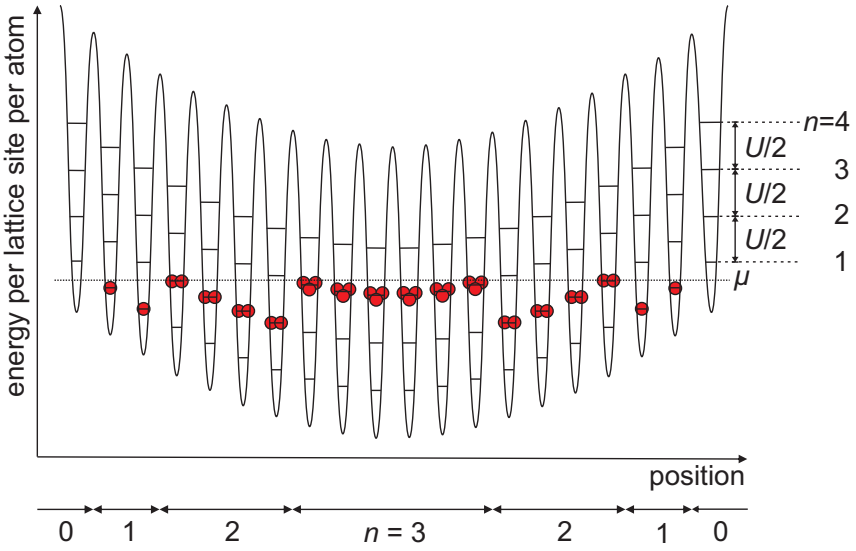

Figure 2.7: Inhomogeneous Mott insulator. Shell structure of the inhomogeneous Mott insulator for zero temperature and $J \to 0$. The external harmonic confinement gives rise to a position-dependent energy offset. The particles fill the lattice sites up to a constant chemical potential μ. In 3D, this leads to a shell structure with shells of constant particle number per site. The cost in interaction energy of moving a particle to another site inside a shell of constant n is U.

filling occur at radial distances where

$$\epsilon_i n_i + \frac{U}{2} n_i(n_i - 1) = \mu n_i \tag{2.15}$$

for some integer n_i. This is schematically shown in Fig. 2.7. The particles fill the lattice up to a constant chemical potential μ. For increasing ϵ_i, the number of particles per site decreases. The shell structure of the inhomogeneous Mott insulator was experimentally resolved in Refs. [Föl06, Cam06].

A model for zero temperature and $J = 0$ [Han06, Vol07] predicts the fraction of atoms at lattice sites occupied with n atoms each as a function of U and the geometric mean of the angular frequency $\bar{\omega}$ of the external harmonic trapping potential. For given U and $\bar{\omega}$, the particle distribution only depends on the total particle number. The model predicts a maximum fraction of particles on doubly-occupied sites of 53% which occurs when a core of triply-occupied sites starts to form.

For finite U/J, the Mott insulator shells are separated by shells of atoms in the superfluid state. The sharp steps in the atom density distribution smear out. In these regions, a gain in tunneling energy makes energy levels accessible that would lie above μ in the case of $J = 0$. Thus, the superfluid state is energetically more favorable than the Mott insulator state in that particular region.

2.3 Inelastic Scattering

The problem of two particles *elastically* scattering off one another is discussed in a large number of textbooks, see e.g. Refs. [Mot65, Tay72, Joa75]. We therefore skip a discussion of this standard topic. Instead, we focus on inelastic scattering in the ultracold limit. This topic is discussed much less frequently and great care is needed to avoid factor-of-two errors in the calculation of loss rates for identical particles.

Section 2.3.1 introduces the central results, namely loss-rate equations for inelastic two-body and three-body collisions with phenomenological rate coefficients. The remainder of Sec. 2.3 is devoted to relating the two-body loss coefficients to the S-matrix and the scattering length. In particular, in Sec. 2.3.2 we describe multichannel scattering of distinguishable particles and derive the scattering cross sections for elastic and inelastic scattering. The special case of identical bosons is considered in Sec. 2.3.3. Loss rate coefficients are derived in Sec. 2.3.4. A description in terms of a Markovian quantum master equation and the effect of the pair correlation function are discussed in Sec. 2.3.5. If one is only interested in the initial loss rate, the master equation formalism can be simplified to an effective Hamiltonian as shown in Sec. 2.3.6.

2.3.1 Rate Equations

Inelastic collisions in an ultracold gas typically convert a significant amount of internal energy into kinetic energy in the relative motion of the particles. If the released kinetic energy is large enough, all particles involved in the inelastic collision are lost from the trap.

Firstly, we consider two-body collisions. As will be derived in the remainder of Sec. 2.3, the density n of bosons in the same spin state obeys a loss-rate equation

$$\frac{d}{dt}n = -K_2\, g^{(2)}(0)\, n^2 \,, \tag{2.16}$$

where K_2 is the two-body loss coefficient for a BEC which is related to the s-wave scattering length by

$$K_2 \;=\; -\frac{2}{\hbar}\mathrm{Im}(g) \;=\; -\frac{8\pi\hbar}{m}\,\mathrm{Im}(a) \;, \tag{2.17}$$

with g from Eq. (2.12). The fact that the loss-rate coefficient is non-negative by definition implies $\mathrm{Im}(a) \leq 0$.

In Eq. (2.16), the pair correlation function at zero relative distance is denoted by $g^{(2)}(0)$. For a weakly interacting Bose gas at zero temperature, $g^{(2)}(0) \approx 1$. If the gas is above the critical temperature for Bose-Einstein condensation, then $g^{(2)}(0) = 2$.

If the atoms are initially in the absolute internal ground state, inelastic two-body collisions cannot occur. In this case, inelastic processes are dominated

by three-body collisions. In a three-body collision two atoms form a molecule. The binding energy is released as kinetic energy in the relative motion of the molecule and the third atom. The released energy is typically much larger than the trap potential so that all three atoms are lost from the trap. This recombination process is forbidden for two-body collisions due to energy and momentum conservation. In analogy to Eq. (2.16) one obtains

$$\frac{d}{dt}n \;=\; -K_3\, g^{(3)}(0)\, n^3 \;, \tag{2.18}$$

with the three-body loss coefficient K_3 and the three-body correlation function $g^{(3)}(0)$. For a BEC $g^{(3)}(0) = 1$ and for a thermal gas above the critical temperature for Bose-Einstein condensation, $g^{(3)}(0) = 6$.

The remainder of Sec. 2.3 is devoted to relating the two-body loss coefficients to the scattering length. This is a rather subtle issue and readers less interested in details may wish to continue with Chapter 3.

2.3.2 Multichannel Scattering

In this section, we discuss scattering of distinguishable particles with spin and derive expressions for elastic and inelastic scattering cross sections for incoming particles in the s-wave limit. The problem can be separated into center-of-mass and relative coordinates. The center-off-mass motion is trivial. The relative motion corresponds to the scattering of a single particle with reduced mass m_r off a potential $V(\mathbf{r})$. The incoming wave is assumed to be a plane wave with wave vector $\mathbf{k}_{\alpha\beta} = m_r \mathbf{v}_{\mathrm{rel},\alpha\beta}/\hbar$ along the positive z-direction, where $\mathbf{v}_{\mathrm{rel},\alpha\beta}$ is the relative velocity. The initial spin states are denoted by $\alpha\beta$. The corresponding kinetic energy is $E = \hbar^2 \mathbf{k}_{\alpha\beta}^2/(2m_r)$. Scattering theory is usually formulated as a time-independent process and the Schrödinger equation reads

$$\left(-\frac{\hbar^2\nabla^2}{2m_r} + V(\mathbf{r})\right)\psi(\mathbf{r}) = E\psi(\mathbf{r}) \;\; . \tag{2.19}$$

For large radius, the scattered wave is proportional to a spherical wave. This leads to the asymptotic wave function for distinguishable particles

$$\psi(\mathbf{r}) \overset{r\to\infty}{=} \frac{1}{\sqrt{\mathcal{V}}}\left(e^{izk_{\alpha\beta}}\,|\alpha\beta\rangle + \sum_{\alpha'\beta'}\frac{e^{irk_{\alpha'\beta'}}}{r} f_{\alpha'\beta',\alpha\beta}(\vartheta,\varphi)\,|\alpha'\beta'\rangle\right) \;. \tag{2.20}$$

Here, r,ϑ,φ are spherical coordinates and $\mathcal{V}$ is a normalization volume. The normalization volume is chosen so that the plane wave component $e^{izk_{\alpha\beta}}/\sqrt{\mathcal{V}}$ contains one particle in the quantization volume. The spin state of the scattered wave is denoted by $\alpha'\beta'$. Internal energy can be converted into kinetic energy during the scattering process and vice versa. As a consequence, the

wave vector k depends on the spin state. The task in scattering theory is to determine the scattering amplitudes $f_{\alpha'\beta',\alpha\beta}(\vartheta,\varphi)$ for a given potential $V(\mathbf{r})$.

In a traditional scattering experiment, a target is hit by a plane wave with flux density $\mathbf{j}_{\text{in}} = n_{\text{in}}\mathbf{v}_{\text{rel},\alpha\beta}$, where n_{in} is the number density of incoming particles. Scattering events occur at a rate Γ, which is used to define the total scattering cross section σ by

$$\Gamma = \sigma j_{\text{in}} N_t \,, \tag{2.21}$$

where N_t is the number of target particles. The flux density for the outgoing part of the wave function $\psi = f_{\alpha'\beta',\alpha\beta}(\vartheta,\varphi)\,|\alpha'\beta'\rangle\, e^{irk_{\alpha'\beta'}}/(r\sqrt{\mathcal{V}})$ is $\mathbf{j}_{\text{out}} = \text{Re}(\psi^*(\hbar/i)\nabla\psi)\,/m_r$. By integrating the radial part of $\mathbf{j}_{\text{out}}$ over a sphere of radius r centered around $r = 0$, the scattering event rate can be calculated. The result is

$$\Gamma = \sum_{\alpha'\beta'} \frac{v_{\text{rel},\alpha'\beta'}}{\mathcal{V}} \int d\Omega |f_{\alpha'\beta',\alpha\beta}(\vartheta,\varphi)|^2 \,, \tag{2.22}$$

where $d\Omega = \sin\vartheta\ d\vartheta\ d\varphi$ is the differential solid angle. Comparison with Eq. (2.21) with $n_{\text{in}} = 1/\mathcal{V}$ and $N_t = 1$ yields the total scattering cross section

$$\sigma_{\alpha\beta} = \sum_{\alpha'\beta'} \sigma_{\alpha'\beta',\alpha\beta} = \sum_{\alpha'\beta'} \frac{k_{\alpha'\beta'}}{k_{\alpha\beta}} \int d\Omega |f_{\alpha'\beta',\alpha\beta}(\vartheta,\varphi)|^2 \,. \tag{2.23}$$

It is normalized to the incoming flux that is proportional to $k_{\alpha\beta}$.

The asymptotic solution Eq. (2.20) can be expanded in terms of spherical harmonics $Y_{l',m_{l'}}(\vartheta,\varphi)$ with angular momentum quantum numbers l' and $m_{l'}$. The primes indicate that these quantum numbers refer to the outgoing wave. We restrict our considerations to the case, where only outgoing partial waves with $m_{l'} = 0$ are populated. This is the case, for example, if the potential is cylindrically symmetric around the z-axis. The scattering amplitudes then read

$$f_{\alpha'\beta',\alpha\beta}(\vartheta) \;=\; \sum_{l'=0}^{\infty} f_{\alpha'\beta'l',\alpha\beta} Y_{l'0}(\vartheta) \sqrt{4\pi(2l'+1)} \,, \tag{2.24}$$

where the partial scattering amplitudes are denoted by $f_{\alpha'\beta'l',\alpha\beta}$. With this expansion the scattering problem can be reformulated. In a first step, the asymptotic solution Eq. (2.20) can be rewritten for a single incoming partial wave l and reads

$$\psi_l(\mathbf{r}) \overset{r\to\infty}{\longrightarrow} (-1)^l \frac{e^{-ikr}}{r} Y_{l0}(\vartheta) - \sum_{\alpha'\beta'} \frac{e^{irk_{\alpha'\beta'}}}{r} \sqrt{\frac{k_{\alpha\beta}}{k_{\alpha'\beta'}}} \sum_{l'=0}^{\infty} S_{\alpha'\beta'l',\alpha\beta l} Y_{l'0}(\vartheta) \,. \tag{2.25}$$

This defines the scattering (or S-) matrix. The factor $k_{\alpha\beta}/k_{\alpha'\beta'}$ is chosen so that the S-matrix is unitary if the number of particles is conserved. The factor $k_{\alpha\beta}/k_{\alpha'\beta'}$ reflects the fact that the outgoing flux is proportional to $k_{\alpha'\beta'}$, while

the cross section is normalized to the incoming flux that is proportional to $k_{\alpha\beta}$. Time reversal invariance implies that the S-matrix is symmetric. In a following step, the incoming partial waves in Eq. (2.25) are superimposed with suitable amplitudes to obtain an incoming plane wave. This yields

$$f_{\alpha'\beta'l',\alpha\beta} = \frac{1}{2i\sqrt{k_{\alpha\beta}k_{\alpha'\beta'}}} \sum_{l=0}^{\infty} \sqrt{\frac{2l+1}{2l'+1}} \left(S_{\alpha'\beta'l',\alpha\beta l} - \delta_{\alpha'\alpha}\delta_{\beta'\beta}\delta_{l'l}\right) , \tag{2.26}$$

where δ is the Kronecker symbol. Thus the total scattering cross section can be rewritten as

$$\sigma_{\alpha\beta} = \sum_{\alpha'\beta'} \frac{k_{\alpha'\beta'}}{k_{\alpha\beta}} \sum_{l'=0}^{\infty} 4\pi(2l'+1)|f_{\alpha'\beta'l',\alpha\beta}|^2 . \tag{2.27}$$

It is customary to define the scattering phases $\eta_{\alpha\beta l}$ based on the diagonal elements of the S-matrix

$$S_{\alpha\beta l,\alpha\beta l} = e^{2i\eta_{\alpha\beta l}} . \tag{2.28}$$

Note that the phases are only defined modulo π. If the S-matrix is diagonal in $\alpha\beta l$, then unitarity of the S-matrix implies that the scattering phases are real.

For ultracold gases, the limit of vanishing energy of the incoming wave is important. This limit is called the dissociation threshold. For sufficiently low energies the centrifugal barrier prevents partial waves with $l \neq 0$ from penetrating into the central region of the scattering potential. The higher partial waves do not probe the actual scattering potential and the lowest partial wave ($l = 0$) dominates over all other partial waves. This defines the s-wave limit. If the scattering potential is short ranged, i.e. $V(r) \propto r^{-s}$ with $s > 3$ for large r, it can be shown that $\eta_{\alpha\beta 0} = \mathcal{O}(k_{\alpha\beta})$ for $k_{\alpha\beta} \to 0$ [Tay72]. Here, the scattering process can be fully described by the s-wave scattering length

$$a_{\alpha\beta} = -\lim_{k_{\alpha\beta}\to 0} \frac{\tan\eta_{\alpha\beta 0}}{k_{\alpha\beta}} , \tag{2.29}$$

which is defined for each incoming spin state $\alpha\beta$.

The cross section for an incoming s-wave is obtained from Eq. (2.26) and Eq. (2.27)

$$\sigma_{\alpha'\beta'l',\alpha\beta 0} = \frac{\pi}{k_{\alpha\beta}^2} |S_{\alpha'\beta'l',\alpha\beta 0} - \delta_{\alpha'\alpha}\delta_{\beta'\beta}\delta_{l'0}|^2 . \tag{2.30}$$

For elastic scattering the outgoing wave is also in the s-wave limit. By using Eq. (2.28) and Eq. (2.29), the elastic cross section yields [Bal97]

$$\sigma_{\mathrm{el}} \overset{k_{\alpha\beta}\to 0}{=} 4\pi|a_{\alpha\beta}|^2 . \tag{2.31}$$

For inelastic collisions, internal energy can be converted into kinetic energy in the collision. Therefore, the outgoing wave can be outside the s-wave limit. The total inelastic cross section is calculated by summing over $\alpha'\beta'l'$. Near threshold, one obtains

$$\sigma_{\text{inel}} \overset{k_{\alpha\beta}\to 0}{=} \frac{\pi}{k_{\alpha\beta}^2} \sum_{\alpha'\beta'\neq\alpha\beta} \sum_{l'} \left|S_{\alpha'\beta'l',\alpha\beta 0}\right|^2 . \tag{2.32}$$

The first sum extends over all spin channels $\alpha'\beta'$, except for the incoming one $\alpha\beta$. For the sum including the initial spin state, unitarity of the S-matrix implies $\sum_{\alpha'\beta'} \sum_{l'} |S_{\alpha'\beta'l',\alpha\beta 0}| = 1$, so that [Bal97]

$$\begin{aligned} \sigma_{\text{inel}} &\overset{k_{\alpha\beta}\to 0}{=} \frac{\pi}{k_{\alpha\beta}^2} \left(1 - \left|S_{\alpha\beta 0,\alpha\beta 0}\right|^2\right) \\ &\overset{k_{\alpha\beta}\to 0}{=} -\frac{4\pi}{k_{\alpha\beta}} \text{Im}(a_{\alpha\beta}) \ . \end{aligned} \tag{2.33}$$

Hence, the imaginary part of the scattering length represents the sum over all inelastic cross sections. Note that for low energies ($k_{\alpha\beta} \to 0$) the inelastic cross section diverges while the elastic cross section becomes constant. Furthermore, σ_{inel} is non-negative by definition which implies $\text{Im}(a_{\alpha\beta}) \leq 0$.

2.3.3 Identical Bosons

To extend the scattering cross sections to identical bosons with spin, the wave function Eq. (2.20) has to be symmetrized (see Appendix A). The scattering amplitudes $f_{\alpha'\beta',\alpha\beta}(\vartheta)$ and $f_{\alpha'\beta',\beta\alpha}(\pi-\vartheta)$ interfere. A useful quantity for s-wave collisions is the symmetrized scattering length defined as

$$a_{\alpha\beta}^{\text{sym}} = \frac{a_{\alpha\beta,\alpha\beta} + a_{\alpha\beta,\beta\alpha}}{1+\delta_{\alpha\beta}} , \tag{2.34}$$

in accordance with the symmetrized S-matrix [Sto88]. The elastic and inelastic scattering cross sections for bosons become [Bur99]

$$\sigma_{\text{el}}^{\text{boson}} \overset{k_{\alpha\beta}\to 0}{=} (1+\delta_{\alpha\beta})\, 4\pi \left|a_{\alpha\beta}^{\text{sym}}\right|^2 \tag{2.35}$$

$$\sigma_{\text{inel}}^{\text{boson}} \overset{k_{\alpha\beta}\to 0}{=} -(1+\delta_{\alpha\beta})\, \frac{4\pi}{k_{\alpha\beta}} \text{Im}\left(a_{\alpha\beta}^{\text{sym}}\right) , \tag{2.36}$$

where the factor $(1+\delta_{\alpha\beta})$ accounts for interference of identical bosons.

2.3.4 Loss Rates Caused by Inelastic Collisions

In an inelastic collision the kinetic energy of the outgoing wave is different from the kinetic energy of the incoming wave. Typically, the gain in kinetic energy

for the outgoing wave is so large that both particles involved in the collision escape from the trapping potential. For identical particles the calculation of the resulting loss rates is a tricky issue which can often lead to factor-of-two errors if one is not careful.

We follow the approach of Ref. [Sto88] based on a quantum Boltzmann equation. The relaxation rate from initial states $\alpha\beta$ to final states $\mu\nu$ in a gas of identical bosons in the s-wave limit is given by [Sto88]

$$G_{\alpha\beta\to\mu\nu} = \left\langle \frac{\pi\hbar}{m_r k_{\alpha\beta}} \left| S_{\{\mu\nu\},\{\alpha\beta\}} - \delta_{\{\mu\nu\},\{\alpha\beta\}} \right|^2 \right\rangle_{\rm th} , \tag{2.37}$$

where the curly brackets indicate that the S-matrix has to be calculated in a symmetrized basis. The thermal average is denoted by $\langle \ldots \rangle_{\rm th}$. As discussed in Ref. [Sto89], the thermal average over a Bose-Einstein distribution coincides with the average over a Maxwell-Boltzmann distribution for temperatures T above the critical temperature T_C for Bose-Einstein condensation (BEC). Deviations occur only for $T < T_C$. For $T = 0$ the relaxation rate is a factor of $1/2$ smaller than for $T > T_C$. In the following we consider a thermal gas with $T > T_C$. To calculate the total inelastic relaxation coefficient we sum over all final states not equal to the initial state and use the unitarity of the S-matrix to arrive at

$$\sum_{\{\mu\nu\}\neq\{\alpha\beta\}} G_{\alpha\beta\to\mu\nu} \;=\; -\left\langle \frac{4\pi\hbar}{m_r} \mathrm{Im}\big(a^{\rm sym}_{\alpha\beta}\big) \right\rangle_{\rm th} . \tag{2.38}$$

This result does not depend on $k_{\alpha\beta}$ and we can drop the thermal average.

The operational significance of the relaxation rates Eq. (2.37) is a redistribution of population between spin states according to [Sto88]

$$\frac{d}{dt} n_\alpha \;=\; \sum_\beta \sum_{\{\mu\nu\}} (1+\delta_{\alpha\beta}) \left(G_{\mu\nu\to\alpha\beta} n_\mu n_\nu - G_{\alpha\beta\to\mu\nu} n_\alpha n_\beta \right) \tag{2.39}$$

This describes the temporal evolution of the density n_α of particles in spin state α. The first term describes particles that enter the state α in a collision and the second term accounts for particles leaving state α. We assume that only one spin state α is present initially. Hence,

$$\frac{d}{dt} n_\alpha = n_\alpha^2 \sum_\beta (1+\delta_{\alpha\beta}) G_{\alpha\alpha\to\alpha\beta} - 2 n_\alpha^2 \sum_{\{\mu\nu\}} G_{\alpha\alpha\to\mu\nu} . \tag{2.40}$$

If each inelastic collision removes both involved particles from the trap, we must remove all terms in the first sum except the elastic term $\alpha = \beta$. As a result the particle density decays as

$$\frac{d}{dt} n_\alpha = -2 n_\alpha^2 \sum_{\{\mu\nu\}\neq\{\alpha\alpha\}} G_{\alpha\alpha\to\mu\nu} = \frac{8\pi\hbar}{m_r} \mathrm{Im}(a^{\rm sym}_{\alpha\alpha})\; n_\alpha^2 . \tag{2.41}$$

As mentioned above, this expression holds for an uncondensed thermal gas.

2.3.5 Master Equation and Correlations

In the previous section, we mentioned the factor of two difference in collision rates between $T = 0$ and $T > T_C$. Now we show that this can be interpreted in terms of the pair correlation function. This approach has the advantage that it is also applicable for strongly correlated systems in 1D.

In this approach, the inter-atomic interaction potential is replaced by a pseudo potential [Hua87] $g\delta^{(3)}(\mathbf{r})\frac{\partial}{\partial r}r$ with interaction strength g as defined in Eq. (2.12). This contact (or zero-range) potential is designed so that it mimics the correct s-wave scattering properties.

In a further approximation, this contact potential is replaced by an even simpler delta potential [Hua87] $g\delta^{(3)}(\mathbf{r})$. This potential may only be used in first Born approximation where it reproduces the correct s-wave scattering properties. The full Born series yields no s-wave scattering for the delta potential. Using the delta potential, the Hamiltonian for a many-body system of identical bosons with two-body interactions reads [Pit03]

$$\begin{aligned}\hat{H} \;=\; & \int d^3r\, \hat{\Psi}^\dagger(\mathbf{r}) \left(-\frac{\hbar^2}{2m}\nabla^2 + V(\mathbf{r})\right) \hat{\Psi}(\mathbf{r}) \\ & + \frac{\mathrm{Re}(g)}{2} \int d^3r\, \hat{\Psi}^{\dagger 2}(\mathbf{r})\hat{\Psi}^2(\mathbf{r}) \;,\end{aligned} \tag{2.42}$$

where m is the mass of a boson and $\hat{\Psi}(\mathbf{r})$ is the field operator that annihilates a boson at position $\mathbf{r}$. This Hamiltonian is Hermitian and conserves the number of particles. It represents only the elastic part of the interactions. Inelastic interactions and the resulting loss are described by a Markovian quantum master equation [Bre02]

$$\frac{\partial}{\partial t}\rho = -\frac{i}{\hbar}[\hat{H}, \rho] + \mathcal{D}\rho \;. \tag{2.43}$$

The action of the dissipator $\mathcal{D}$ on the statistical operator ρ is given by

$$\mathcal{D}\rho = \mathcal{D}_{\mathrm{loss}}\rho + \mathcal{D}_{\mathrm{gain}}\rho \tag{2.44}$$

$$\mathcal{D}_{\mathrm{loss}}\rho = -\frac{\mathrm{Im}(g)}{2\hbar} \int d^3r \left(-\hat{\Psi}^{\dagger 2}\hat{\Psi}^2\rho - \rho\hat{\Psi}^{\dagger 2}\hat{\Psi}^2\right) \tag{2.45}$$

$$\mathcal{D}_{\mathrm{gain}}\rho = -\frac{\mathrm{Im}(g)}{2\hbar} \int d^3r\; 2\hat{\Psi}^2\rho\hat{\Psi}^{\dagger 2} \;. \tag{2.46}$$

We refrain from presenting a rigorous derivation of this result, but we motivate its plausibility: The two terms in $\mathcal{D}_{\mathrm{loss}}$ are obtained by analytic continuation of those terms in the master equation that result from the two-body interaction terms contained in $\hat{H}$. As $\mathrm{Re}(g)$ can be continued to g or g^*, the signs of these two terms remain to be determined. The relative sign is obtained from the requirement that ρ is Hermitian at all times, which implies $\frac{\partial}{\partial t}(\rho - \rho^\dagger) = 0$. $\mathcal{D}_{\mathrm{loss}}$

leads to loss of population from states containing two or more particles. This reduces $\mathrm{Tr}\{\rho\}$, where $\mathrm{Tr}\{\ldots\}$ denotes the trace. $\mathcal{D}_{\mathrm{gain}}$ is needed to refill the lost population incoherently into states with exactly two particles removed. This conserves $\mathrm{Tr}\{\rho\}$. The resulting dissipator $\mathcal{D}$ has a Lindblad form [Bre02, Lin76]. The overall sign of $\mathcal{D}$ is determined from $\mathrm{Im}(g) \leq 0$ combined with the fact that $\mathcal{D}$ is supposed to describe loss (not gain) of particles. The resulting overall sign of $\mathcal{D}$ is consistent with the fact that the factor outside the integral must be non-negative for all Lindblad forms [Bre02]. Note that in the integral, $\hat{\Psi}$ and $\hat{\Psi}^\dagger$ depend on $\mathbf{r}$, while ρ does not.

We are interested in the temporal evolution of the particle-density $\hat{n}(\mathbf{r}) = \hat{\Psi}^\dagger(\mathbf{r})\hat{\Psi}(\mathbf{r})$. A calculation that employs bosonic commutation relations for $\Psi^\dagger(\mathbf{r})$ and $\hat{\Psi}(\mathbf{r})$ yields

$$\begin{aligned} \left.\frac{d}{dt}\langle\hat{n}(\mathbf{r})\rangle\right|_{\mathrm{loss}} &= \mathrm{Tr}\{\hat{n}(\mathbf{r})\,\mathcal{D}\rho\} \\ &= \frac{2\mathrm{Im}(g)}{\hbar}\left\langle\hat{\Psi}^{\dagger 2}(\mathbf{r})\hat{\Psi}^2(\mathbf{r})\right\rangle . \end{aligned} \tag{2.47}$$

We define the pair correlation function

$$g^{(2)}(\mathbf{r},\mathbf{r}') = \frac{\left\langle\hat{\Psi}^\dagger(\mathbf{r})\hat{\Psi}^\dagger(\mathbf{r}')\hat{\Psi}(\mathbf{r})\hat{\Psi}(\mathbf{r}')\right\rangle}{\langle\hat{n}(\mathbf{r})\rangle\,\langle\hat{n}(\mathbf{r}')\rangle}, \tag{2.48}$$

where we use K_2 fomr Eq. (2.17) and obtain the central result

$$\frac{d}{dt}\langle\hat{n}(\mathbf{r})\rangle = -K_2 g^{(2)}(\mathbf{r},\mathbf{r})\,\langle\hat{n}(\mathbf{r})\rangle^2 . \tag{2.49}$$

Note that this result as well as Eq. (2.42) and Eq. (2.44) rely on the delta potential approximation. In 3D this is only valid if the interactions do not deform the wave functions (first Born approximation). This is the case in the weakly interacting regime, i.e. if $n|a|^3 \ll 1$. In 1D, a strongly interacting many-body system is correctly described by the delta potential approximation and the expressions derived here are valid for arbitrary interaction strength.

Particle loss is proportional to $g^{(2)}$ at $\mathbf{r} = \mathbf{r}'$. If the system is translationally invariant, then $g^{(2)}$ depends only on the relative coordinate $\mathbf{r} - \mathbf{r}'$. In this case, we abbreviate $g^{(2)}(\mathbf{r},\mathbf{r})$ as $g^{(2)}(0)$. The correlation functions for a weakly interacting Bose gas are

$$g^{(2)}(0) = \begin{cases} 1 & \text{for} \quad T = 0 \\ 2 & \text{for} \quad T > T_C. \end{cases} \tag{2.50}$$

Note that the loss rate for $T > T_C$ obtained with this approach is identical to Eq. (2.41). For a BEC $g^{(2)}(0)$ is reduced by a factor of 2 compared to a thermal gas [Yas96, Ött05, Sch05]. This is the quantum mechanical analog of the Hanbury-Brown and Twiss effect [Han56]. More generally, the n-body function is reduced by $n!$ [Kag85, Bur97].

2.3.6 Effective Hamiltonian

If one is only interested in the initial loss rate of a system, then the master equation formalism can be simplified to an effective Hamiltonian. The treatment presented here is a standard approach on which quantum-jump Monte-Carlo methods are based. This treatment starts with the observation that $\mathcal{D}_{\text{loss}}$ in Eq. (2.45) acts on ρ in a way that looks like a commutator. Indeed, $\mathcal{D}_{\text{loss}}$ can be absorbed in the Hamiltonian by replacing $\text{Re}(g)$ in Eq. (2.42) by g. The resulting non-Hermitian operator is called effective Hamiltonian $\hat{H}_{\text{eff}}$. The master equation (2.43) can be rewritten as

$$\frac{\partial \rho}{\partial t} = -\frac{i}{\hbar}\left(\hat{H}_{\text{eff}}\rho - \rho\hat{H}_{\text{eff}}^{\dagger}\right) + \mathcal{D}_{\text{gain}}\rho \; . \tag{2.51}$$

In the following, we consider the simple case, where ρ initially represents a Fock state with N particles, $\rho = |N\rangle\langle N|$. The time evolution at short time will be

$$\rho(t) = (1-\xi t)\,|N\rangle\langle N| + \xi t\,|N-2\rangle\langle N-2| + \mathcal{O}(t^2), \tag{2.52}$$

where ξ is related to $\text{Im}(g)$ and to the density of particles. The loss rate of particle number is $\frac{dN}{dt}\big|_{t=0} = -2\xi$. If we are only interested in calculating the loss rate at short times, we can obviously neglect the action of the operator $\mathcal{D}_{\text{gain}}$ (2.46) that only refills the population into state $|N-2\rangle$. If we drop $\mathcal{D}_{\text{gain}}$ from the master equation, we obtain $\frac{d}{dt}\text{Tr}\{\rho\}\big|_{t=0} = -\xi$. Hence, the loss of particle number in a model including $\mathcal{D}_{\text{gain}}$ is related to the decay of $\text{Tr}\{\rho\}$ in the model that ignores $\mathcal{D}_{\text{gain}}$ by

$$\left.\frac{dN}{dt}\right|_{t=0} = 2\left.\frac{d}{dt}\text{Tr}\{\rho\}\right|_{t=0} \; . \tag{2.53}$$

The crucial point is that with ρ initially prepared in a pure quantum state $|\psi\rangle$ and with $\mathcal{D}_{\text{gain}}$ neglected, the master equation is equivalent to a usual Schrödinger equation using the effective Hamiltonian

$$i\hbar\frac{\partial}{\partial t}|\psi\rangle = \hat{H}_{\text{eff}}\,|\psi\rangle \tag{2.54}$$

with $\rho = |\psi\rangle\langle\psi|$ as usual. The resulting decay of $\langle\psi|\psi\rangle = \text{Tr}\{\rho\}$ yields the loss rate of the particle number according to Eq. (2.53). Hence,

$$\left.\frac{dN}{dt}\right|_{t=0} = \frac{2}{i\hbar}\langle\psi|\left(\hat{H}_{\text{eff}} - \hat{H}_{\text{eff}}^{\dagger}\right)|\psi\rangle \; . \tag{2.55}$$

For a right eigenstate of the effective Hamiltonian, $\hat{H}_{\text{eff}}\,|\psi\rangle = E\,|\psi\rangle$, we obtain

$$\left.\frac{dN}{dt}\right|_{t=0} = \frac{4}{\hbar}\text{Im}(E) \; . \tag{2.56}$$

In conclusion, a calculation of the initial loss rate is possible using a Schrödinger equation with the effective Hamiltonian instead of the master equation. The imaginary part of E is always negative and represents the initial loss rate.

3 Experimental Setup

The prerequisite for all experiments presented in this thesis is a Bose-Einstein condensate (BEC) of ^{87}Rb atoms. The apparatus used to produce the BEC is briefly described in Sec. 3.1. Section 3.2 is devoted to the creation of high magnetic fields required to observe Feshbach resonances. For a detailed description the reader is referred to Refs. [San01, Sch02, Mar03]. In Sec. 3.3.1 the optical lattice setup is summarized and the experimental sequence for the creation of an atomic Mott insulator as well as a Mott-like state of molecules is described. Section 3.4 explains blast schemes to remove atoms from a mixed cloud of atoms and molecules. More technical details can be found in Refs. [Han06, Vol07].

3.1 Bose-Einstein Condensation

The onset of Bose-Einstein condensation in a three-dimensional gas of indistinguishable, non-interacting bosons is determined by the condition [Pet02]

$$n\lambda_{\mathrm{dB}} \geq 2.612\,, \tag{3.1}$$

where n is the density and $\lambda_{\mathrm{dB}} = h/\sqrt{2\pi m k_B T}$ the thermal de-Broglie wavelength of the particles with temperature T. Starting from a dilute Rb vapor at room temperature, 19 orders of magnitude of phase-space density must be bridged to reach the BEC phase transition. This "phase-space odyssey" is illustrated in Fig. 3.1. First, a combination of laser-cooling and trapping techniques is employed. In a next step, the magnetically trapped atoms are evaporatively cooled to reach BEC. In the following, the individual components of the experimental setup are presented.

3.1.1 Double-MOT System

Figure 3.2 shows a sketch of the apparatus. Two vacuum chambers that are connected by a differential pumping stage make up the main part of the setup. The upper chamber houses a magneto-optical trap (MOT). The MOT is optimized for fast loading of large atom numbers. The atoms are loaded from a background gas of ^{87}Rb with a vapor pressure of $\sim 10^{-7}$ mbar. Typical loading rates are $\sim 5 \times 10^{10}\,\mathrm{s}^{-1}$. Short, near-resonant laser pulses transfer the atoms over a distance of ~ 35 cm to the lower MOT which is located inside a glass

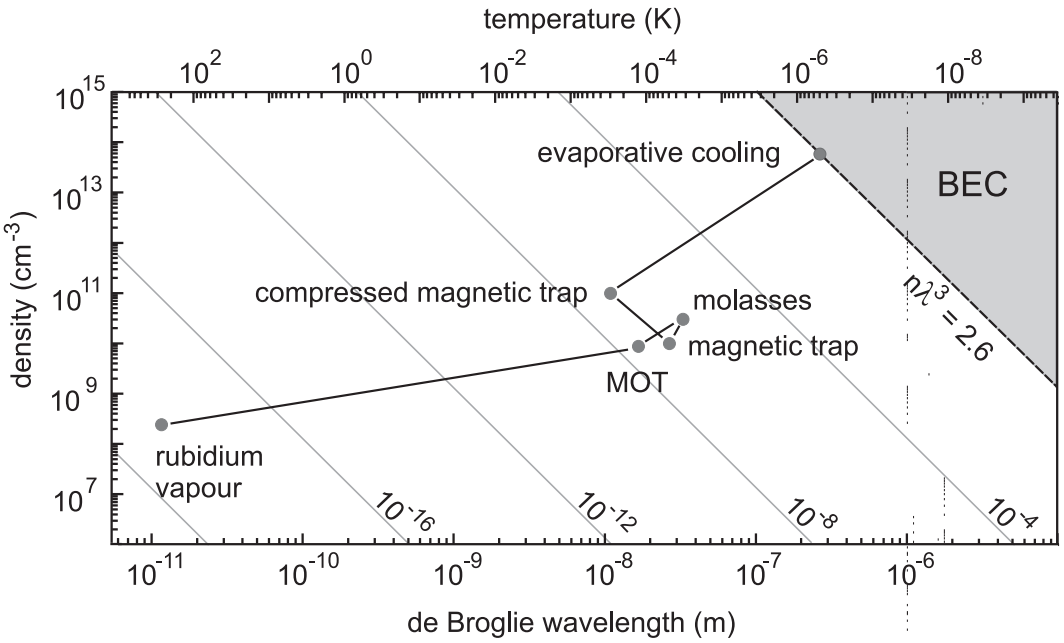

Figure 3.1: Phase space odyssey. To reach the BEC phase transition, the phase-space density has to be increased strongly. This is achieved by employing a combination of laser-cooling techniques and evaporative cooling.

cell. The single shot transfer efficiency is $\sim 15\%$. After 2 s of loading with 15 transfer shots, about $2 - 4 \times 10^9$ atoms are trapped in the lower MOT. After the last transfer shot, polarization gradient cooling is applied to reduce the temperature to $40 - 50\,\mu$K. The low background pressure of $\sim 10^{-11}$ mbar ensures long lifetimes of the atoms in the magnetic trap.

The atomic transitions are shown in Fig. 3.3. The MOT beams, which are aligned in a standard σ^+-σ^-configuration, are slightly red-detuned with respect to the cycling transition $5S_{1/2}f = 2 \leftrightarrow 5P_{3/2}f = 3$. A repumping laser drives the transition $5S_{1/2}f = 1 \leftrightarrow 5P_{3/2}f = 2$. The spontaneous decay rate of the excited states is $\Gamma_{\mathrm{sp}} = 2\pi \times 6.065\,\mathrm{MHz}$ [Vol96].

The light that addresses all transitions involving $5S_{1/2}f = 2$ is produced by a titanium-sapphire laser (Coherent MBR 110) with an output power of $\sim 1.3\,$W. The repumping light is provided by an external-cavity diode-laser (Toptica DL 100) with $\sim 120\,$mW output power. Both lasers are stabilized on atomic transitions using Doppler-free saturation spectroscopy. The respective root mean square (rms) linewidths are 40 kHz and 400 kHz (measured on a timescale of 50 ms for a bandwidth of 1 MHz).

3.1.2 Magnetic Trap

After polarization gradient cooling, the atomic cloud is spin-polarized by optical pumping prior to transferring it to the magnetic trap. Two beams with σ^+-

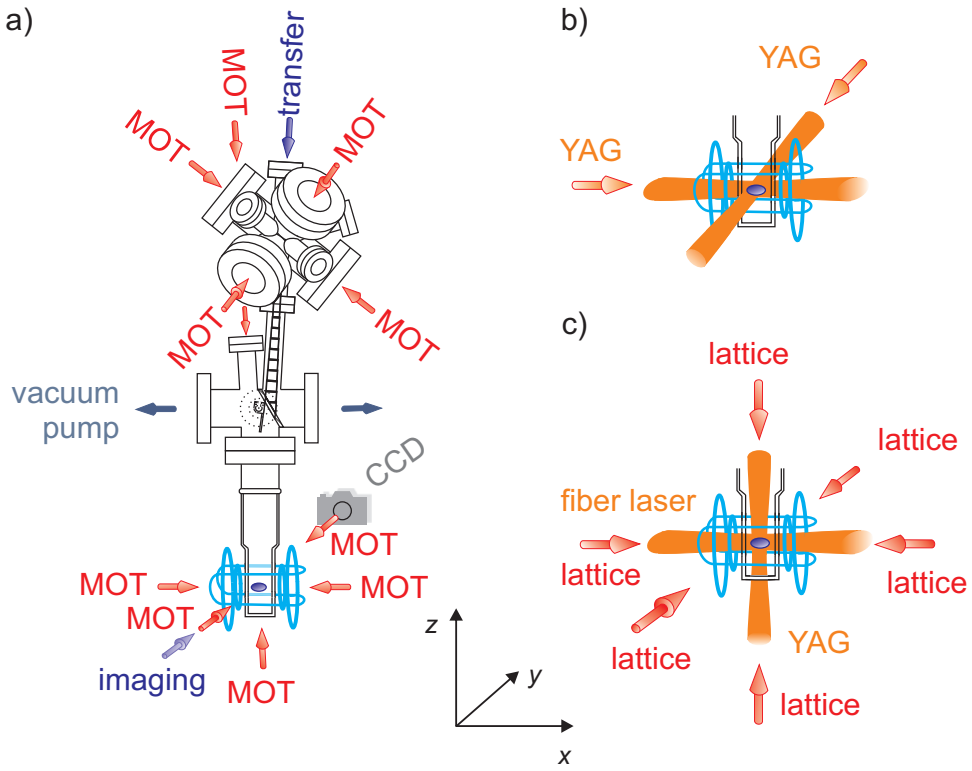

Figure 3.2: Experimental setup. (a) Vacuum system made up of an upper chamber housing a vapor-cell MOT and, connected by a differential pumping stage, a glass cell housing the lower MOT. The magnetic trap and the imaging system are also shown. (b) Crossed dipole trap in configuration A. One beam propagates along the x-axis and the other beam crosses orthogonally and subtends an angle of 25° with the y-axis. (c) Crossed dipole trap in configuration B and lattice beams. The horizontal beam of the dipole trap has a tight focus in the z-direction and a weak focus in the y direction. The ratio of the beam waists is 1 : 15.

and π-polarization resonantly drive the transition $5S_{1/2}f = 2 \leftrightarrow 5P_{3/2}f = 2$ and approximately 50% of the population is transferred into the low-field seeking state $|f, m_f\rangle = |1, -1\rangle$. This state is magnetically-trappable.

Figure 3.4 shows the coil configuration of the magnetic trap. The coils generate a Ioffe-Pritchard field configuration [Pri83]. The radial confinement is provided by a two-dimensional quadrupole field generated by four linear rods (the "bars") with alternating current directions. The magnetic bottle-field generated by two "pinch" coils confines the atoms axially. To prevent a reduction of the radial confinement by the strong fields of the "pinch" coils, a homogeneous field created by a pair of compensation coils in Helmholtz configuration is superimposed. The field in the trap center is thus reduced to a small offset value. The finite magnetic-field in the trap center is necessary

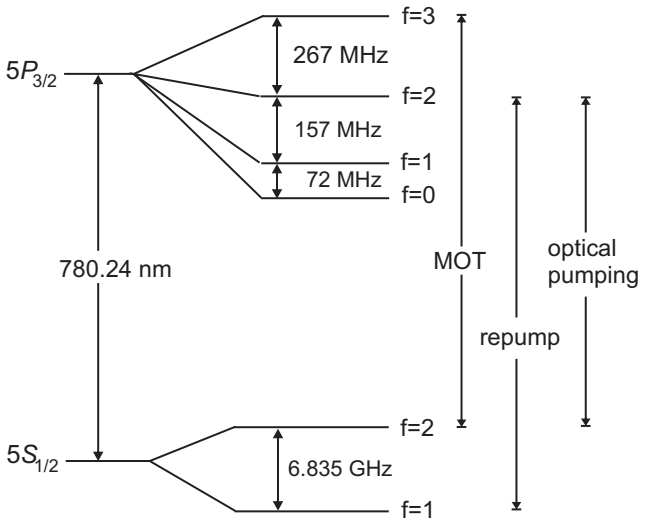

Figure 3.3: Level scheme of ^{87}Rb. Labeled hyperfine transitions are used in the experiment.

to prevent Majorana spin-flips to non-trappable Zeeman states [Mig85]. The offset-field stability of the magnetic trap is $< 1\,\mathrm{mG}$ (rms) over 1 hour.

Close to the trap center, the trapping potential is harmonic in all three directions. It is characterized by the axial and radial angular trap frequencies, ω_a and ω_r, which can be adjusted independently of each other. For efficient loading of the magnetic trap, the position of the cloud after polarization gradient cooling is matched to the position of the trap center. The trap frequencies

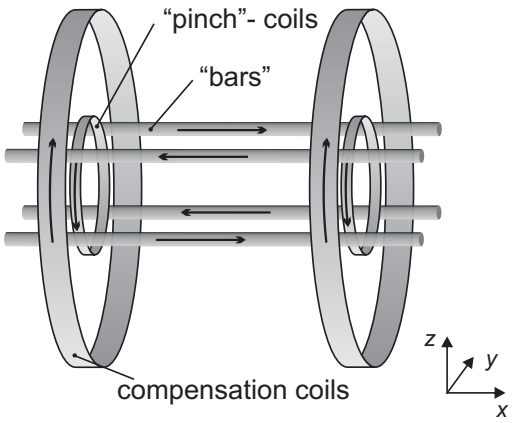

Figure 3.4: Ioffe-Pritchard magnetic trap. The "bars" generate a 2D quadrupole field for radial confinement. The "pinch" coils provide the axial harmonic confinement. The compensation coils in Helmholtz configuration reduce the field in the trap center to a small offset value. They are also used to generate the homogeneous magnetic field to address the Feshbach resonances (see Sec. 3.2)

.

are chosen to be $\omega_a = \omega_r = 2\pi \times 8.5\,\mathrm{Hz}$. Together with the fast switch-on times of $\sim 1\,\mathrm{ms}$ this ensures that the phase-space density is not altered during the loading process.

3.1.3 Evaporative Cooling

The phase space density is further increased by forced evaporative cooling until the critical value for BEC is reached. For this purpose, a radio-frequency (rf) field is applied to the magnetically trapped atomic cloud. If the frequency ν_{rf} matches the resonance condition $h\nu_{\mathrm{rf}} = m_f g_f \mu_B B(\mathbf{r})$, where g_f is the Landé factor of the atomic state, μ_B is the Bohr magneton and $B(\mathbf{r})$ denotes the magnitude of the magnetic field, transitions to non-trappable Zeeman states are induced locally.

Since atoms with high kinetic energy can reach regions of higher magnetic field than low-energy atoms, high-energy atoms are removed from the trap at higher ν_{rf}. By sweeping ν_{rf} from high to low values, the hottest atoms are continuously removed from the sample. In the experiment, ν_{rf} is swept from 50 MHz to 2 MHz in 5 s.

A high collision rate is essential to ensure fast thermalization and thus efficient evaporative cooling. To increase the collision rate, the cloud in the magnetic trap is compressed prior to the evaporation process. The trap frequencies of the compressed trap are $\omega_a = 2\pi \times 14\,\mathrm{Hz}$ and $\omega_r = 2\pi \times 108\,\mathrm{Hz}$. After evaporation, a BEC of typically 2×10^6 atoms is produced.

3.1.4 Optical Dipole Trap

The Feshbach resonances used in the experiments performed within the framework of this thesis occur for atoms in hyperfine states that are not magnetically trappable. Therefore, the atoms are transferred from the magnetic trap to an optical dipole trap which can trap atoms and molecules regardless of their internal state. Here, the basic principle of dipole traps is presented for atoms. For a detailed discussion see for example Ref. [Gri00].

An optical dipole trap is created by far-detuned laser light. The oscillating electric field $\mathbf{E}$ induces an oscillating electric dipole moment

$$\mathbf{d} = \alpha(\omega)\mathbf{E}\,, \tag{3.2}$$

where $\alpha(\omega)$ is the frequency-dependent complex polarizability of the atom. The potential energy of the dipole in the external field $\mathbf{E}$ is given by

$$V_{\mathrm{dip}} = -\frac{1}{2}\left\langle \mathbf{d}\cdot\mathbf{E}\right\rangle_t = -\frac{1}{2\epsilon_0 c}\mathrm{Re}(\alpha)\, I\,, \tag{3.3}$$

where $\langle \ldots \rangle_t$ denotes the time average, and the laser intensity is denoted by I. A non-zero imaginary part of the polarizability causes absorption from the

laser beam followed by re-emission. The corresponding photon scattering rate is given by

$$\Gamma_{\mathrm{sc}} = \frac{1}{\hbar\omega}\left\langle\left(\frac{d}{dt}\mathbf{d}\right)\cdot\mathbf{E}\right\rangle_t = \frac{1}{\hbar\epsilon_0 c}\mathrm{Im}(\alpha)\, I\ . \tag{3.4}$$

The polarizability is usually calculated in a semi-classical approach treating the atom as a quantum-mechanical two-level system. This leads to simple formulas for the dipole potential and the scattering rate [Gri00]

$$V_{\mathrm{dip}}(\mathbf{r}) = \frac{3\pi c^2\Gamma_{\mathrm{sp}}}{2\omega_0^3}\frac{I(\mathbf{r})}{\Delta}, \tag{3.5}$$

$$\Gamma_{\mathrm{sc}}(\mathbf{r}) = \frac{3\pi c^2\Gamma_{\mathrm{sp}}^2}{2\hbar\omega_0^3}\frac{I(\mathbf{r})}{\Delta^2}\ . \tag{3.6}$$

Here, $\Delta = \omega - \omega_0$ denotes the detuning of the angular frequency ω of the light field with respect to the atomic resonance ω_0. Γ_{sp} is the spontaneous decay rate of the excited state of the atom. The above expressions are valid for detunings which are large compared to the fine-structure splitting but small compared to the atomic resonance frequency ω_0 (rotating wave approximation).

The sign of Δ determines the sign of V_{dip} and therefore the direction of the dipole force. For a red detuned laser beam ($\Delta < 0$), the atoms will be attracted to regions of high intensity. This makes it possible to trap atoms in the focus of a Gaussian laser beam. In order to minimize heating caused by photon scattering, dipole traps are usually operated at large detunings and high intensities.

A rotationally symmetric Gaussian laser beam with waist w_0 and power P has an intensity profile

$$I(r,z) = \frac{2P}{\pi w^2(z)}e^{-2\frac{r^2}{w^2(z)}}\ , \tag{3.7}$$

where $w(z) = w_0\sqrt{1+(z/z_R)^2}$ is the $1/e^2$ radius of the intensity, $z_R = \pi w_0^2/\lambda$ the Rayleigh length and λ the wavelength. Such an intensity profile leads to a cylindrically symmetric dipole trap. Close to the center, the trapping potential is approximately harmonic

$$V_{\mathrm{dip}}(r,z) \approx -V_0\left(1 - 2\left(\frac{r}{w_0}\right)^2 - \left(\frac{z}{z_R}\right)^2\right)\ , \tag{3.8}$$

and is characterized by the radial and axial angular trapping frequencies

$$\omega_r = \sqrt{\frac{4V_0}{mw_0^2}} \quad \text{and} \quad \omega_z = \sqrt{\frac{2V_0}{mz_R^2}}\ , \tag{3.9}$$

where $V_0 = |V_{\mathrm{dip}}(\mathbf{r}=0)|$. Since z_R typically is a factor of $\frac{\pi w_0}{\lambda} \gg 1$ larger than w_0, the axial confinement is much weaker than the radial confinement.

In order to obtain similar confinement in all three directions, a crossed dipole trap created by two intersecting laser beams with mutually orthogonal linear polarization is employed.

We use two different dipole trap configurations. In configuration A, as shown in Fig. 3.2(b), one beam propagates along the axis of the magnetic trap (x-axis) and the second beam propagates in the yz-plane subtending an angle of 25° with the y-axis. The light for both beams is provided by a Nd:YAG laser (Innolight Mephisto 2000) which delivers up to 2 W of output power in single-frequency operation at a wavelength of 1064 nm. Typical numbers are 50 μm for the waist and $50 - 100$ mW for the laser power per beam.

In configuration B, an elliptical beam with a waist of 60 μm in the z-direction and a waist of 900 μm in the y-direction propagates along the axis of the magnetic field. The light for this beam is provided by a fiber laser (IPG Fiber Laser YLR-20-LP-SF) with up to 20 W of output power and a wavelength of 1064 nm. The specified linewidth is 100 kHz at -3 dB. The laser power at the position of the atoms is typically $2 - 3$ W. The second beam has a waist of 55 μm and is derived from the above-mentioned Nd:YAG laser. It propagates along the vertical direction from the bottom of the glass cell and has a typical power of up to 170 mW.

Trap frequencies are measured by parametric heating [Sav97]. Typical values are $(\omega_x, \omega_y, \omega_z) \simeq 2\pi \times (80, 110, 170)$ Hz for configuration A and $(\omega_x, \omega_y, \omega_z) \simeq 2\pi \times (30, 30, 80)$ Hz for configuration B. These values were measured in the presence of a strong magnetic field ~ 1000 G (see Sec. 3.2). The finite depth of the crossed dipole trap can be used for evaporation. It makes it possible to adjust the particle number between 3×10^4 and 5×10^5.

3.1.5 Imaging System

Absorption imaging at zero magnetic field is used for the detection of the atomic density distribution [Mar03]. A laser beam which is near-resonant with the $5S_{1/2}f = 2 \leftrightarrow 5P_{3/2}f = 3$ transition propagates along the imaging axis (y-axis). The atomic cloud absorbs part of the light and casts a shadow in the beam. The shadow is imaged onto a CCD-camera (Theta System SIS1-s285M).

From the recorded two-dimensional intensity distribution $I_T(x, z)$, the column density $\tilde{n}(x, z) = \int dy\, n(\mathbf{r})$ can be calculated according to Beer's law. For an incident beam with intensity $I_0(x, z)$ well below the saturation intensity of the atomic transition one obtains

$$\tilde{n}(x, z) = \frac{1}{\sigma_{\text{abs}}} \ln \frac{I_0(x, z)}{I_T(x, z)} , \tag{3.10}$$

where σ_{abs} is the absorption cross section of a photon by an atom.

Before imaging, the atomic cloud is released from the trap and is allowed to fall and expand freely for $2 - 20$ ms (time-of-flight method). For long-enough expansion times the spatial image recorded by the camera represents

the initial momentum distribution of the atoms if the atom-atom interactions are negligible.

To observe particles with different magnetic moments such as atoms in different Zeeman states simultaneously, we use a Stern-Gerlach separation method. To this end, a magnetic-field gradient is applied after release from the trap. Due to their different magnetic moments, the particles in different Zeeman states experience different forces and thus different accelerations which lead to spatial separation along the direction of the magnetic-field gradient. The magnetic-field gradient is created by the coils of the lower MOT. Typically, the gradient has a magnitude of $4 - 12\,\mathrm{G/cm}$ and is applied for $1 - 2\,\mathrm{ms}$.

Absorption imaging of molecules is difficult because the molecules typically have no cycling transition and only very few photons would be scattered from each molecule leading to very small signals. However, it was demonstrated in ^{6}Li that very weakly bound Feshbach molecules can be imaged by absorption imaging close to the Feshbach resonance [Chi06b]. In our experiment, we dissociate the molecules and image the resulting atoms.

3.2 Magnetic Field for Feshbach Resonances

Feshbach resonances in ^{87}Rb are very narrow and occur at high magnetic fields [Mar02]. To observe these resonances, an accurately stabilized magnetic field is required. The magnetic field stability must be better than the ratio of resonance width to resonance position. In ^{87}Rb, this ratio is 2×10^{-4} at best.

The magnetic field is created by the compensation coils of the magnetic trap. The coils are driven by four power supplies (Agilent 6690A) providing currents up to 1760 A. A home-built servo loop stabilizes the current so that the magnetic-field noise caused by current fluctuations is below 4 mG (rms). The magnitude of the magnetic field at the position of the atomic cloud is measured using microwave spectroscopy. From the transition frequency, the magnetic field can be inferred according to the Breit-Rabi formula [Ram56]. The direction of the magnetic field is opposite to the center field in the magnetic trap and the weak guiding field in the dipole trap. Atoms which were in the hyperfine state $|f, m_f\rangle = |1, -1\rangle$ in the dipole trap are transferred to the state $|1, 1\rangle$ with almost 100% efficiency by rapidly switching on the strong field (typically in $\sim 2\,\mathrm{ms}$). By deliberately creating an angle between the weak guiding field and the strong field, the ratio of atoms in states $|1, -1\rangle$, $|1, 0\rangle$ and $|1, 1\rangle$ can be adjusted in a limited range with very good reproducibility. The angle between the fields is created by superimposing weak offset fields along the y- and z-axis.

The strong homogeneous offset field is not perfectly aligned in Helmholtz configuration. At $\sim 1005\,\mathrm{G}$ we observe magnetic field gradients with a magnitude of $(2.1, 7.9, 2.2)\,\mathrm{G/cm}$ along the (x, y, z)-axis, respectively. These gradi-

ents lead to an additional force on the atoms that shifts the cloud away from the center of the dipole trap. This force also pulls atoms out of the dipole trap supporting evaporative cooling.

To control the dynamics of the atoms close to the Feshbach resonance and to associate and dissociate molecules, fast magnetic field ramps are desirable. To this end, we use two additional coils to create a magnetic field of a few Gauss that is added to the strong background field. Due to the small inductance of the coils, ramp speeds up to $\sim 1\,\mathrm{G}/\mu\mathrm{s}$ are possible. The servo loop for these coils has a step-response time of $\sim 1\,\mu\mathrm{s}$.

3.3 Optical Lattice

3.3.1 Setup and Calibration

Optical lattices are periodic potentials generated by far-detuned standing-wave light fields. A great variety of lattice configurations can be created by superimposing several standing-waves in different beam geometries at different wavelengths and power. For an overview see Ref. [Jes96]. The simplest three-dimensional (3D) configuration is a simple cubic lattice as shown in Fig. 3.5(a). It can be created by superimposing three standing-waves with Gaussian shape at right angles with mutually orthogonal polarization. The dipole force creates the following potential

$$V_{\mathrm{lat}}(\mathbf{r}) \;=\; -\sum_{j=x,y,z}\left(V_j\cos^2\left(k_{\mathrm{lat}}r_j\right)+\frac{m}{2}\omega_j^2 r_j^2\right)\;, \tag{3.11}$$

where $\lambda_{\mathrm{lat}} = 2\pi/k_{\mathrm{lat}}$ is the lattice wavelength. The lattice depth V_j is calculated from Eq. (3.5) and yields

$$\frac{V_j}{E_r} \;=\; -\frac{3mc^2}{\hbar^2 k_{\mathrm{lat}}^2\omega_0^3}\frac{8P_j}{w_{0j}^2}\frac{\Gamma_{\mathrm{sp}}}{\Delta}\;, \tag{3.12}$$

where P_j is the power and w_{0j} the waist of the beam j. The lattice depth is conveniently expressed in terms of the recoil energy from Eq. (2.6).

For a red-detuned lattice potential ($\Delta < 0$), the particles are trapped at the anti-nodes of the standing-waves. Close to its center, each lattice site forms an approximately harmonic potential in each direction with angular trapping frequency

$$\omega_{\mathrm{lat,j}} = \sqrt{\frac{2V_j k_{\mathrm{lat}}^2}{m}}\;. \tag{3.13}$$

The angular trapping frequency ω_j in Eq. (3.11) accounts for an external, slowly varying, harmonic potential created by an additional trap, e.g a dipole

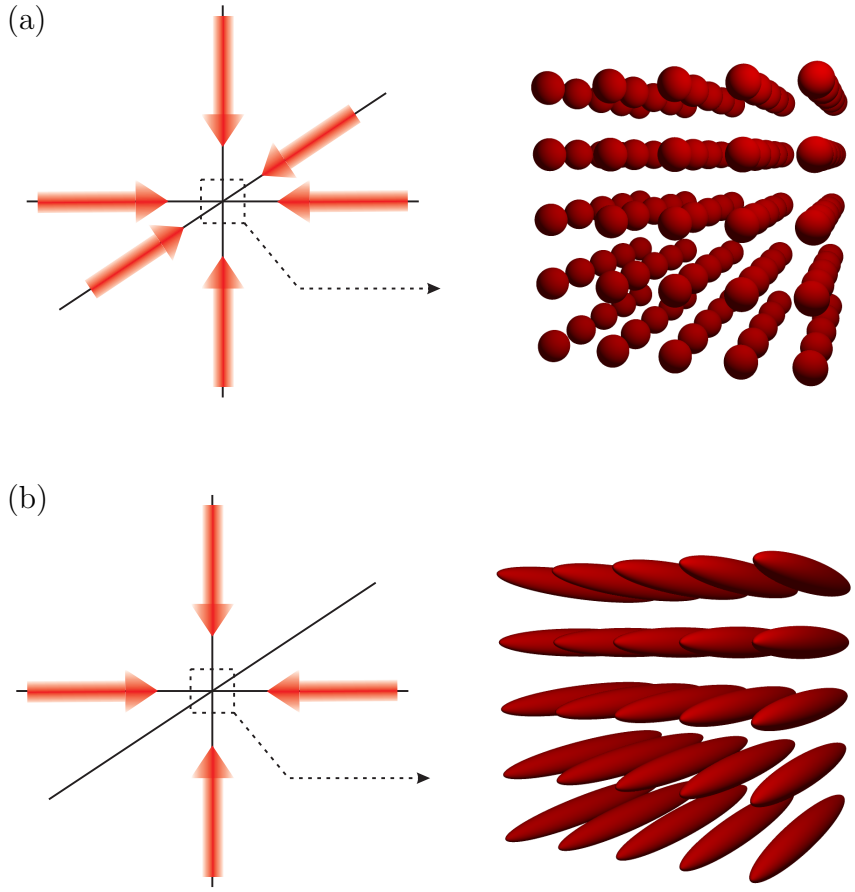

Figure 3.5: Schematic representation of lattice potentials. (a) A 3D simple-cubic lattice potential is formed at the intersection of three mutually orthogonal standing waves. (b) Two orthogonally intersecting standing waves create a 2D array of tube-shaped atom traps.

trap, and by the Gaussian lattice beams. The angular trap frequencies due to the Gaussian beam shape are given by

$$\omega_x^2 = \frac{4}{m}\left(\frac{V_y}{w_{0y}^2} + \frac{V_z}{w_{0z}^2}\right) , \quad \omega_y, \omega_z \text{ by cyclic permutation.} \tag{3.14}$$

By orthogonally superimposing two standing waves, a 2D array of tube-shaped traps is formed as depicted in Fig. 3.5(b). This geometry can be used to confine particles in 1D.

For a detailed description of the optical lattice setup see Refs. [Han06, Vol07]. In brief, the lattice light is provided by a titanium-sapphire laser (Coherent MBR110) with an output power of up to 1.9 W at a wavelength of 830.440 nm. The laser is frequency-stabilized to an internal reference cavity and has a linewidth of 100 kHz (rms) measured at a timescale of 10 ms with a band-

width of 50 kHz). The light is split into three beams. The power in each beam is controlled separately by an acoustic-optic modulator (AOM) and a shutter. The beams are mode-cleaned by optical fibers and intersect almost orthogonally with mutually orthogonal linear polarization at the position of the atomic cloud. By additionally detuning the frequencies of the beams from each other by a few tens of MHz, any remaining interference effects due to non-perfect orthogonal polarization average to zero on a time scale much faster than the atomic motion. The beam waists are $w_{0j} = 135\,\mu$m and the maximal power per beam at the position of the atoms is $P_j \sim 200\,$mW resulting in a lattice depth of up to $\sim 35E_r$ for atoms.

To calibrate the lattice depth, we use a method from Ref. [Hec02]. A BEC of atoms is released from the dipole trap and one lattice beam is pulsed on for a short time. This creates diffraction peaks in the time-of-flight images because the zero-momentum state $|p = 0\rangle$ is coupled to higher momentum states $|\pm 2\hbar k_{\mathrm{lat}}\rangle, |\pm 4\hbar k_{\mathrm{lat}}\rangle, \ldots$ by the lattice potential. The population in the diffraction peaks oscillates as a function of pulse time (Rabi oscillations). For low enough lattice depth, only momentum states $|\pm 2\hbar k_{\mathrm{lat}}\rangle$ are populated. By measuring the angular frequency Ω_{lat} of the Rabi-oscillations in the population of these momentum states, the depth of the lattice V_{lat} can be inferred from $\hbar\Omega_{\mathrm{lat}}/2 = \sqrt{4E_r^2 + V_{\mathrm{lat}}^2/8}$ [Han06]. With this method, V_{lat} is measured for each standing wave separately with an accuracy of $\sim 10\%$.

3.3.2 Creating a Mott-like state of molecules

The creation of a Mott-like state of molecules, where each lattice site contains exactly one molecule, is described in detail in Refs. [Vol06, Vol07, Dür06]. Here, the experimental sequence is briefly summarized. Typically $\sim 8 \times 10^4$ atoms in the state $|f = 1, m_f = 1\rangle$ are prepared in an atomic Mott insulator [Gre02, Gre03] with a core that contains exactly $n = 2$ atoms at each lattice site. The lattice depth is $V_{\mathrm{lat}}^a = 31.7E_r^a$, where V_{lat}^a is the lattice depth seen by an atom and E_r^a is the atomic recoil energy. Next, we linearly ramp the laser power of the dipole trap light to zero within 5 ms. This prevents molecule loss due to absorption of photons from the dipole trap light. Subsequently, we ramp the magnetic field linearly from 1008.8 G to 1005.5 G at a speed of 1.6 G/ms. This ramp crosses the Feshbach resonance at 1007.4 G and associates molecules. The lattice depth seen by the molecules is $V_{\mathrm{lat}}^m = 2V_{\mathrm{lat}}^a$ since their polarizability is twice the polarizability of a single atom. According to Eq. (2.6), the molecular recoil energy is $E_r^m = E_r^a/2$ because the molecules have twice the mass of a single atom. Thus the lattice depth seen by a molecule is $V_{\mathrm{lat}}^m = 127E_r^m$.[1] At lattice sites with a filling of $n = 1$, the magnetic field ramp has no effect,

[1] Note that the angular trap frequencies $\omega_x, \omega_y, \omega_z$ from Eq. (3.14) and ω_r from Eq. (3.9) describing the external harmonic confinement due to the finite waist of the lattice beams and the crossed dipole trap are identical for atoms and molecules.

at sites with $n > 1$ atom pairs are associated to molecules. If sites with $n > 2$ are occupied initially, the molecules will collide inelastically with other atoms or molecules leading to fast loss of the molecule and its collision partner. Typically, we lose about 10% of the overall atom number during the association ramp. This might be due to the fact, that we work close to the point where a core of $n = 3$ is formed. In addition, loss might also come from the superfluid regions between the Mott shells. For lattice sites with $n = 2$ the molecule association efficiency is above 90%. The maximum fraction of atoms that is converted into molecules is 47(3)% which is close to the theoretical limit of 53% (see Sec. 2.2.4). In a next step, we remove the remaining atoms by applying a blast scheme as described in Sec. 3.4. This does not influence the number of molecules.

3.4 Blast Scheme

After molecule association in the optical dipole trap or in the optical lattice, remaining atoms can be expelled from the trapping potential using the radiation pressure of light [Xu03, Tha06]. Since the trap is much deeper than the photon recoil energy, several recoil kicks are needed to remove the atoms. Therefore, a cycling transition is required.

We use the σ^+ transition $|f = 2, m_f = 2\rangle \leftrightarrow \left|m_i' = 3/2, m_f' = 3\right\rangle$[2], which is 1405 MHz blue detuned (at 1005.8 G) from the $B = 0$ MOT transition (see Fig. 3.3). The light for the cycling transition is provided by an external cavity diode laser (Toptica DL100) with up to 120 mW output power. The laser is frequency-stabilized by a beat lock to the titanium-sapphire laser at 780 nm.

When starting with atoms in state $|f, m_f\rangle = |1, 1\rangle$, a closed cycling transition does not exist and the atoms are transferred to $|2, 2\rangle$. For the transfer, we use two different approaches. The first is an all-optical scheme using pump light that is 62 MHz red detuned (at 1005.8 G) from the $B = 0$ repump transition. The light is obtained from the repump laser using an AOM and resonantly drives the π transition $|f = 1, m_f = 1\rangle \leftrightarrow \left|m_i' = 3/2, m_f' = 1\right\rangle$. From the excited state populated by this pump light, atoms can decay back to the initial state, into the desired state $|f = 2, m_f = 2\rangle$ or into the undesired state $|f = 2, m_f = 1\rangle$. The experiment shows, that the branching ratio for decay into the undesired state is only a few percent. We still use a third light field to deplete this state. We employ another AOM to obtain light that is 87 MHz red detuned (at 1005.8 G) from the $B = 0$ MOT transition. This light resonantly drives the σ^+ transition $|f = 2, m_f = 1\rangle \leftrightarrow \left|m_i' = 3/2, m_f' = 2\right\rangle$. Note that the excited state $\left|m_i' = 3/2, m_f' = 1\right\rangle$ cannot decay into ground states with $m_f = 0$,

[2] The blast light is applied while the atoms are at ~ 1005 G. The used hyperfine ground states are characterized by good quantum number f, m_f, while the excited states are characterized by good quantum numbers m_i', m_f'.

because at $\sim 1005\,\mathrm{G}$ the quantum number $m_i = 3/2$ is conserved during the decay and the $j = 1/2$ ground state does not have sub-states with $m_j = -3/2$.

All three blast fields are operated a factor of ten or more above saturation intensity. They are on simultaneously. The trap depth is typically a few μK, so that approximately five directed photon recoil momenta should add sufficient kinetic energy for an atom to leave the trap. This momentum should be accumulated after $0.2\,\mu$s. The estimated acceleration is $10^5\,\mathrm{m/s^2}$, so that the cloud radius of $10\,\mu$m is estimated to be traversed in $15\,\mu$s. The experiment shows that the blast light needs to be on for 300 μs, in order to remove all atoms from the trap. The origin of this discrepancy is not clear. Application of the three blast beams reduces the molecule number by approximately 30%.

In a second scheme, adapted from Ref. [Tha06], the two pump lasers are replaced by a microwave pulse that drives the $|f = 1, m_f = 1\rangle \leftrightarrow |f = 2, m_f = 2\rangle$ transition. The transition frequency is 9125.48 MHz at 1005.8 G. The microwave signal is provided by a synthesizer. After passing through an amplifier the signal has an output power of $\sim 30\,\mathrm{dBm}$. It is emitted by a microwave wave guide mounted $\sim 12\,\mathrm{cm}$ from the position of the cloud. Typically, a pulse duration of $\sim 500\,\mu$s transfers 50% of the population to $|f = 2, m_f = 2\rangle$. If the microwave and the cycling laser with an intensity of less than $0.1\,\mathrm{mW/cm^2}$ well below saturation intensity are on simultaneously for 2 ms, all atoms can be removed from the trap without reducing the molecule number. Rabi-oscillations on the $|f = 1, m_f = 1\rangle \leftrightarrow |f = 2, m_f = 2\rangle$ transition could not be observed. This is presumably due to magnetic field gradients.

4 Collisional Decay

Inelastic few-body collisions limit the lifetime of ultracold gases of atoms and diatomic molecules. In Sec. 4.1 we investigate inelastic two-body collisions of Feshbach molecules with other molecules or atoms leading to loss of the colliding particles from the cloud. We present measurements of the two-body molecule-molecule and atom-molecule loss coefficients [Sya06].

For atoms in their internal ground state, two-body collisions cannot be inelastic. In this case, the loss is dominated by inelastic three-atom collisions, also refered to as three-body recombination. Here, two of the three particles form a weakly-bound molecule and the binding energy is released as kinetic energy in the relative motion of the molecule and the third atom. Section 4.2 reports on measurements of the three-body loss-rate coefficient close to the 1007 G-Feshbach resonance [Smi07]. The data exhibit a dramatic magnetic-field dependence, which agrees with a theoretical model.

4.1 Inelastic Collisions of Feshbach Molecules

Diatomic molecules associated from ultracold atomic gases using Feshbach resonances are in highly-excited rovibrational states. An inelastic collision with another atom or molecule can lead to a vibrational de-excitation of the molecule. The difference in binding energy is released as kinetic energy in the relative motion of the molecule and the collision partner. This energy is typically much larger than the trap depth, so that both particles escape from the trap.

Here, we present a measurement of the loss-rate coefficients K_{am} and K_{mm}^{th} for inelastic atom-molecule and molecule-molecule collisions, respectively. The molecules are associated from atomic ^{87}Rb using the Feshbach resonance at 1007.4 G [Mar02] with a width of $\Delta B = 0.21$ G [Vol03, Dür04a]. The loss measurements are performed at 1005.8 G. In one measurement, atoms and molecules are in the trap simultaneously. In this case, the loss is dominated by inelastic atom-molecule collisions and reveals K_{am}. In another measurement, remaining atoms are removed from the trap using an all-optical blast scheme after associating the molecules (see Sec. 3.4). The loss in this measurement is dominated by inelastic molecule-molecule collisions and reveals K_{mm}^{th}. Both measurements are performed in thermal clouds.

The molecules are associated from atoms in their absolute ground state.

Spontaneous dissociation of Feshbach molecules into unbound atom pairs with lower-lying spin states as observed in ^{85}Rb is therefore impossible [Tho05a]. A previous measurement in ^{87}Rb using photo-associated molecules set an upper limit of $K_{am} < 8 \times 10^{-11}\,\mathrm{cm}^3/\mathrm{s}$ [Wyn00]. This limit is not applicable in the present experiment because a different rovibrational state is investigated and the experiment is performed at a very different magnetic field.

4.1.1 Experimental Sequence

The experiment starts with the preparation of an ultracold gas of ^{87}Rb atoms in the hyperfine state $|f = 1, m_f = -1\rangle$ in the magnetic trap. The radio-frequency induced evaporation is stopped near the critical temperature T_C of the phase transition to BEC. The atoms are then transferred into the crossed-beam optical dipole trap in configuration A as described in Sec. 3.1.4. The measured trap frequencies are $(\omega_x, \omega_y, \omega_z) = 2\pi \times (95, 154, 200)\,\mathrm{Hz}$.

After transfer into the dipole trap, a magnetic field of $B = 1007.6\,\mathrm{G}$ is turned on rapidly and the spin of the atoms is transferred to the hyperfine state $|f = 1, m_f = 1\rangle$. Then, B is ramped across the Feshbach resonance at a rate of $0.4\,\mathrm{G/ms}$. This associates atom pairs to molecules. As soon as molecules are forming during the ramp, they can undergo inelastic collisions. For molecules made from bosonic atoms, the inelastic collision rates are enhanced near the Feshbach resonance [Xu03]. Hence the molecule number can be maximized by jumping the magnetic field away from the resonance as fast as possible once the molecules are created [Mar05]. To this end, B is jumped from $1007.35\,\mathrm{G}$ to $1005.8\,\mathrm{G}$. We find experimentally that this combination of ramp speed and start point for the magnetic-field jump produces the maximum molecule number.

Immediately after jumping the field to $1005.8\,\mathrm{G}$, remaining atoms can be removed from the trap by applying the all-optical blast scheme for $0.3\,\mathrm{ms}$. This is followed by a variable hold time in the trap. This time is scanned in the loss measurements described below. After the hold time, the trap is switched off. Directly after release from the trap, the molecules are separated from remaining atoms using the Stern-Gerlach effect by applying a magnetic-field gradient of $120\,\mathrm{G/cm}$ for $1\,\mathrm{ms}$. Immediately after this, the magnetic field is jumped to $1006.9\,\mathrm{G}$ and subsequently the molecules are dissociated into unbound atom pairs by ramping the magnetic field back across the Feshbach resonance to $1007.7\,\mathrm{G}$ at a rate of $0.8\,\mathrm{G/ms}$. At the end of this ramp, the magnetic field is switched off rapidly. Finally, $7\,\mathrm{ms}$ after release from the trap, an absorption image is taken.

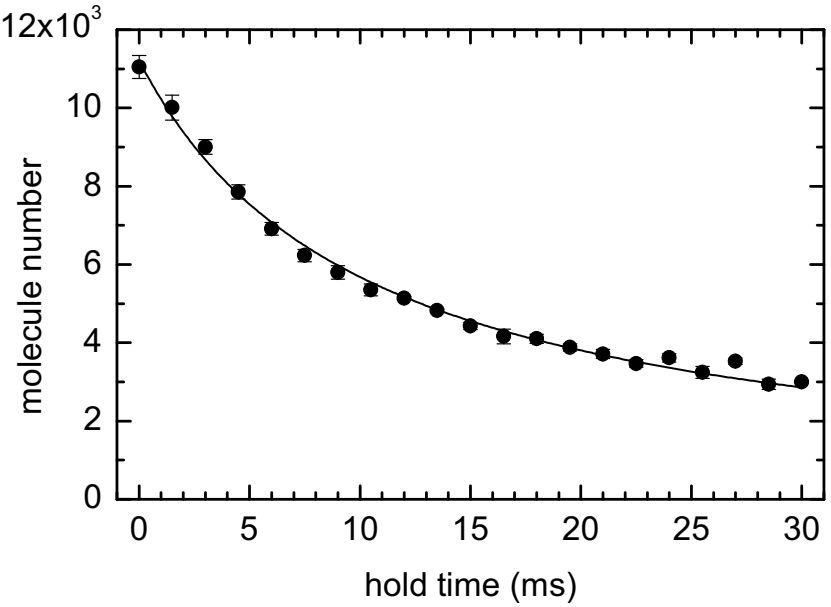

Figure 4.1: Loss of molecules from the trap. After blasting away the atoms, the molecules decay due to inelastic collisions. The line shows a fit of Eq. (4.4) to the data (•) yielding K_{mm}^{th}.

4.1.2 Molecule Loss from the Trap

The molecule number decays as a function of hold time between the association of the molecules and their release from the trap. The loss of molecules from the trap can be described by the rate equation

$$\frac{d}{dt}n_m = -K_m n_m - K_{am} n_a n_m - K_{mm}^{th} n_m^2 \,, \tag{4.1}$$

where n_a and n_m are the particle densities of atoms and molecules and K_{am} and K_{mm}^{th} are the loss-rate coefficients caused by inelastic atom-molecule and molecule-molecule collisions, respectively. K_{mm}^{th} is defined as $K_{mm}^{th} = g^{(2)}(0) \times K_{mm}$ with $g^{(2)}(0) = 2$ because the measurements are performed for an uncondensed gas of bosons. K_{am} does not depend on whether any of the clouds are Bose condensed. K_m represents molecule loss mechanisms which do not rely on collisions with other cold atoms or molecules. Such loss could be caused by background gas collisions, photo-dissociation by the dipole-trap light, or spontaneous decay into lower rovibrational levels. The experimental results show that K_m is negligible. The loss of atoms during the hold time is also found to be negligible. This is because the atom number is either zero or much higher than the molecule number, so that inelastic atom-molecule collisions can only lead to loss of a small fraction of the atoms.

Volume integration of Eq. (4.1) yields

$$\frac{d}{dt}N_m = -K_m N_m - \frac{K_{am}}{V_{am}} N_a N_m - \frac{K^{th}_{mm}}{V_{mm}} N_m^2 \,, \tag{4.2}$$

where N_a and N_m are the total number of atoms and molecules, respectively. The effective volume is defined as

$$\frac{1}{V_{im}} = \frac{1}{N_i N_m} \int n_i n_m \, d^3x \tag{4.3}$$

for i equal to a or m for atoms or molecules, respectively. V_{im} depends on the shape of the cloud, but not on the particle number. Note that $\langle n_m \rangle = N_m/V_{mm}$ is often referred to as the average density. Assuming that N_a, V_{am}, and V_{mm} are time independent, Eq. (4.2) can be integrated analytically yielding

$$N_m(t) = \frac{N_0 \Gamma}{-N_0\beta + (N_0\beta + \Gamma)e^{\Gamma t}} \,, \tag{4.4}$$

where $\beta = K^{th}_{mm}/V_{mm}$ and $\Gamma = K_m + K_{am}N_a/V_{am}$ and N_0 is the molecule number at $t = 0$.

Figure 4.1 shows experimental results of the molecule loss obtained after blasting away the atoms. In this measurement, $\Gamma = K_m$ because $N_a = 0$. An unconstrained fit of Eq. (4.4) to the data yields a slightly negative value for Γ which is unphysical. We therefore fix $\Gamma = 0$ and obtain $\beta = 8(1) \times 10^{-3}$ /s from the fit. The error bar is statistical.

Figure 4.2 shows experimental results without blasting away the atoms. Obviously, the presence of the atoms reduces the molecule lifetime substantially. An unconstrained fit of Eq. (4.4) to the data yields a slightly negative value for β which is unphysical. We therefore fix β to the value from Fig. 4.1 and obtain $\Gamma = 0.9(1)$ /ms from the fit. Again, the error bar is statistical.

In order to extract the loss-rate coefficients K^{th}_{mm} and K_{am}, the effective volumes V_{mm} and V_{am} have to be determined. This requires knowledge of the density distributions of the atomic and molecular cloud, which is a delicate issue because the small cloud size makes direct measurements of the spatial distributions in the trap very difficult. Theoretical modeling is also difficult. Even the distributions at the beginning of the loss measurements are hard to model because the time evolution during molecule association is nontrivial. This is because, first, atomic pair correlations are crucial for a realistic treatment of the association process [Gór04]. Second, the loss rate coefficients K^{th}_{mm} and K_{am} become relevant as soon as molecules start to form during the ramp. Third, these coefficients exhibit an unknown magnetic-field dependence near the Feshbach resonance.

During the loss measurement, anharmonicities in the trap potential and elastic collisions between particles tend to randomize the motion leading towards a thermal distribution. Inelastic collisions, however, remove particles

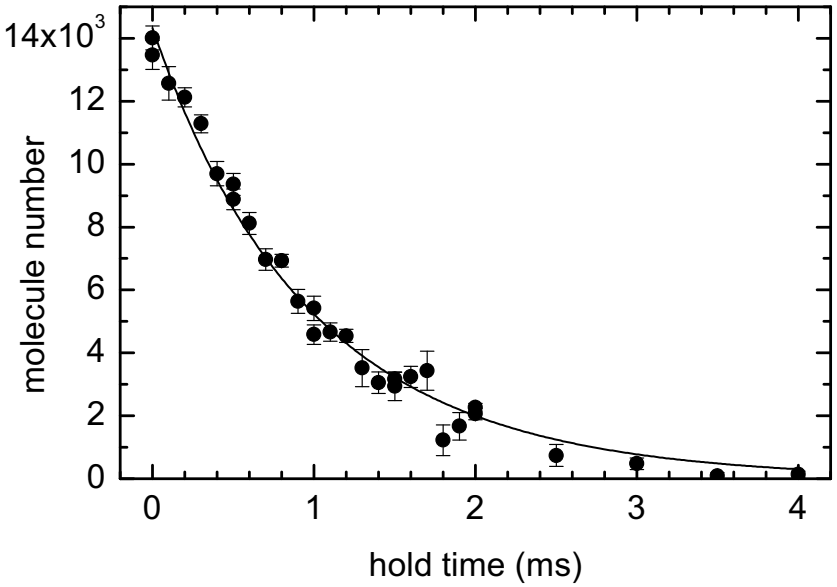

Figure 4.2: Loss of molecules in the presence of atoms. After blasting away the atoms the molecules decay due to inelastic collisions. The line shows a fit of Eq. (4.4) to the data (•), yielding K_{am}. Clearly, the loss is much faster than in Fig. 4.1.

preferentially at the trap center where the density is highest. The elastic scattering cross section for the molecules are unknown. Hence it is not clear which process dominates at what stage of the loss measurement. The evolution of the density distributions during the loss measurement is therefore a complex process with unknown parameters and unknown initial conditions.

4.1.3 Effective Volume and Temperature

In order to obtain an estimate for the effective volumes V_{am} and V_{mm}, we assume that particles of the same species (atoms or molecules) are in thermal equilibrium. Our model does allow for a temperature difference between atoms and molecules. With this approximation, the spatial density distributions n_a and n_m are Gaussian and Eq. (4.3) yields the effective volume for species i

$$V_{im} = (2\pi)^{3/2} \prod_{k=1}^{3} \sqrt{\sigma_{i,k}^2 + \sigma_{m,k}^2}\,, \tag{4.5}$$

where the index k refers to the three directions in space. The one-dimensional (1D) root-mean-square (rms) radii of the Gaussians are $\sigma_{i,k} = \sqrt{k_B T_i/(m_i \omega_{i,k}^2)}$. The mass and temperature of species i are labeled m_i and T_i, respectively. The polarizability and the mass of a molecule are twice as large as for one atom, so that the trap frequencies for atoms and molecules are identical, i.e. $\omega_{a,k} = \omega_{m,k}$.

The temperature of the atoms and molecules is determined from time-of-flight measurements. For the atoms, the cloud size evolves as

$$\sigma_{a,k}(t) = \sqrt{\sigma_{a,k}^2(0) + \sigma_{v,a}^2 t^2}\ , \tag{4.6}$$

where the trap is switched off at $t = 0$ and $\sigma_{v,i} = \sqrt{k_B T_i/m_i}$ is the 1D rms-velocity of species i, which is independent of the spatial direction if the species is in thermal equilibrium. For the molecules extra kinetic energy is added in the dissociation process [Muk04, Dür04b] so that

$$\sigma_{m,k}(t) = \sqrt{\sigma_{m,k}^2(0) + \sigma_{v,m}^2 t^2 + \sigma_{v,\mathrm{dis}}^2 t_{\mathrm{rem}}^2}\ . \tag{4.7}$$

Again, $t = 0$ is chosen at the time of release from the trap. $\sigma_{v,\mathrm{dis}}$ reflects the extra kinetic energy released in the dissociation. t_{rem} is the remaining time of flight between dissociation and detection. In order to determine $T_m \propto \sigma_{v,m}^2$, we scan the time t between release and detection in such a way that t_{rem} remains fixed. A fit of Eq. (4.7) is then equivalent to a fit of Eq. (4.6) with a modified value for $\sigma(0)$. Thus the extracted temperature is insensitive to the dissociation heating.

The atomic cloud before molecule association typically contains 3.6×10^5 atoms at a temperature of $0.5\,\mu$K very close to T_C. The cloud is almost purely thermal with only 6×10^3 BEC atoms. The molecule association is accompanied by noticeable heating and substantial loss. The remaining atomic cloud contains $N_a = 1.9 \times 10^5$ atoms at a temperature of $T_a = 1.0\ \mu$K. There is no BEC in the remaining atomic cloud. The molecular cloud has a temperature of $T_m = 1.5\,\mu$K resulting in a peak phase-space density of $\sim 10^{-3}$ for the molecules. The center-of-mass motion of an atom pair is unchanged in the association, and in a dilute thermal cloud the atomic pair correlations are uncorrelated from the center-of-mass motion of the pairs. Our experiment should produce molecules with the same temperature as the initial atoms. This agrees reasonably with our measurements. The measured values of N_a, T_a, and T_m vary by less than 10% during the loss measurement. This justifies the assumption that they are time-independent. This assumption was used to derive Eq. (4.2).

4.1.4 Results

The above values for T_m and T_a yield effective volumes of $V_{mm} = 3.8 \times 10^{-8}\,\mathrm{cm}^3$ and $V_{am} = 4.6 \times 10^{-8}\,\mathrm{cm}^3$. The resulting loss-rate coefficients are $K_{mm}^{th} = 3 \times 10^{-10}\,\mathrm{cm}^3/\mathrm{s}$ and $K_{am} = 2 \times 10^{-10}\,\mathrm{cm}^3/\mathrm{s}$. The value of K_{mm}^{th} for a quantum degenerate cloud would be $K_{\mathrm{mm}} = 1.5 \times 10^{-10}\,\mathrm{cm}^3/\mathrm{s}$ (see Sec. 2.3.5). Statistical errors on the rate coefficients are negligible compared to systematic errors.

The dominant systematic error arises from the problematic assumption that the clouds are in thermal equilibrium. For reasons discussed above, it is hard to

measure or model the temporal evolution of the density distributions. On one hand, the association process preferentially populates the trap center, because the association is less efficient at low atomic density. On the other hand, inelastic collisions preferentially deplete the trap center. Both effects can lead to a misestimation of V_{am} but the trends go into opposite directions. It is not clear which effect dominates. The resulting systematic error is hard to quantify. We speculate that a factor of 3 seems possible for K_{am} as well as for K_{mm}^{th}.

A recent theoretical model predicts $K_{am} = 3 \times 10^{-10}\,\mathrm{cm}^3/\mathrm{s}$ at 1005.8 G [Smi07]. This value is a factor of 1.5 larger than the measured value but agrees within the systematic uncertainty. Previous models [Bra04, Pet04a] are only applicable if the magnetic field is less than ΔB away from the Feshbach resonance, which is not the case in the present experiment.

Measurements of loss-rate coefficients for other bosonic systems, ^{23}Na and ^{133}Cs, reveal values of typically $5 \times 10^{-11}\,\mathrm{cm}^3/\mathrm{s}$ [Muk04, Chi05].

4.2 Three-Body Recombination

Three-body recombination is the transition from three initially unbound atoms to a weakly-bound dimer molecule and a remnant atom. The binding energy is released as kinetic energy in the relative motion of the collision partners. As a result, all three atoms are expelled from the trap. When inelastic two-body collisions are absent, the trap lifetime is determined by three-body recombination. This is the case for atoms in the absolute ground state.

In 1970, V. Efimov predicted that for three identical bosons with a resonant two-body interaction, an infinite series of trimer bound states exists [Efi70, Efi71]. These states, now known as Efimov states, even exist in the absence of a corresponding two-body bound state. A theoretical description of the three-atom problem is difficult. It is simplified to some degree if one restricts the considerations to the range where the elastic two-body scattering length a is much larger than all other length scales in the system. In this regime, one often assumes that all two-body potentials that produce the same a have the same universal three-body behavior. For a recent review on universality in few-body systems see Ref. [Bra06]. Assuming universality, all properties of the three-body collision can be expressed in terms of a. For dimensional reasons, the three-body loss rate coefficient K_3 can be expressed as $K_3 = C\hbar a^4/2m$, where C is a dimensionless constant factor [Fed96b]. Here, K_3 is the loss coefficient for a BEC. The proportionality to a^4 was demonstrated experimentally in ^{133}Cs [Web03].

More recent models including non-universal properties of the system predict that C is a periodic function with $C(a) = C(22.7a)$ that oscillates between 0 and 68 [Bra01, Bra06]. The maxima and minima in $C(a)$ correspond to

Efimov's prediction that an infinite sequence of trimer bound states exists near a pole of a [Esr99]. Therefore, it is particularly interesting to study the magnetic-field dependence of K_3 close to a Feshbach resonance. Note that minima in K_3 are routinely used for the creation of BECs in ^{85}Rb and ^{133}Cs [Cor00, Kra04].

First experimental evidence of Efimov states was found recently based on a measurement of three-body recombination in ^{133}Cs [Kra06]. In principle, Efimov states should exist in three-body systems in many fields of physics. But so far experimental efforts in beam experiments with clusters of ^{4}He [Brü05] or in neutron halo systems in nuclear physics [Jen04] have remained unsuccessful.

4.2.1 Experimental Sequence

We prepare a BEC with 5×10^5 atoms in the state $|f = 1, m_f = 1\rangle$ in the crossed-beam optical dipole trap in configuration A (see Sec. 3.1.4) at a magnetic field of $\sim 1005\,\mathrm{G}$. The trap frequencies are measured to be $(\omega_x, \omega_y, \omega_z) = 2\pi \times (76, 106, 155)\,\mathrm{Hz}$. Next, the magnetic field is ramped to its final value B and held there. The atom number decays as a function of time. For $B < 1007.2\,\mathrm{G}$, the decay is so slow that the size of the cloud changes adiabatically during the decay. For $B > 1007.2\,\mathrm{G}$ the decay is too fast for the BEC to adiabatically adapt its size. In this regime, we jump the magnetic field from the initial to the final value and measure the loss only on a short time scale during which the cloud keeps its initial size. Finally, after a variable hold time, the trap and the magnetic fields are switched off abruptly and after 19 ms of free fall an absorption image is taken.

4.2.2 Modeling the Decay

For our experimental parameters, $n|a|^3 \leq 0.02$, and therefore the gas is weakly interacting and can be described in terms of the Gross-Pitaevskii (GP) equation [Pit03]. Furthermore, we neglect the kinetic energy term in the GP equation and describe the system in the Thomas-Fermi (TF) approximation. The equilibrium density profile in a harmonic trapping potential with angular trapping frequencies $(\omega_x, \omega_y, \omega_z)$ in the Thomas-Fermi approximation is given by an inverted parabola (see e.g. [Pit03])

$$n(\mathbf{r}) \;=\; \max\left\{ n_{\mathrm{peak}} \left(1 - \sum_{j=x,y,z} \left(\frac{r_j}{r_{\mathrm{TF,j}}} \right)^2 \right), 0 \right\} , \tag{4.8}$$

where the Thomas-Fermi radii $r_{\mathrm{TF,j}}$, the peak density n_{peak} and the effective volume V_{eff} are given by

$$r_{\mathrm{TF,j}} = \frac{\bar{\omega}}{\omega_j}\left(15\bar{a}_{\mathrm{ho}}^4 aN\right)^{1/5} \tag{4.9}$$

$$n_{\mathrm{peak}} = \frac{N^{2/5}}{V_{\mathrm{eff}}} \tag{4.10}$$

$$V_{\mathrm{eff}} = \frac{8\pi}{15^{2/5}}(\bar{a}_{\mathrm{ho}}^4 a)^{3/5}\,. \tag{4.11}$$

The geometric mean of the trapping frequencies $\bar{\omega} = (\omega_x\omega_y\omega_z)^{1/3}$ determines the mean harmonic oscillator length $\bar{a}_{\mathrm{ho}} = \sqrt{\hbar/(m\bar{\omega})}$. The scattering length is denoted by a. As the atoms are prepared in their absolute ground state, a is real. The dependence of a on magnetic field is well described by Eq. (2.3) with $\Gamma = 0$.

Pure three-body loss in a weakly interacting BEC is described by Eq. (2.18) with $g^{(3)}(0) = 1$. Volume integration yields an equation for the total atom number N

$$\frac{dN}{dt} = -K_3\left\langle n^2\right\rangle N\,, \tag{4.12}$$

where $\langle n^2\rangle$ is the mean squared density. It can be shown that for a Thomas-Fermi density profile

$$\left\langle n^2\right\rangle = \frac{1}{N}\int d^3r\, n^3 = \frac{8}{21}n_{\mathrm{peak}}^2\,. \tag{4.13}$$

If the loss is much slower than the smallest trap frequency, the size of the BEC can adiabatically follow the change in atom number. The cloud remains a Thomas-Fermi parabola during the decay and the Thomas-Fermi radius decreases steadily following the loss in the atom number. In this case, the decay is governed by [Söd99]

$$\frac{dN}{dt} = -\frac{8}{21}\frac{K_3}{V_{\mathrm{eff}}^2}N^{9/5}\,. \tag{4.14}$$

The solution to this rate equation is

$$N(t) = \frac{N_0}{(1 + N_0^{(p-1)}(p-1)Lt)^{\frac{1}{p-1}}}\,, \tag{4.15}$$

with $L = 8K_3/(21V_{\mathrm{eff}}^2)$, $p = 9/5$ and the initial atom number N_0. We use Eq. (4.15) to extract K_3 for $B < 1007.2\,\mathrm{G}$.

For fast loss, the cloud cannot adapt its shape to the decay and the above adiabatic approximation is not valid. This is the case for $B > 1007.2\,\mathrm{G}$. For short hold times the cloud is well described by a Thomas-Fermi parabola corresponding to the scattering length *before* the jump to the final magnetic

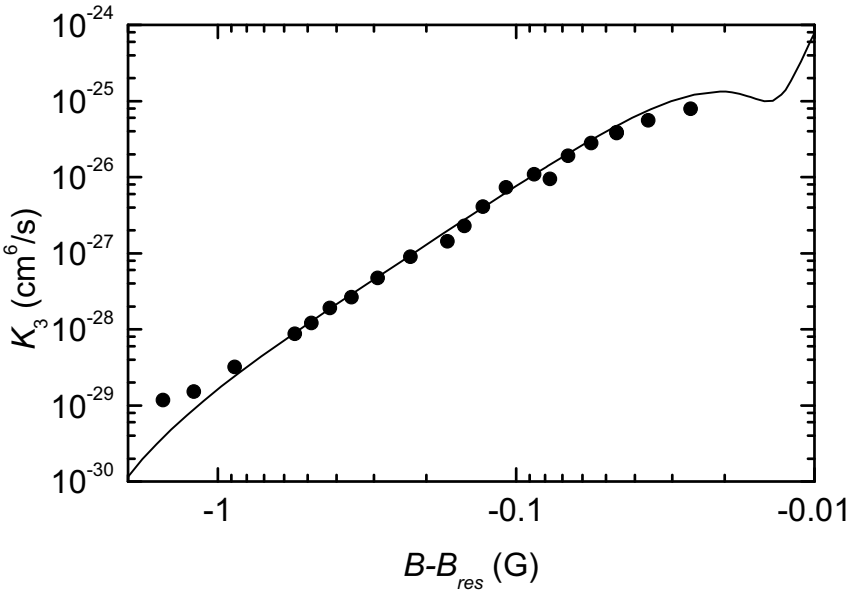

Figure 4.3: Three-body recombination rate. K_3 is determined from time resolved loss measurements at various magnetic fields B near the Feshbach resonance at $B_{\rm res} = 1007.4\,\mathrm{G}$. Measured values of K_3 (•) change over four orders of magnitude and are well described by a theoretical model (line) [Smi07] without any free fit parameters. The model predicts an Efimov minimum 15 mG below the resonance.

field B. Hence instead of $V_{\rm eff}(B)$ we use $V_{\rm eff}^{\rm bg}$, the value obtained for $a = a_{\rm bg}$. The fast jump excites breathing modes in the trap and the time scale for which this approximation is limited by the largest trap frequency and by the speed of the loss. From Eq. (4.14) we obtain

$$\left.\frac{dN}{dt}\right|_{t=0} = -\frac{8}{21}\frac{K_3}{{V_{\rm eff}^{\rm bg}}^2}N_0^{9/5} \tag{4.16}$$

for the initial decay.

4.2.3 Results

Figure 4.3 shows K_3 as a function of magnetic field close to the Feshbach resonance as extracted from fits of Eq. (4.15) and Eq. (4.16) to the decay curves. A variation of K_3 over four orders of magnitude is observed. The data are well described by a theoretical model [Smi07] without any free fit parameters. The model is based on an exact solution of the three-body Schrödinger equation and takes into account the two highest-lying two-body bound states. The predicted local minimum in K_3, 15 mG below the resonance, is an Efimov minimum and can be associated with a trimer bound-state. Unfortunately, its experimental observation is very difficult because of magnetic-field noise.

As a first test for systematic errors, we performed another measurement at $\sim 2\,\mathrm{G}$ with atoms in the state $|f=1, m_f=-1\rangle$ with $n_{\mathrm{peak}}^{\mathrm{BEC}} = 6\times10^{14}\,\mathrm{cm}^{-3}$ and $\bar{\omega} = 2\pi \times 115\,\mathrm{Hz}$. Here, we obtain $K_3^{bg} = 8.5 \times 10^{-30}\,\mathrm{cm}^6/\mathrm{s}$, which is a factor of ~ 1.4 larger than the value $K_3 = 5.8(1.9) \times 10^{-30}\,\mathrm{cm}^6/\mathrm{s}$ from Ref. [Bur97] and agrees with the value obtained in Ref. [Mar03].

Systematic errors in K_3 arise from the uncertainty in the calibration of the trap frequencies and the atom number. These errors lead to an estimated uncertainty of a factor of ~ 3 in K_3. Compared to that, statistical errors are negligible. For data points close to the resonance, the 30 mG accuracy of the magnetic field calibration becomes an issue. Several additional loss processes can cause systematic errors: three-body loss involving thermal atoms, evaporative loss, and avalanche losses. In the following, we discuss these processes in detail.

The cloud has a thermal fraction of atoms with a temperature of $T = 160\,\mathrm{nK}$ and a peak density of $n_{\mathrm{peak}}^{th} \approx 1.0 \times 10^{13}\,\mathrm{cm}^{-3}$. Since the thermal density is much smaller than the initial density $n_{\mathrm{peak}}^{\mathrm{BEC}} = 5.1 \times 10^{14}\,\mathrm{cm}^{-3}$ in the BEC, inelastic three-body collisions involving thermal atoms are negligible.

Evaporative loss can occur because the dipole trap has a depth of only $\sim k_B \times 2\,\mu\mathrm{K}$. The rate of evaporative loss is very sensitive to the trap depth. This quantity is not known accurately because we operate in a regime, where gravitational sag is important. It is therefore difficult to estimate the evaporative loss rate. The experimental observation that K_3^{bg} is close to the value of Ref. [Bur97] suggests that evaporative loss has only little effect on the decay far away from the Feshbach resonance. An increase of the elastic scattering length a can speed up evaporation proportional to a^2 [Lui96, Ket96] and part of the observed loss closer to the Feshbach resonance might in principle be due to evaporation. In practice however, K_3 increases faster than a^2 so that the evaporative loss is expected to contribute only little to the decay.

Collisional avalanches [Sch01] might also contribute to the observed loss. Avalanches can start, if a primary collision producing fast particles is followed by a secondary elastic or inelastic collision with another atom before the fast particles leave the cloud. This secondary collision produces a fast atom, which itself can collide with other particles, etc. Quantitative modeling of the avalanche loss is difficult. The model in Ref. [Sch01] defines the opacity as a measure that can be used to estimate, whether avalanches occur. For a BEC with a Thomas-Fermi density profile, the opacity is $O_s = \frac{5}{12}\,\sigma_{\mathrm{el}}\,\bar{r}_{\mathrm{TF}}\,n_{\mathrm{peak}}^{\mathrm{BEC}}$ [Sch02], where $\bar{r}_{\mathrm{TF}}$ is the geometric mean of the Thomas-Fermi radii $r_{\mathrm{TF,j}}$ and $\sigma_{\mathrm{el}} = 8\pi a^2$ assuming s-wave collisions. An avalanche can start if O_s is of order one or larger. Our experimental parameters far away from the Feshbach resonance yield $O_s \sim 0.8$. The additional measurement of K_3^{bg} was performed at $O_s \sim 1.1$ and the reasonable agreement with the value of Ref. [Bur97] indicates that avalanches have little effect here. For our measurements closer to the Feshbach resonance, O_s increases approximately as a^2. For example,

$O_s \sim 3$ at 1007.2 G so that avalanches should have a noticeable effect. However, Eq. (4.15) fits well to the temporal evolution of the data at this magnetic field, suggesting that avalanches are negligible. At 1007.37 G, $O_s \sim 50$ indicates that avalanche loss should be dominant. Nonetheless, the theoretical prediction shown in Fig. 4.3 agrees well with the data close to resonance, suggesting that losses caused by avalanches contribute only little.

5 Coherent Atom-Molecule Oscillations

Most of the work on molecule association performed so far was based on adiabatically ramping a magnetic field across a Feshbach resonance. Here, we explore a different technique based on coherent atom-molecule oscillations at a Feshbach resonance [Sya07]. Unlike adiabatic ramps, time-resolved coherent oscillations allow for full control over the final superposition state produced. Furthermore, precision measurements might profit from this technique [Chi06a].

Section 5.1 introduces the atom-molecule coupling. A description of the experimental sequence follows in Sec. 5.2. The observation of coherent atom-molecule oscillations is presented in Sec. 5.3. Furthermore, in Sec. 5.4 we show that confinement-induced molecules exist not only below the lowest band of the lattice [Mor05], but also in band gaps. Section 5.5 presents a measurement of the magnetic-field dependence of the scattering length based on excitation spectroscopy of a Mott insulator.

5.1 Atom-Molecule Coupling

The pioneering experiment on molecule association recorded Ramsey oscillations between the atomic and the molecular state, but this experiment observed coherent oscillations only "over a very limited range" of the magnetic field [Don02]. In a subsequent experiment, atom-molecule oscillations with 6% amplitude were induced using a radio-frequency field [Tho05b]. Atom-molecule oscillations were also reported in a photoassociation experiment [Ryu05]. In addition, oscillations between two bound molecular states were observed recently [Mar07]. We observe time-resolved coherent oscillations between the atomic and the molecular state with large amplitude. The oscillations are weakly damped and the data show oscillations up to the 29^{th} cycle.

The observation of coherent atom-molecule oscillations requires a pulse shape that is rectangular or at least strongly diabatic. In free space, such pulses populate the continuum of above-threshold entrance-channel states [Don02] thus leading to oscillations between many levels, typically with small molecular amplitude. We avoid this by working in a deep three-dimensional optical lattice where the entrance-channel states are discrete. For weak enough coupling, the

coupling of the molecular state to only one entrance-channel state is noticeable. In addition, the lattice isolates the molecules from each other, thus suppressing loss due to inelastic collisions [Tha06]. We use an optical lattice that is deep enough that tunneling is negligible. Here each lattice site represents a simple harmonic trap with angular frequency $\omega_{\mathrm{ho}} = k_{\mathrm{lat}}\sqrt{2V^a_{\mathrm{lat}}/m}$, where $2\pi/k_{\mathrm{lat}}$ is the wavelength of the lattice light and V^a_{lat} is the lattice depth seen by an atom. In contrast to the free-space case, the closed-channel molecular state $|\psi_m\rangle$ is coupled to only one discrete state, namely the motional ground state $|\psi_a\rangle$ of two entrance-channel atoms at one lattice site. The matrix element $H_{\mathrm{am}} = \langle\psi_a| H |\psi_m\rangle$ of the Hamiltonian H is given by Eq. (B.9). At resonance coherent oscillations between the two states are expected to occur with angular frequency $\Omega_{\mathrm{res}} = 2H_{am}/\hbar$.

In addition to the coupling in Eq. (B.9), $|\psi_m\rangle$ can couple to excited s-wave trap states of the relative motion of two entrance-channel atoms [Köh06]. This coupling between many states can lead to quite complex dynamics. In order to avoid this, we need a Feshbach resonance with $\Omega_{\mathrm{res}} \ll \omega_{ho}$. For very small Ω_{res}, the magnetic field noise δB_{rms} [Dür04a] becomes an issue, resulting in the condition

$$\frac{\delta B_{\mathrm{rms}}\Delta\mu}{\hbar} \ll \Omega_{\mathrm{res}} \ll \omega_{\mathrm{ho}} \,. \tag{5.1}$$

In the experiment, we choose the Feshbach near 414 G with both incoming atoms in the hyperfine state $|f = 1, m_f = 0\rangle$ [Mar02]. A coupled-channels calculation predicts $a_{\mathrm{bg}} = 100.8\,\mathrm{a_B}$ and $\Delta B = 18\,\mathrm{mG}$ [Kok], where a_B is the Bohr radius. The Breit-Rabi formula predicts $\Delta\mu = 2\pi\hbar \times 111\,\mathrm{kHz/G}$. This is an unusually small value that helps reducing Ω_{res} and the sensitivity to magnetic-field noise.

5.2 Experimental Sequence

The experiment starts with an almost pure BEC of atoms at $\sim 412\,\mathrm{G}$ with more than 90% of the population in state $|f = 1, m_f = 0\rangle$. Then, the system is prepared in an atomic Mott insulator where the central region contains exactly two atoms at each lattice site [Vol06, Vol07]. In a next step, the magnetic field is jumped to a value very close to the 414 G Feshbach resonance. In response to the step in the externally applied field, eddy currents build up. We therefore use two subsequent steps of the magnetic field. The first step begins 2.4 G below the Feshbach resonance and ends typically 50 mG away from the Feshbach resonance, where mixing between states $|\psi_a\rangle$ and $|\psi_m\rangle$ is negligible. 250 μs later the eddy currents have fully settled and the second step is applied. The height of the second step is small enough that eddy currents have a negligible effect. After this step, we hold the magnetic field for a variable time. Finally, magnetic field, lattice, and dipole trap are abruptly switched off

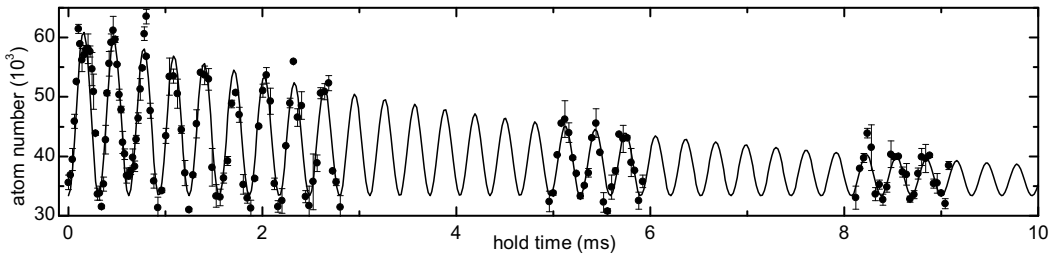

Figure 5.1: Coherent atom-molecule oscillations. Time-resolved oscillations between the atomic and the molecular state at $V^a_{\rm lat} = 15E^a_r$. The experimental data (•) show the number of entrance-channel atoms. The line shows a fit of Eq. (5.2) that yields $\Omega = 2\pi \times 3.221(2)$ kHz and $\tau = 5.9(4)$ ms.

and after 4 ms of free flight an absorption image is taken. The imaging light is resonant with an atomic transition so that molecules remain invisible.

5.3 Observation of Coherent Atom-Molecule Oscillations

5.3.1 Resonant Oscillations

The number of atoms as a function of hold time right at the Feshbach resonance $B_{\rm res}$ is shown in Fig. 5.1. The experimental data clearly show atom-molecule oscillations up to the $29^{\rm th}$ cycle. The signal has a minimum at $t = 0$ because for this data set, the first magnetic-field step ends 50 mG above the Feshbach resonance. Hence, the eddy currents effectively lead to an adiabatic ramp across the Feshbach resonance and associate molecules, as in Ref. [Mar05]. The data show damping in a way that the minimum atom number is essentially unchanged. This suggests that the decay is due to loss of population as opposed to dephasing which would lead to damping towards the mean atom number. We therefore fit

$$N(t) = N_1 + N_2 e^{-t/\tau} \frac{1 - \cos(\Omega t)}{2} \tag{5.2}$$

to the data. Here, N_1 is the particle number of the atomic background, N_2 the oscillation amplitude, τ the damping constant and Ω the frequency of the oscillation. Both, $|\psi_m\rangle$ and $|\psi_a\rangle$ can decay into lower-lying open two-atom channels. We measured the decay of population in state $|\psi_a\rangle$ 2.4 G below the Feshbach resonance and obtained a decay rate of less than 1 /s. We therefore attribute the decay fully to the state $|\psi_m\rangle$. During an oscillation period, half of the time is spent in this state. Hence the decay rate Γ of population in $|\psi_m\rangle$ can be extracted from the fit Eq. (5.2) yielding $\Gamma = 2/\tau = 0.34(2)$ /ms.

The fraction of the population that participates in the oscillation at short time is $N_2/(N_1 + N_2) = 0.46(1)$. This value reflects the fraction of lattice

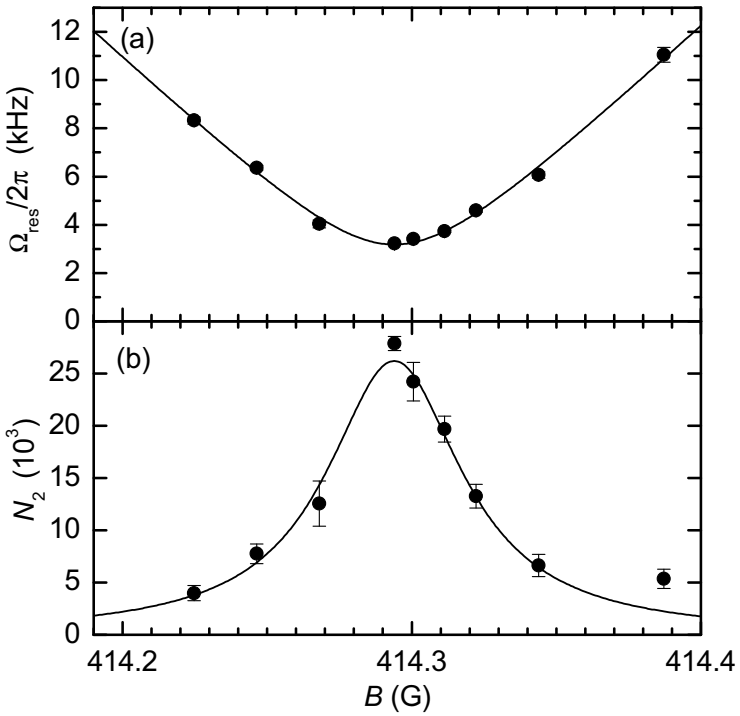

Figure 5.2: Dependence on the magnetic field. The frequency (a) and the amplitude (b) of the atom-molecule oscillations are shown in the vicinity of the Feshbach resonance for $V^a_{\rm lat} = 15E^a_r$. The lines show fits of Eq. (5.3) and Eq. (5.4) to the experimental data (•), respectively.

sites that are initially occupied by two atoms and agrees reasonably with the theoretical prediction of 0.53. The conversion efficiency at these sites is almost 100%. We repeated the measurements of Ref. [Vol06] in order to verify that the state produced here is really a quantum state in which the central region of the cloud contains exactly one molecule.

5.3.2 Magnetic-Field Dependence

The frequency and amplitude of the coherent oscillations depend on the magnetic-field value during the hold time. This dependence is shown in Fig. 5.2. As in any two-level system, the frequency is expected to follow a hyperbola

$$\Omega(B) = \sqrt{\Omega^2_{\rm res} + [(B - B_{\rm res})\Delta\mu/\hbar]^2}\,, \tag{5.3}$$

where $B_{\rm res}$ is the resonance position which depends on the lattice depth $V^a_{\rm lat}$, as discussed further below. A fit to the data is shown in Fig. 5.2(a). The best-fit values are $\Omega_{\rm res} = 2\pi \times 3.2(1)\,$kHz and $\Delta\mu = 2\pi\hbar \times 112(2)\,$kHz/G, in good agreement with the result of Fig. 5.1 and the theoretical prediction, respectively.

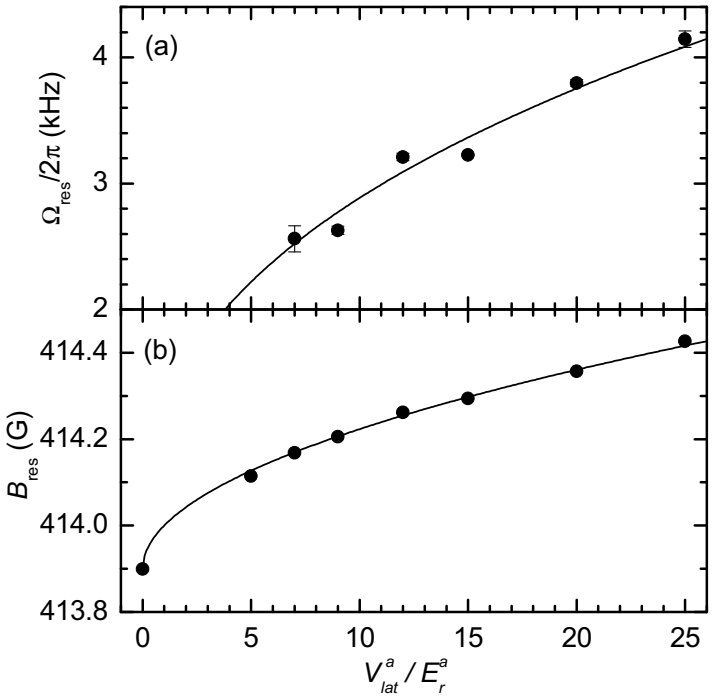

Figure 5.3: Dependence on the harmonic confinement. The on-resonance oscillation frequency (a) and the Feshbach resonance position (b) are shown as a function of lattice depth $V^a_{\rm lat}$. The lines show fits of Eq. (B.9) and Eq. (5.5) to the data (•).

The amplitude of the oscillation is plotted as a function of magnetic field in Fig. 5.2(b). This amplitude follows a Lorentzian

$$N_2(B) \;=\; N_{\rm res}\frac{\Omega^2_{\rm res}}{\Omega^2(B)}\;, \tag{5.4}$$

which is shown in Fig. 5.2(b). We use only $N_{\rm res}$ as a free fit parameter and copy the values of the other parameters from the fit to Fig. 5.2(a).

5.3.3 Dependence on the Harmonic Confinement

The oscillation frequency $\Omega_{\rm res}$ depends on the atomic density in the entrance-channel state. In Eq. (B.9) the corresponding effective volume is $(\sqrt{2\pi}a_{ho})^3/(1+0.49a_{bg}/a_{ho})$. We varied the lattice depth $V^a_{\rm lat}$ in order to verify this density dependence. Results are shown in Fig. 5.3(a). The line shows a fit of Eq. (B.9) to the data, where the only free fit parameter is the overall amplitude. As $\Delta\mu$ and a_{bg} can typically be predicted much more accurately than ΔB, we use this fit to determine $\Delta B = 15(1)\,$mG which agrees fairly well with the theoretical expectation [Kok]. The dominant contribution to the error in ΔB comes from the calibration of $V^a_{\rm lat}$ which we perform in terms of a frequency measurement

(see Sec. 3.3.1). We estimate the relative error in $V^a_{\rm lat}$ to be $\sim 10\,\%$. This determination of ΔB is independent of the atom-number calibration because only lattice sites with exactly two atoms contribute to the oscillation.

The increase of the harmonic confinement also leads to a shift of the Feshbach resonance position $B_{\rm res}$. This is shown in Fig. 5.3(b) as a function of $V^a_{\rm lat}$. Based on the zero-point energy of the three-dimensional harmonic oscillator for the relative motion of the two atoms, one expects $B_{\rm res} = B_0 + 3\hbar\omega_{ho}/2\Delta\mu$ [Mor05], where B_0 is the value at $V_{\rm lat} = 0$. The background scattering length a_{bg} causes a correction [Bus98] yielding

$$B_{\rm res} = B_0 + \frac{\hbar\omega_{ho}}{\Delta\mu}\left(\frac{3}{2} + \sqrt{\frac{2}{\pi}}\,\frac{a_{bg}}{a_{ho}}\right) . \tag{5.5}$$

For magnetic fields between B_0 and $B_{\rm res}$, the confinement thus stabilizes the molecules against dissociation that would occur in free space [Mor05].

We measured $B_0 = 413.90\,\mathrm{G}$ for the free space resonance position. This value is $0.44\,\mathrm{G}$ smaller than in Ref. [Mar02]. We attribute the discrepancy to the fact that the loss feature observed in Ref. [Mar02] at this particular resonance was extraordinarily broad making an accurate determination of the resonance position difficult in Ref. [Mar02]. We fit Eq. (5.5) to the data in Fig. 5.3(b). The only free fit-parameter is $V^a_{\rm lat}$ entering the equation in $\omega_{ho}(V^a_{\rm lat})$ and $a_{ho}(V^a_{\rm lat})$. The fit yields a value of $V^a_{\rm lat}$ that is a factor of 1.20(2) larger than our independent calibration of the lattice depth. This deviation can be explained by the assumption that our independent calibration of $V^a_{\rm lat}$ is worse than estimated. A second explanation presumes that other mechanisms have a significant effect. For example, the harmonic approximation used to derive Eq. (5.5) might be too inaccurate. Alternatively, the observed deviation might be explained as a differential ac-Stark shift between states $|\psi_a\rangle$ and $|\psi_m\rangle$ induced by the lattice light. The magnitude of the differential ac-Stark shift would have to equal 2% of the total ac-Stark shift.

5.4 Molecule Dissociation in the Lattice

To investigate the dissociation of $|\psi_m\rangle$ into excited trap states of the entrance channel, we first induce oscillations as in Fig. 5.1. In a next step, we stop the oscillations at a point where the molecule fraction is large by jumping the magnetic field to a different value typically far above the lowest oscillator state. We hold the magnetic field there for $250\,\mu$s and then switch it off.

The observed number of entrance-channel atoms is shown in Fig. 5.4. The peak near $414.5\,\mathrm{G}$ corresponds to the lowest oscillator state. The signal at this peak is fairly small because the dissociation pulse duration of $250\,\mu$s happens to be close to a minimum of the oscillations where only few molecules are dissociated. The peaks are approximately equidistant with a separation of

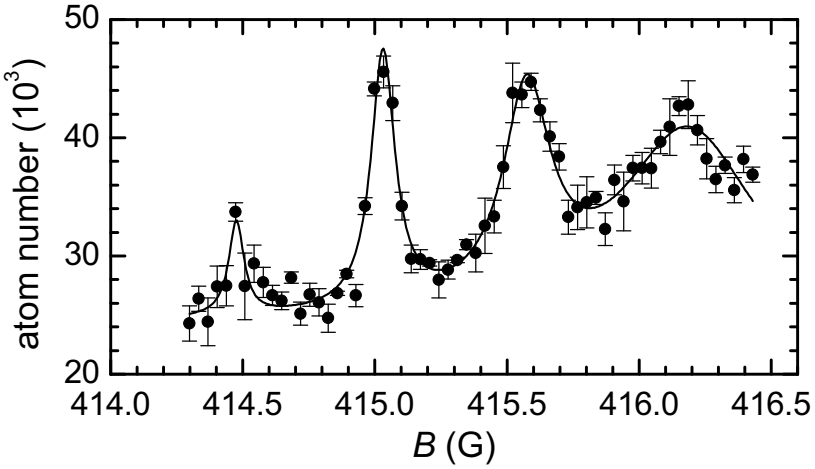

Figure 5.4: Mapping the band structure by molecule dissociation. The separation of the peaks corresponds to $\sim 2\hbar\omega_{ho}$, i.e. the molecules dissociate into even bands. Dissociation is suppressed in the band gaps showing the existence of confinement-induced band-gap molecules. The data were obtained at $V^a_{\rm lat} = 25E^a_r$. The line is a guide to the eye.

$\sim 0.57\,\mathrm{G}$ corresponding to an energy difference of $\sim 2\pi\hbar \times 63\,\mathrm{kHz}$ that is close to $2\hbar\omega_{ho} = 2\pi\hbar \times 66\,\mathrm{kHz}$. The exact energies of the peaks can be obtained from a band structure calculation for two interacting atoms [Nyg08].

Figure 5.4 shows a suppression of dissociation into odd bands of the lattice as well as into band gaps. The suppression in the gaps demonstrates that confinement-induced molecules can be created not only below the lowest band [Mor05], but also in three-dimensional band gaps. We attribute the suppression of dissociation into odd bands to the fact that these bands have odd parity at quasi-momentum zero. Hence the s-wave state $|\psi_m\rangle$ cannot dissociate at quasi-momentum zero. It has to be noted that this measurement also profits from the reduced sensitivity to magnetic-field noise due to the small value of $\Delta\mu$.

We see no oscillations for dissociation into the second band near 415 G even when avoiding eddy-currents as above. We attribute this to single-atom tunneling, which has an amplitude of $J = 2\pi\hbar \times 3.8\,\mathrm{kHz}$ in the second band and leads to decoherence.

5.5 Elastic Scattering Length

Here, an independent method to determine the characteristic parameters ΔB, a_{bg} and Γ (see Eq. (2.3)) of the 414 G Feshbach resonance is presented. It is based on measuring the real part of the scattering length close to resonance by recording the excitation spectrum of a Mott insulator. As compared to

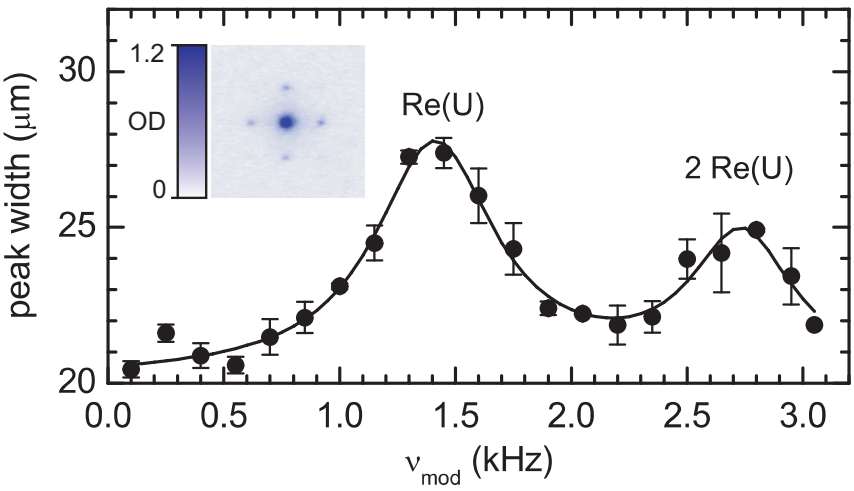

Figure 5.5: Excitation spectrum of a Mott insulator. The spectrum is measured by amplitude modulation of one of the lattice beams at $B = 415.4\,\mathrm{G}$. The width of the central interference peak observed in the time-of-flight absorption picture (see inset) after restoration of phase coherence is measured as a function of modulation frequency ν_{mod}. The gap as well as the two peaks in ν_{mod} corresponding to the on-site interaction energy $\mathrm{Re}(U)$ and $\mathrm{Re}(2U)$ are clearly visible. The line is a fit of two Lorentzian to the data (•).

the procedure presented in Ref. [Vol03], where the real part of the scattering length was extracted from a mean-field driven expansion of a BEC, the method presented here has the advantage that no atom number calibration is required.

The excitation spectrum of an atomic Mott insulator can be probed by modulation spectroscopy of one of the lattice beams [Stö04, Vol06]. The intensity modulation with frequency ν_{mod} creates sidebands on the lattice light. These sidebands drive a two-photon carrier-sideband transition and add energy to or remove energy from the system. For an atomic $n = 1$ Mott insulator, energy is added only if $h\nu_{\mathrm{mod}} \approx \mathrm{Re}(U)$. This is the energy an atom has to overcome when it tunnels to a neighboring site already occupied by another atom. Close to the resonance at $h\nu_{\mathrm{mod}} = \mathrm{Re}(U)$, energy is added to the system leading to heating. This is observed as a broadening of the interference peaks observed in time-of-flight images when the lattice is ramped back down into the superfluid regime [Gre02, Vol06].

To record the excitation spectrum, the following experimental sequence is applied. After the preparation of the atomic Mott-insulator state, the magnetic field is quickly jumped to the final magnetic-field value B without inducing atom-molecule oscillations and held there. Then the lattice light is modulated at constant ν_{mod} with a peak-to-peak modulation amplitude of 20% for 20 ms to allow for enough time for tunneling processes to occur. Next the lattice is ramped down linearly to $5E_r^a$ within 10 ms. Finally a time-of-flight absorption image is taken. A typical image is shown in the inset of Fig. 5.5. The procedure

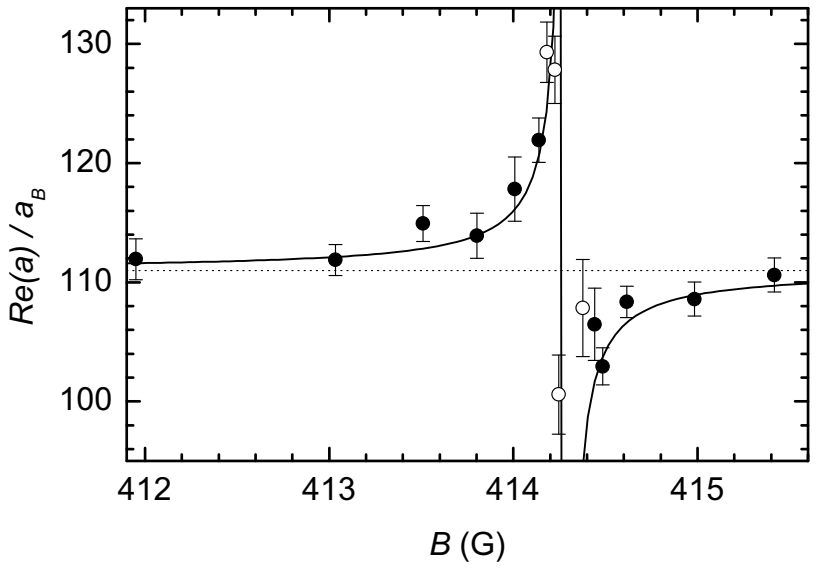

Figure 5.6: Real part of the scattering length close to resonance. The data (•) are extracted from excitation spectra of atoms in a Mott insulator at $V^a_{\rm lat} = 15E^a_r$ (see Fig. 5.5). The solid line shows a fit of Eq. (2.3) to the data. Data points (◦) close to resonance are excluded from the fit due to systematic uncertainties. The vertical solid line represents the resonance position $B_{\rm res}$, the horizontal dashed line the background scattering length $a_{\rm bg}$.

is repeated for different $\nu_{\rm mod}$.

Figure 5.5 shows an excitation spectrum measured at $V^a_{\rm lat} = 15E^a_r$ and $B = 415.4\,\mathrm{G}$. The peak width is extracted from the central peak of the interference pattern (see inset). The gap for low $\nu_{\rm mod}$, which is a characteristic property of the Mott insulator, can be seen clearly in the spectrum. The peak in $\nu_{\rm mod}$ corresponding to $\mathrm{Re}(U)$ is due to excitations where an atom on a singly occupied site hops onto another singly occupied site. The peak corresponding to $2\mathrm{Re}(U)$ is due to excitations where an atom hops onto a site already occupied by $n \geq 2$ atoms [Gre03]. The peak positions are extracted from a Lorentzian fit to the data.

Excitation spectra are recorded for different values of the magnetic field close to the Feshbach resonance and the real part of the scattering length is extracted by using Eq. (2.11). The result is shown in Fig. 5.6. A fit of Eq. (2.3) to the data yields a molecular decay rate $\Gamma = 39(3)\,/\mathrm{ms}$ that is two orders of magnitude larger than the value obtained in Sec. 5.3.1. This indicates that the dispersive feature in $\mathrm{Re}(a)$ is broadened by $\sim 30\,\mathrm{mG}$. The mechanism that causes the broadening remains unclear. Therefore, it is questionable whether Eq. (2.3) correctly describes the data close to resonance. Thus we exclude data points in a range of $\pm 100\,\mathrm{mG}$ around the resonance and fit Eq. (2.3) with $\Gamma = 0$ to the data. The fit yields a resonance position of $B_{\rm res} = 414.29(3)\,\mathrm{G}$

that agrees well with the measurements in Sec. 5.3.3. Furthermore, we obtain $a_{\mathrm{bg}} = 111(1)\,\mathrm{a_B}$ and $\Delta B = 13(2)\,\mathrm{mG}$. The errors are purely statistical. Systematic errors are larger. The uncertainty in the calibration of the lattice depth (see Sec. 3.3.1) leads to an uncertainty of $\sim 10\%$ in a_{bg}. The broadening of the dispersive feature might cause additional systematic errors. Within the experimental uncertainty, the values agree well with the theoretical prediction [Kok] as well as with the experimental results obtained in Sec. 5.3.3.

6 Dissipation Fermionizes a 1D Gas of Bosonic Molecules

Many-body systems usually behave differently depending on whether the particles are bosons or fermions. However, bosons are forced to behave much like fermions if the system is one-dimensional (1D) and the interactions dominate the dynamics. This strongly correlated system is called a Tonks-Girardeau gas [Ton36, Gir60] and was observed with atoms in optical lattices [Par04, Kin04]. All this work dealt with conservative interactions. Here we demonstrate a surprising generalization, namely that inelastic collisions produce a dissipative analogue of the Tonks-Girardeau gas [Sya08]. The experiment is performed with Feshbach molecules confined to 1D in the optical lattice. Inelastic collisions between the molecules create strong correlations that suppress the molecule loss rate. We dramatically increase this suppression by adding a lattice along the 1D direction. This work offers perspectives to create other, and possible new, strongly correlated states using dissipation [Sac99, Wen04].

In Sec. 6.1 we summarize the theory of strongly interacting bosons in 1D for elastic interactions and generalize the Lieb-Liniger model to the case of inelastic interactions. The experimental observation of the strongly correlated system is presented in Sec. 6.2. In Sec. 6.3 we develop theory to describe the system if a shallow lattice is applied along the 1D direction. Its experimental realization is demonstrated in Sec. 6.4.

6.1 Strongly Interacting Bosons in 1D

6.1.1 Elastic Interactions

The historic development of the theory of one-dimensional gases dates back to 1936, when L. Tonks theoretically analyzed a one-dimensional classical gas of hard elastic spheres of finite size [Ton36]. He found that this system of impenetrable particles obeys the equation of state of an ideal gas with a volume that is reduced by the volume of the particles. He also showed that the gas obeys the Maxwell-Boltzmann distribution.

In 1960, M. Girardeau established a relationship between one-dimensional systems of bosons with infinitively strong repulsive interactions and non-interacting, spinless fermions [Gir60]. Due to the infinitely strong interaction, the bosons are impenetrable. Girardeau found that the many-body wave function

in position representation for the bosonic system is equivalent to the many-body wave function of the fermionic system multiplied by a position dependent constant $+1$ or -1. As a consequence, the many-body wave function for the bosonic system vanishes whenever the relative coordinate of two-particles is zero as for a non-interacting Fermi gas.

Lieb and Liniger extended Girardeau's model to the case of repulsive elastic interactions modeled by a delta-function potential with finite strength g_{1D} [Lie63]. They considered a one-dimensional gas of N bosons in a box with length L with periodic boundary conditions. The Hamiltonian reads

$$\hat{H}_{\mathrm{LL}} = -\frac{\hbar^2}{2m}\sum_j \frac{\partial^2}{\partial x_j^2} + g_{1D}\sum_{j<i}\delta(x_j - x_i)\ , \tag{6.1}$$

where x_j is the position of the jth boson. The particle density n_{1D} can be used to introduce a dimensionless interaction strength [Lie63]

$$\gamma \ = \ \frac{m g_{1D}}{\hbar^2 n_{1D}}\ . \tag{6.2}$$

Counter-intuitively, in 1D the gas becomes more interacting with decreasing density. In the strongly correlated regime a Tonks-Girardeau gas is realized. This regime is reached for $|\gamma| \gg 1$.

For $\gamma \gg 1$ and $N \gg 1$ Lieb and Liniger found an analytic expression for the energy eigenvalue of the ground state [Lie63]

$$E \ = \ N\frac{\hbar^2\pi^2 n_{1D}^2}{6m}\left(\frac{\gamma}{\gamma+2}\right)^2\ . \tag{6.3}$$

For $\gamma \to \infty$ the energy per particle approaches the Fermi energy $\hbar^2 k_F^2/2m$ with $k_F = \pi n_{1D}$ as for non-interacting fermions.

In 1998, M. Olshanii proposed that the Tonks-Girardeau gas could be realized by confining particles to a cylindrical trap with very tight radial confinement [Ols98]. At sufficiently low temperature, the radial motion of the particles is essentially frozen and particles can only move axially. For harmonic confinement, characterized by the angular harmonic oscillator frequency $\omega_\perp$, the radial motion is governed by the ground-state wave function with harmonic oscillator length $a_\perp = \sqrt{\hbar/m\omega_\perp}$, where m is the mass of one particle. Two-body interactions between the bosons in the cylindrical trap can be modeled by a delta-potential with interaction strength [Ols98]

$$g_{1D} \ = \ \frac{2\hbar^2 a}{m a_\perp^2}\left(1 + \frac{a}{\sqrt{2}\,a_\perp}\,\zeta\left(\frac{1}{2}\right)\right)^{-1}\ , \tag{6.4}$$

where a is the three-dimensional scattering length and ζ denotes the Riemann zeta function with $\zeta(\frac{1}{2}) \approx -1.46$.

Particle loss due to inelastic interactions can serve as a direct experimental probe of the pair correlation function. This is because two-body collision rates are proportional to finding two particles at the same position. Hence, the loss rate caused by inelastic two-body collisions is proportional to $g^{(2)}(0)$ as already discussed in Sec. 2.3.1. Gangardt and Shlyapnikov calculated $g^{(2)}(0)$ for strongly interacting bosons with repulsive interactions with $\gamma \gg 1$ and obtained [Gan03]

$$g^{(2)}(0) = \frac{4\pi^2}{3\gamma^2} \,. \tag{6.5}$$

In the strongly correlated regime, $g^{(2)}(0)$ is strongly suppressed as observed in Ref. [Kin05] and reaches $g^{(2)}(0) = 0$ for $\gamma = \infty$ as for non-interacting fermions. On the other hand, in the *weakly* interacting regime with $\gamma \ll 1$, a gas of identical bosons at zero temperature has $g^{(2)}(0) \approx 1$. Analogous statements hold for three-body collisions [Kag85, Gan03, Bur97, Lab04].

6.1.2 Inelastic Interactions

The interaction between ultracold bosons is described by the scattering length a. The real and imaginary part of a represent elastic and inelastic collisions, respectively (see Sec. 2.3.2). Obviously, a strong repulsive interaction makes it energetically unfavorable that two bosons are at the same position. We show that a strong inelastic interaction also produces a strong reduction of the probability to find two bosons at the same position. This surprising behavior becomes plausible from an analogy in classical optics, where absorption is expressed by an imaginary part of the refractive index. If an electromagnetic wave impinges perpendicularly on a surface between two media with complex refractive indices n_1 and n_2, then a fraction $|(n_1-n_2)/(n_1+n_2)|^2$ of the intensity will be reflected. In the limit $|n_2| \to \infty$, the light is perfectly reflected off the surface, no matter what the value of $\arg n_2$, where $n_2 = |n_2|e^{i \arg n_2}$. This is due to index mismatch. In our system, bosons interacting with large imaginary a almost perfectly reflect off each other for an analogous reason. This leads to an almost vanishing boundary condition at zero relative distance, which strongly suppresses the probability to find two bosons at the same position.

As discussed in Sec. 2.3.1, loss caused by inelastic two-body collisions can be described by a negative imaginary part of the scattering length. Here we generalize the Lieb-Liniger model to the case of inelastic interactions characterized by complex a. We present the main arguments and the reader is referred to Ref. [GR08] for a detailed derivation.

We first note following the calculations in Ref. [Ols98] that Eq. (6.4) for the 1D interaction strength remains valid if a is complex. Next, we consider the boundary condition for the wave function. It is well known, that the delta-potential in Eq. (6.1) can be replaced by a boundary condition for the wave

function ψ at positions where the relative coordinate $x_{ij} = x_i - x_j$ vanishes

$$\left.\frac{d\psi}{dx_{ij}}\right|_{x_{ij}\to 0^+} - \left.\frac{d\psi}{dx_{ij}}\right|_{x_{ij}\to 0^-} = \frac{mg_{1D}}{\hbar^2}\,\psi|_{x_{ij}=0}\ . \tag{6.6}$$

Bosonic symmetry implies that on the left-hand side, the first term equals minus the second term. Expanding ψ in a power series around $x_{ij} = 0$, Eq. (6.6) can be rewritten as

$$\psi(x_1, \ldots, x_N) \propto \frac{2\hbar^2}{mg_{1D}} + |x_{ij}| + \mathcal{O}(x_{ij}^2)\ , \tag{6.7}$$

where the proportionality contains the dependence on all remaining coordinates.

The energy eigenstates of the generalized Lieb-Liniger model can be divided into two classes: gaseous states and bound states. For real γ, the momenta of all particles are real valued for gaseous states whereas at least one momentum is complex for bound states. Furthermore, for $\gamma \to \pm\infty$ all momenta converge to finite values for gaseous states, whereas at least one momentum diverges to $\pm i\infty$ for bound states. The latter is exemplified by a state where particles i and j are bound. Here $\psi \propto \exp(mg_{1D}|x_{ij}|/2\hbar^2)$ for $x_{ij} \to 0$, which corresponds to an imaginary momentum that diverges for $\gamma \to \infty$. Bound states exist only if $\mathrm{Re}(\gamma) < 0$. The case of real and negative γ was considered in Ref. [Ast05].

We consider the case of complex γ, where all momenta are usually complex, but the convergence or divergence of the momenta for $|\gamma| \to \infty$ can still be used to distinguish between gaseous and bound states. As a consequence, ψ and $d\psi/dx_{ij}$ remain finite for $|\gamma| \to \infty$ for all gaseous states. Equation (6.6) then implies

$$\psi|_{x_{ij}=0} \to 0 \quad \text{for} \quad |\gamma| \to \infty \tag{6.8}$$

for all gaseous states, because the left-hand side of Eq. (6.6) must remain finite. The same result can be obtained from Eq. (6.7), because the term proportional to $|x_{ij}|$ must remain finite so that the proportionality factor must remain finite.

In the limit $|\gamma| \to \infty$, the interaction for all gaseous states is fully described by the boundary condition Eq. (6.8). The crucial point is that this boundary condition is independent of $\arg(\gamma)$ and it is precisely this boundary condition that yields a Tonks-Girardeau gas. Hence, the wave functions of all gaseous states turn exactly into Girardeau's solutions in the limit $|\gamma| \to \infty$, no matter what the value of $\arg(\gamma)$. Attraction, repulsion, and dissipation all produce the Tonks-Girardeau gas in the limit of infinite interaction strength.

Note that in this experiment, $\mathrm{Im}(a)$ is large and negative while $\mathrm{Re}(a)$ in negligible. One can show [GR08] that for $\mathrm{Im}(\gamma) \to -\infty$ and finite $\mathrm{Re}(\gamma)$, no bound states exist, no matter what the sign of $\mathrm{Re}(\gamma)$. Bound states are

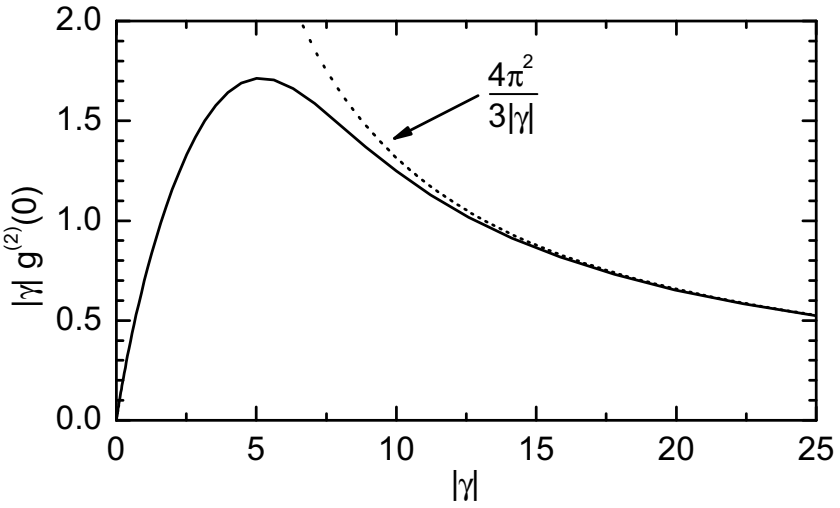

Figure 6.1: Loss rate for purely inelastic interaction. For $\mathrm{Re}(\gamma) = 0$, the loss rate $dn_{1D}/dt \propto |\gamma| g^{(2)}(0)$ (solid line) shows a maximum as a function of the interaction strength $|\gamma|$. The dotted line shows the asymptotic behavior according to Eq. (6.12). For large $|\gamma|$ it scales as $\propto 1/|\gamma|$. Thus, for large $|\gamma|$ the system is strongly correlated, and the loss rate drops $\propto 1/|\gamma|$.

therefore of little relevance in our experiment. In particular, the ground state is gaseous.

We now calculate the pair-correlation function $g^{(2)}(0)$ for complex γ. In 3D, the rate equation describing losses due to inelastic two-body interaction is given by Eq. (2.16) with $K_2 = -2\mathrm{Im}(g)/\hbar$ from Eq. (2.17). In 1D, the analogous relation reads

$$\frac{dn_{1D}}{dt} = -K_2^{1D}\, n_{1D}^2\, g^{(2)}(0) \tag{6.9}$$

with

$$K_2^{1D} = -\frac{2}{\hbar}\mathrm{Im}(g_{1D}) \ . \tag{6.10}$$

Following the calculations in Ref. [Lie63], it can be shown that Eq. (6.3) remains valid for complex γ. This equation describes the lowest-lying state of the system. If there are no bound states, then this is the ground state. The initial loss rate of this state is obtained by inserting Eq. (6.3) into Eq. (2.56). In order to obtain $g^{(2)}(0)$, we spatially integrate Eq. (6.9) and solve for $g^{(2)}(0)$. Hence,

$$g^{(2)}(0) = \frac{2\mathrm{Im}(E)}{N n_{1D} \mathrm{Im}(g_{1D})} \ . \tag{6.11}$$

Insertion of Eq. (6.3) to lowest order in $1/\gamma$ yields the pair-correlation function for $|\gamma| \gg 1$

$$g^{(2)}(0) = \frac{4\pi^2}{3|\gamma|^2} \ , \tag{6.12}$$

which is independent of $\arg(\gamma)$. In particular $g^{(2)}(0) \to 0$ for $|\gamma| \to \infty$ independent of $\arg(\gamma)$. The suppression of $g^{(2)}(0)$ characteristic for a strongly correlated regime can be reached equally well with elastic or inelastic interactions. This is a consequence of the boundary condition Eq. (6.8).

For purely inelastic interaction, i.e. $\mathrm{Re}(\gamma) = 0$, the loss rate dn_{1D}/dt from Eq. (6.9) shows an interesting behavior as a function of K_2. This is shown in Fig. 6.1 as as function of the dimensionless interaction strength $|\gamma| \propto K_2$. For small $|\gamma|$, the system is weakly correlated and $g^{(2)}(0) \approx 1$. Therefore $dn_{1D}/dt \propto |\gamma| g^{(2)}(0)$ increases linearly with $|\gamma|$. When $|\gamma| \sim 5$, dn_{1D}/dt has a maximum, and for large $|\gamma|$ the system is strongly correlated and dn_{1D}/dt drops proportionally to $1/|\gamma|$. Figure 6.1 shows an exact numerical solution of the Lieb-Liniger model for $N = 40$ particles, where $g^{(2)}(0)$ is obtained from Eq. (6.11). The result for $N = 20$ is almost identical so that finite size effects are negligible.

6.2 Observation of Strong Correlations

6.2.1 Experimental Sequence

The experiment starts with the preparation of a Mott-like state of molecules as described in Sec. 3.3.2. The optical-lattice potential seen by a molecule is given by Eq. (2.5) with

$$V_\parallel^m = V_x^m \qquad V_\perp^m = V_y^m = V_z^m \tag{6.13}$$

and $\lambda_{\mathrm{lat}} = 830.440\,\mathrm{nm}$. At the end of the state preparation, the lattice depth is $V_\parallel^m = V_\perp^m = 127 E_r^m$, where E_r^m is the molecular recoil energy (see Sec. 3.3.2).

After state preparation, $V_\parallel^m$ is linearly ramped to its final value with $V_\parallel^m \ll V_\perp^m$ resulting in an array of tubes as shown in Fig. 3.5(b). We choose a ramp duration of 0.5 ms. For much faster ramps, we observe a substantial broadening of the momentum distribution along the tubes. For much slower ramps, particle loss during the ramp becomes noticeable. The system is allowed to evolve for a variable hold time at the final value of $V_\parallel^m$. During this hold time, the relevant loss occurs. After the hold time, all molecules are dissociated into atom pairs using a magnetic field ramp with 1.6 G/ms across the Feshbach resonance to 1008.7 G. The dissociation terminates the loss. Finally, the magnetic field and the lattice light are switched off simultaneously, and the number of atoms is determined from a time-of-flight absorption image. The lattice beams that create $V_\perp^m$ have a finite waist. This results in a harmonic confinement with angular frequency $\omega_\parallel = 2\pi \times 71\,\mathrm{Hz}$ along the tubes.

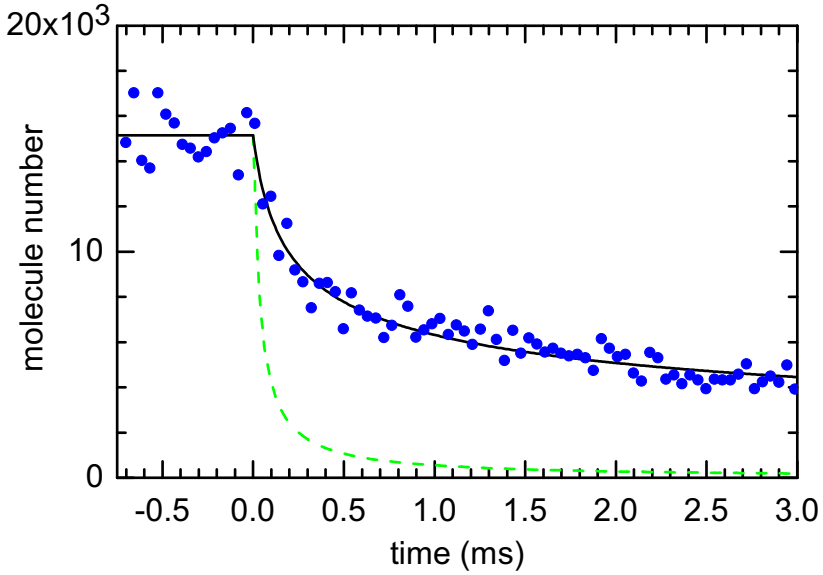

Figure 6.2: Time-resolved loss of molecules at $V_{\parallel}^{m} = 0$. The loss begins at $t = 0$. The solid line shows a fit of Eq. (6.16) to the experimental data (•) with $t \leq 1$ ms. The best-fit value is $\chi n_{1D}^{3}(0) = 4.3/\mathrm{ms}$, corresponding to $K_2 = 2.2 \times 10^{-10}$ cm^3/s, and, at $t = 0$, to $g^{(2)}(0) = 0.11$. The dashed line shows the expectation for an uncorrelated system. The observed loss is much slower than the dashed line because of strong correlations.

6.2.2 Results

The decay of the molecule number as a function of hold time at $V_{\parallel}^{m} = 0$ is shown in Fig. 6.2. The ramp down of $V_{\parallel}^{m}$ begins at $t = -0.5\,\mathrm{ms}$ and ends at $t = 0$. The data do not show noticeable loss during the ramp down. In order to avoid complications due to the harmonic confinement $\omega_{\parallel}$ along the tubes, we process only data for $t \leq 1\,\mathrm{ms}$.

To model the decay, we combine Eqs. (6.2), (6.4), (6.9), (6.12). This yields

$$\frac{dn_{1D}}{dt} = -\chi\, n_{1D}^{4} \tag{6.14}$$

$$\chi = \frac{4\pi^2 \hbar a_{\perp}^{2}}{3m}\,\mathrm{Im}\left(\frac{1}{a}\right) . \tag{6.15}$$

Time integration of Eq. (6.14) gives $n_{1D}(t) = n_{1D}(0)(1 + 3t\chi n_{1D}^{3}(0))^{-1/3}$. The experimental data represent an average over a large number of tubes of different lengths. This is not critical because the initial 1D density $n_{1D}(0) = 2/\lambda$ is identical in all tubes. Spatial integration yields the total particle number

$$N(t) = \frac{N(0)}{\left(1 + 3t\chi n_{1D}^{3}(0)\right)^{1/3}} . \tag{6.16}$$

A fit of Eq. (6.16) to the data with $t \leq 1\,\mathrm{ms}$ in Fig. 6.2 yields $\chi n_{1D}^3(0) = 4.3(4)\,/\mathrm{ms}$, corresponding to $\mathrm{Im}(1/a) = 1/24\,\mathrm{nm}$, according to Eq. (6.15). The error is purely statistical.

This value of $\mathrm{Im}(1/a)$ might have contributions from $\mathrm{Re}(a)$ and $\mathrm{Im}(a)$. The identity

$$\mathrm{Re}(a)^2 = -\mathrm{Im}(a)^2 - \frac{\mathrm{Im}(a)}{\mathrm{Im}(1/a)} \tag{6.17}$$

shows that $\mathrm{Re}(a)^2$ is a parabola as a function of $\mathrm{Im}(a)$ at fixed $\mathrm{Im}(1/a)$. This yields an upper bound $|\mathrm{Re}(a)| \leq 1/(2\mathrm{Im}(1/a)) = 12\,\mathrm{nm}$. This information can be combined with our previous studies [Vol06, Dür06] of excitation spectra at $V_\parallel^m = V_\perp^m = 15E_r^m$. With the upper bound for $|\mathrm{Re}(a)|$, the excitation spectra should yield a resonance at a frequency below 1.4 kHz. Our measurements show no such resonance, even in a much broader frequency range. This can only be explained if $|\mathrm{Re}(a)| \ll |\mathrm{Im}(a)|$, because in this case the resonance becomes very broad and shallow, so that it might be undetectable. We conclude that $|\mathrm{Re}(a)| \ll |\mathrm{Im}(a)|$. As a result $\mathrm{Im}(1/a) \approx -1/\mathrm{Im}(a)$.[1]

With $|\mathrm{Re}(a)| \ll |\mathrm{Im}(a)|$ we obtain $\mathrm{Im}(a) = -24\,\mathrm{nm}$ and $K_2 = 2.2(2) \times 10^{-10}\,\mathrm{cm}^3/\mathrm{s}$. At $t = 0$ this corresponds to $|\gamma| = 11(1)$ and $g^{(2)}(0) = 0.11(1)$. This shows that the inelastic interaction brings the experiment into the strongly-correlated regime. As the loss proceeds, n_{1D} decreases and according to Eq. (6.2) $|\gamma|$ increases, so that the system becomes even more strongly correlated.

The value of K_2 obtained here agrees fairly well with the measurements discussed in Sec. 4.1 at 1005.8 G that yield $K_2 = 1.5 \times 10^{-10}\,\mathrm{cm}^3/\mathrm{s}$. For comparison we note that if the system were weakly correlated, i.e. $g^{(2)}(0) \approx 1$, then the loss should follow the dashed line in Fig. 6.2 which is calculated with K_2 from Sec. 4.1. Clearly, the observed loss is drastically inhibited. We conclude that our system is strongly correlated.

Further support for this conclusion comes from the time dependence of our data. If the system were weakly correlated, then $g^{(2)}(0) = 1$ would be time independent. Spatial integration of Equation (6.9) would then predict $dN/dt \propto N^2$ instead of $dN/dt \propto N^4$ in the strongly correlated regime. We fit $dN/dt \propto N^q$ with an arbitrary power q to the data with $t \leq 1\,\mathrm{ms}$. This yields $q = 4.3(6)$ in good agreement with $q = 4$.

The above data analysis relies on the approximation that the system is in the ground state at all times. This approximation is not a major concern because the relevant excited states are fermionized as well and their behavior is similar. But there is a more fundamental aspect to this issue: as the loss proceeds,

[1] The 1D measurements (no matter if $V_\parallel^m = 0$ or $V_\parallel^m \neq 0$) yield an experimental value for $\mathrm{Im}(1/a)$ while the 3D measurement in Sec. 4.1 yields a value for $\mathrm{Im}(a)$ at 1005.8 G. In principle, these two values could be inserted into Eq. (6.17) to extract a value (not just an upper bound) for $|\mathrm{Re}(a)|$. But in practice the systematic uncertainty in the measurement of Sec. 4.1 is so large, that we cannot constrain $|\mathrm{Re}(a)|$ any further.

the particle number changes and the ground state changes correspondingly. A simple estimate for the temporal evolution of the energy can be obtained when assuming that the kinetic energy per particle E^{kin}/N would remain constant during the loss. This is to be compared to the evolution of the ground state: in a harmonic oscillator, the kinetic energy of the fermionized ground state scales as $E_g^{\mathrm{kin}} \propto N^2$. As the loss proceeds, the system automatically evolves away from the ground state, because $E^{\mathrm{kin}}(t)/E_g^{\mathrm{kin}}(t) = N(0)/N(t)$. Hence, for the data with $t \leq 1$ ms that we analyze in Fig. 6.2, $E^{\mathrm{kin}}/E_g^{\mathrm{kin}}$ is estimated to increase by a factor of ~ 2 during the loss.

Detailed calculations [GR08] including the excited states show that the above estimate is too pessimistic. In fact, the loss rate from a fermionized state is proportional to its kinetic energy E^{kin}, i.e. the loss preferentially depletes excited states. The dynamics of this preferential depletion is beyond the scope of this thesis. We only note that $E^{\mathrm{kin}}/E_g^{\mathrm{kin}}$ increases by a factor of less than ~ 2. Hence, it is reasonable to approximate the loss rate as being that of the ground state.

6.3 Strongly Correlated Bosons in the Lattice

Strongly correlated systems in solid state physics usually contain some lattice potential along all directions. It is therefore interesting to study whether similar physics as above is obtained in the case where the lattice depth along the tubes $V_\parallel^m$ is nonzero, but still much smaller than $V_\perp^m$ [Stö04, Par04]. In fact, we observe a much stronger suppression of $g^{(2)}(0)$. In addition, the system with $V_\parallel^m \neq 0$ has the advantage that it is more easily accessible for analytic and numerical calculations.

For $V_\parallel^m \ll V_\perp^m$, the motion perpendicular to the tubes remains frozen out as before, but the motion along the tubes is now described as hopping between discrete lattice sites. This system can be modelled with a Bose-Hubbard Hamiltonian Eq. (2.9) with tunneling amplitude J and on-site interaction matrix element $\mathrm{Re}(U)$. If two particles occupy the same lattice site and tunneling is negligible, this population will decay as $\exp(-\Gamma t)$ (see Sec. 6.3.2), where we abbreviate

$$\Gamma = -\frac{2}{\hbar}\mathrm{Im}(U) \ . \tag{6.18}$$

6.3.1 Analytic Model for the Loss Rate

Here we develop a simple analytic model for the loss rate. We begin by calculating the loss rate from the initial state $|1\rangle$ with exactly one particle at each lattice site. We consider a state $|2\rangle$ that is obtained from state $|1\rangle$ by one tunneling event. States $|1\rangle$ and $|2\rangle$ are coherently coupled by the matrix element $\langle 1|H|2\rangle = -\sqrt{2}J$. We define the angular coupling frequency as

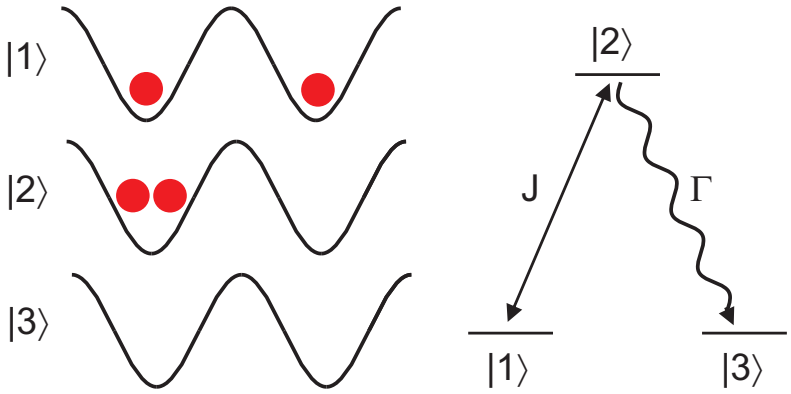

Figure 6.3: Levels involved in the analytic model for loss at $V_{\parallel}^{m} \neq 0$. Left: The initial level $|1\rangle$ contains exactly one particle at each lattice site. State $|2\rangle$ is obtained after one tunneling process with amplitude J. Population in state $|2\rangle$ decays incoherently into state $|3\rangle$ with rate Γ. Right: A more schematic way of drawing these levels: States $|1\rangle$ and $|2\rangle$ are coherently coupled with interaction strength J. State $|2\rangle$ decays incoherently into state $|3\rangle$ with rate Γ. Initially, all population is in state $|1\rangle$.

$\Omega = (2/\hbar)|\langle 1|H|2\rangle| = \sqrt{8}J/\hbar$. In state $|2\rangle$, two particles occupy the same lattice site, so that the state decays with rate coefficient Γ. These states are depicted in Fig. 6.3. While the figure shows the simple case of only two lattice sites, this approach is applicable for an arbitrary number of sites.

States $|1\rangle$ and $|2\rangle$ form a two-level system that fits into a very general pattern: state $|1\rangle$ is initially populated and coherently coupled to state $|2\rangle$, which suffers from incoherent loss. Such a two-level system is a textbook example of an open quantum system. In the fast-loss regime $\Omega \ll \Gamma$, the population decay of the initial state $|1\rangle$ follows $\exp(-\Gamma_{\text{eff}}t)$ with [CT92]

$$\Gamma_{\text{eff}} = \frac{\Omega^2}{\Gamma}\left(1 + \left(\frac{2\Delta E}{\hbar\Gamma}\right)^2\right)^{-1} , \tag{6.19}$$

where $\Delta E = \text{Re}(U)$ is the energy difference between states $|1\rangle$ and $|2\rangle$.

In a tube containing L lattice sites, there are $2(L-1)$ possible tunneling processes, because there are $L-1$ barriers and tunneling through each barrier can occur from the left or right. The loss rates of the initial state $|1\rangle$ for all these possible decay channels add up incoherently. The initial loss rate of the particle number N is twice as large as the population decay of state $|1\rangle$, because two particles are lost per inelastic collision. Hence, for $N \gg 1$ and $\hbar\Gamma \gg J$

$$\left.\frac{dN}{dt}\right|_{t=0} = -(L-1)\kappa , \tag{6.20}$$

where we abbreviate $\kappa = 4\Gamma_{\text{eff}}$. Combination with Eq. (6.18) and $\Omega = \sqrt{8}J/\hbar$ yields

$$\kappa = \frac{32J^2}{\hbar^2\Gamma}\left(1 + \left(\frac{\text{Re}(U)}{\text{Im}(U)}\right)^2\right)^{-1} . \tag{6.21}$$

Note that combination of Eq. (6.21) with Eq. (6.2) yields $\kappa \propto \text{Im}(1/a)$. We recall from Eq. (6.15) that $\chi \propto \text{Im}(1/a)$ and see that κ and χ scale identically with the scattering properties. This illustrates that the two regimes, $V_{\parallel}^m = 0$ and $V_{\parallel}^m \neq 0$, represent similar physics.

For $|\text{Re}(a)| \ll |\text{Im}(a)|$, Eq. (6.21) yields a counter-intuitive effect: the larger the loss coefficient Γ, the smaller the actual loss rate κ. In the experiment, this means that fast on-site loss tends to preserve the initial state and thus suppresses tunneling in the many-body system. This can be interpreted as a manifestation of the continuous quantum Zeno effect [Mis77]: fast dissipation freezes the system in its initial state. Without this Zeno effect, one might naively estimate that tunneling would occur at a rate $\sim 2J/\hbar$. If each such tunneling event would lead to immediate particle loss, then $2J/\hbar$ should set the timescale for the loss, but this estimate is too naive, as discussed below.

An estimation of the loss at longer times must take into account that tunneling of a particle to a previously empty lattice site does not lead to loss. For $\hbar\Gamma \gg J$ we obtain $\hbar\kappa \ll J$. Hence, we assume that between two subsequent loss events, the particles have enough time to redistribute completely randomly along the tube under the constraint that no lattice site is occupied more than once. The probability that the lattice sites next to a specific tunneling barrier are both occupied is then $p = N(N-1)/L(L-1)$.[2] Tunneling through this barrier will lead to loss, only if both sites are occupied. Hence, Eq. (6.20) must be multiplied by p, yielding

$$\frac{dN}{dt} = -\frac{\kappa}{L}\,N^2 , \tag{6.22}$$

for $N \gg 1$. Time integration with $N(0) = L$ yields

$$N(t) = \frac{N(0)}{1+\kappa t} . \tag{6.23}$$

In order to test the quality of the analytic model, we performed much more rigorous analytical and numerical calculations [GR08]. The analytic calculations reveal that the system maps to a very good approximation to a fermionized model. The numerical results show that the system loses its memory

[2] There are $\binom{L}{N}$ possibilities to distribute N distinguishable particles onto L sites with at most one particle per site. For a specific pair of neighboring sites that are occupied by one particle each, the remaining $N-2$ particles can be distributed over the remaining $L-2$ sites, thus giving $\binom{L-2}{N-2}$ distributions. Division by the total number of distributions yields the probability $p = \binom{L-2}{N-2}/\binom{L}{N}$ that two neighboring sites are occupied.

about the initial state in a time $\sim 1/\Gamma$. During this very short time only little loss occurs, and after this transient the loss is well described by Eq. (6.21) and Eq. (6.22). In addition, the numerical results can be fitted fairly well with Eq. (6.23) only, not trying to model the initial transient. The best-fit values for κ obtained this way agree with Eq. (6.21) within 20% for $J/\hbar\Gamma \leq 0.04$, which corresponds to $V_{\parallel}^{m} \geq 1.7 E_r^m$.

6.3.2 Pair-Correlation Function

To calculate the pair correlation function for $V_{\parallel}^{m} \neq 0$, one should note the translational invariance is broken and $g^{(2)}(\mathbf{r},\mathbf{r})$ can depend on $\mathbf{r}$. We start with Eq. (6.9), spatial integration yields

$$\frac{dN}{dt} = -K_2 \int d^3r \; g^{(2)}(\mathbf{r},\mathbf{r}) \left\langle \hat{n}(\mathbf{r}) \right\rangle^2 \; . \tag{6.24}$$

We use a tight-binding Wannier function $w(\mathbf{r}-\mathbf{r}_j)$, Eq. (2.8), to describe the wave function centered at lattice site j. Large contributions to the integral in Eq. (6.24) arise only if $\mathbf{r}$ is close to the center of some lattice site $\mathbf{r}_j$. We only consider this situation. Here the Wannier functions centered at all other lattice sites are negligible and we obtain

$$\begin{aligned}
\left\langle \hat{n}(\mathbf{r}) \right\rangle^2 &= \left\langle \hat{n}_j \right\rangle^2 |w(\mathbf{r}-\mathbf{r}_j)|^4 & (6.25)\\
\left\langle \hat{\Psi}^{\dagger 2}(\mathbf{r}) \hat{\Psi}^2(\mathbf{r}) \right\rangle &= \left\langle \hat{n}_j(\hat{n}_j-1) \right\rangle |w(\mathbf{r}-\mathbf{r}_j)|^4 & (6.26)\\
g^{(2)}(\mathbf{r},\mathbf{r}) &= \frac{\left\langle \hat{n}_j(\hat{n}_j-1) \right\rangle}{\left\langle \hat{n}_j \right\rangle^2} \; , & (6.27)
\end{aligned}$$

where the operator $\hat{n}_j$ describes the particle number at site j. Interestingly, $g^{(2)}(\mathbf{r},\mathbf{r})$ is independent of $\mathbf{r}$, as long as $\mathbf{r}$ is so close to $\mathbf{r}_j$, that the integrand in Eq. (6.24) is large. In order to express the dependence on j instead of $\mathbf{r}$, we write $g_j^{(2)}(0)$. Equation (6.24) becomes

$$\frac{dN}{dt} = -K_2 \sum_{j=1}^{L} g_j^{(2)}(0) \left\langle \hat{n}_j \right\rangle^2 \int d^3r |w(\mathbf{r}-\mathbf{r}_j)|^4 \; . \tag{6.28}$$

We consider L lattice sites with periodic boundary conditions. In this case $\langle \hat{n}_j \rangle$ and $g_j^{(2)}(0)$ are independent of j and $\sum_{j=1}^{L} \langle \hat{n}_j \rangle = N$ yields $\langle \hat{n}_j \rangle = N/L$. In addition, we take the imaginary part on both sides of Eq. (2.11) and combine this with Eq. (6.18) and $K_2 = -2\mathrm{Im}(g)/\hbar$. This yields

$$\Gamma \; = \; K_2 \int d^3r |w(\mathbf{r}-\mathbf{r}_j)|^4. \tag{6.29}$$

Hence,

$$\frac{dN}{dt} = -\frac{\Gamma}{L}\, N^2\, g^{(2)}(0)\ . \tag{6.30}$$

For the strongly correlated state, comparison with the loss rate in Eq. (6.22) yields

$$g^{(2)}(0) \;=\; \frac{\kappa}{\Gamma}\ . \tag{6.31}$$

Interestingly, $g^{(2)}(0)$ is independent of density, in contrast to the case $V_\parallel^m = 0$.

Finally, we consider the case where tunneling is negligible and assume that each lattice site initially contains exactly two particles. Equation (6.27) yields $g_j^{(2)}(0)|_{t=0} = 1/2$. Combination with $N|_{t=0} = 2L$ and Eq. (6.30) yields

$$\left.\frac{dN}{dt}\right|_{t=0} = -\Gamma N|_{t=0}\ . \tag{6.32}$$

Hence, N decays exponentially with $\exp(-\Gamma t)$ because the lattice sites decay independently of each other.

6.4 Observation of Strong Correlations in the Lattice

We performed time-resolved measurements of the molecule number similar to that shown in Fig. 6.2 with the same experimental sequence as described in Sec. 6.2.1 for various values of the lattice depth $V_\parallel^m$. Such measurements are shown in Fig. 6.4. Since our model neglects the harmonic confinement $\omega_\parallel$ along the tube, we evaluate the loss at short times only. As the particles have to tunnel between discrete sites, this condition is less stringent here. We fit Eq. (6.23) to the data with $N(t) \geq N(0)/2$. The resulting best-fit values κ are shown in Fig. 6.5(a). We then fit the analytic results Eq. (6.18) and Eq. (6.21) to the data. With our above conclusion $|\mathrm{Re}(a)| \ll |\mathrm{Im}(a)|$, there is only one free fit parameter. The best-fit value is $K_2 = 1.7(3) \times 10^{-10}\,\mathrm{cm}^3/\mathrm{s}$, which is close to the result of Fig. 6.2. Data for $V_\parallel^m > 10E_r^m$ (not shown in Fig. 6.5) cannot be used for the fit. They only represent the $\sim 10\,/\mathrm{s}$ decay rate of a single, isolated molecule. As $V_\parallel^m/E_r^m$ increases from 1.7 to 10, Γ increases from 45/ms to 82/ms. The dashed line in Fig. 6.5(a) shows the naive estimate $2J/\hbar$ which drops from 3.4/ms to 0.40/ms and lies far off the data.

The value of K_2 extracted from Fig. 6.5(a) is used to calculate Γ and thus $g^{(2)}(0)$ using Eq. (6.31) for each experimental data point. The results are shown in Fig. 6.5(b) and agree well with the theoretical expectation (solid line) based on the same value of K_2. The smallest measured value of $g^{(2)}(0) = 4.6(7)\times 10^{-4}$ represents an improvement of more than two orders of magnitude over previous experiments [Kin05].

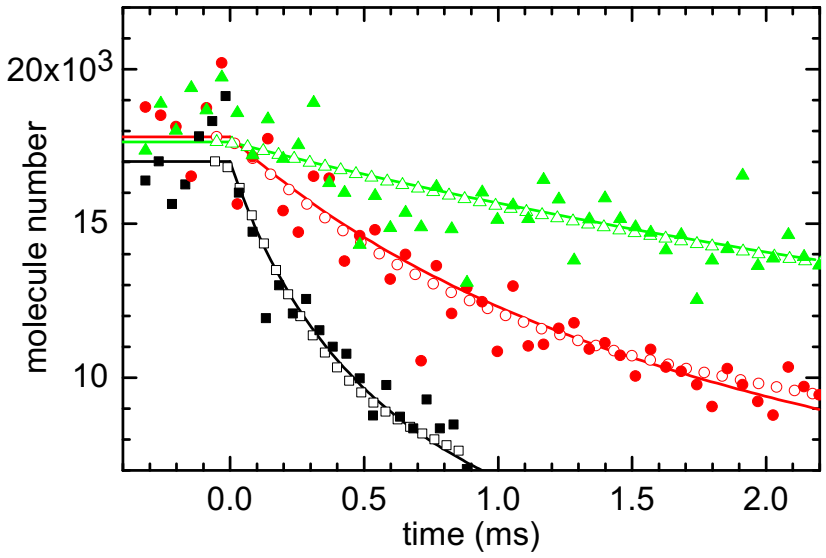

Figure 6.4: Time-resolved loss of molecules at $V_{\parallel} \neq 0$. The loss begins at $t = 0$. Solid lines show fits of the analytic model Eq. (6.23) to the experimental data (filled symbols) with $N(t) > N(0)/2$. Open symbols show results of the numerical calculations. Squares, circles, and triangles correspond to $V_{\parallel}/E_r^m = 1.8$, 3.9, and 6.0 respectively.

Note that a non-interacting gas would have $g^{(2)}(0) = 1$ at any lattice depth. The observed suppression of $g^{(2)}(0)$ is caused by the inelastic interactions, not by the lattice itself. If the molecules were uncorrelated, the loss would follow $dN/dt = -\Gamma N^2/L$ according to Eq. (6.30) with $g^{(2)}(0) = 1$.

In conclusion, we showed that strong dissipation can bring a 1D gas of bosons deeply into the fermionized regime and create a dissipative analogue of the Tonks-Girardeau gas. Measured loss rates yield $g^{(2)}(0) \approx 1/10$. Application of a weak optical lattice along the weakly confined dimension increases this suppression to $g^{(2)}(0) = 1/2000$. Note that our previous experiments in Refs. [Vol06, Dür06] relied on atom-atom interactions to create a strongly correlated state. In a deep lattice where particles hardly tunnel, molecules were associated and the atom-atom correlations were converted into molecule-molecule correlations. This is in sharp contrast to the present experiment, where the molecule-molecule interactions create the molecule-molecule correlations. Future investigations might explore the regime of small but nonzero $V_{\parallel}$ that should connect the two regimes studied here.

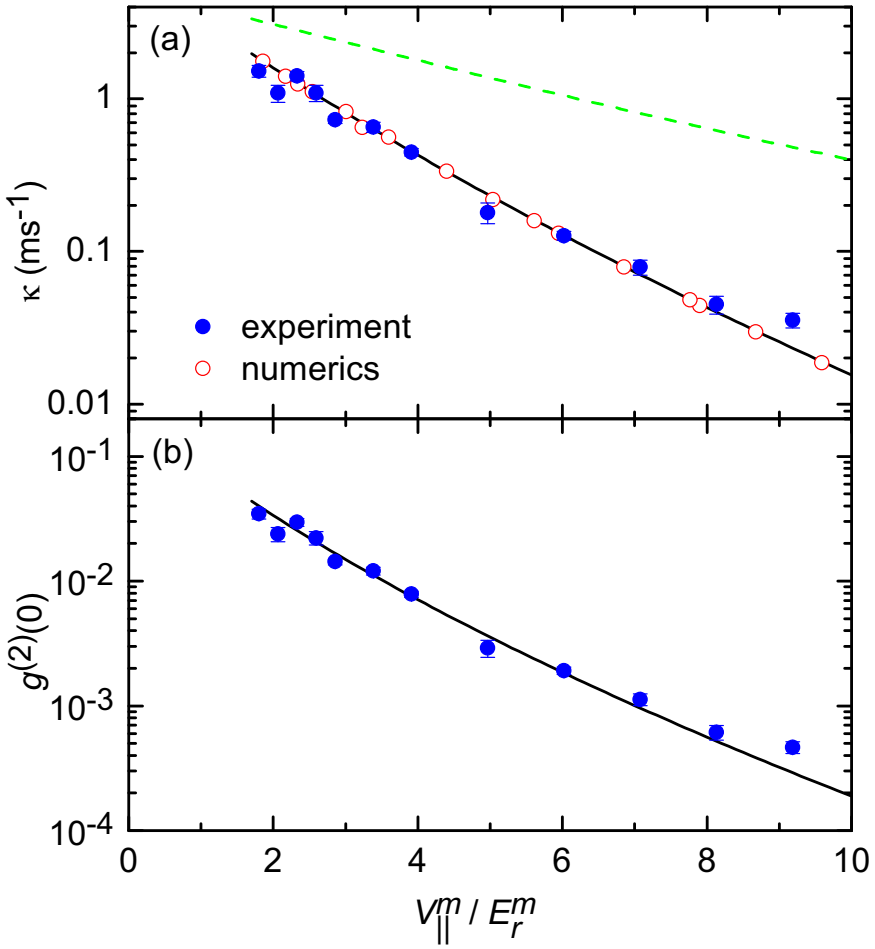

Figure 6.5: (a) Loss at different lattice depths $V_{\parallel}^{m}$. Experimental results (•) for κ are extracted from fits of Eq. (6.23) to time-resolved loss data as shown in Fig. 6.4. A fit of Eq. (6.18) and Eq. (6.21) to the data yields the solid line. The best-fit value is $K_2 = 1.7(3) \times 10^{-10}\,\mathrm{cm}^3/\mathrm{s}$. The experimental data and the analytical model agree well with results of the numerical calculations (○). For comparison, the dashed line shows the naive estimate $2J/\hbar$ which lies far off the data. (b) Pair correlation function calculated from the data in (a) using Eq. (6.31).

7 Outlook

The association of ultracold molecules using Feshbach resonances was a breakthrough in the field of quantum gases. The experiments described in this thesis reveal important aspects of interacting ultracold molecules that are relevant for further experiments.

In particular, the observation that an increased loss coefficient can slow down the actual loss from the correlated many-body system of molecules could be used to increase the lifetime of other systems that suffer from loss by drastically increasing the loss coefficient, e.g. using photoassociation or Feshbach resonances. In the long run, the demonstration that dissipation can be used to reach the strongly correlated regime opens up new perspectives for the observation of spin liquid behavior or topological effects [Sac99, Wen04], especially in 2D.

The coherent atom-molecule oscillations presented in this thesis demonstrate how atomic scattering properties can be inferred from a frequency measurement. Since frequencies can be measured with high accuracy, this technique offers perspectives in high-precision measurements, e.g. in experiments searching for drifts of fundamental constants [Chi06a].

Ultracold molecules in a Mott-like state, as created in the experiments performed here, serve as a good starting point to transfer the molecules into the rovibrational ground state. This can be achieved by a sequence of Raman laser pulses. The absence of inelastic interactions would then allow to ramp down the optical lattice and to create a BEC of molecules in their internal ground state [Jak02]. Recently, a first step in this direction has been taken already [Win07, Lan08].

Ultracold molecules in their rovibrational ground state are of particular interest if they are heteronuclear. In this case, they can have a large permanent electric dipole moment. As a consequence, these polar molecules show a long-range electric dipole-dipole interaction. Based on the dipole-dipole interaction, new quantum phases in optical lattices could be created [Gór02, Mic06, Bar06]. In addition, polar molecules could also be employed for the realization of novel schemes for quantum computation [DeM02, Lee05]. Moreover, precision measurements might also profit from ultracold polar molecules, e.g. in experiments that search for a permanent electric dipole moment of the electron [Hud05, Ber91]. First experiments demonstrating the creation of cold polar molecules [Man04, Sag05] and the association of ultracold heteronuclear molecules using a Feshbach resonance were already reported [Osp06, Pap06].

A Scattering Cross Section for Identical Bosons

We consider the case of two identical bosons with spin scattering off one another. The wave function Eq. (2.20) needs to be symmetric under particle exchange. In the center-of-mass frame particle exchange is equivalent to the parity operation combined with swapping the spin states, i.e. $\vartheta \to \pi - \vartheta$, $\varphi \to \varphi + \pi$ and $|\alpha\beta\rangle \to |\beta\alpha\rangle$. For a spherically symmetric scattering potential the bosonically symmetrized wave function has the asymptotic form

$$\begin{aligned} \psi(\mathbf{r}) \quad &\overset{r\to\infty}{=} \quad \frac{1}{\sqrt{2\mathcal{V}}}\left(e^{izk_{\alpha\beta}}\,|\alpha\beta\rangle + e^{-izk_{\beta\alpha}}\,|\beta\alpha\rangle\right) \\ &+ \quad \frac{1}{\sqrt{2\mathcal{V}}}\sum_{\alpha'\beta'}\frac{e^{irk_{\alpha'\beta'}}}{r} f_{\alpha'\beta',\alpha\beta}(\vartheta)\,|\alpha'\beta'\rangle \\ &+ \quad \frac{1}{\sqrt{2\mathcal{V}}}\sum_{\alpha'\beta'}\frac{e^{irk_{\alpha'\beta'}}}{r} f_{\beta'\alpha',\beta\alpha}(\pi-\vartheta)\,|\beta'\alpha'\rangle\ . \end{aligned} \tag{A.1}$$

The normalization volume $\mathcal{V}$ is chosen so that the plane-wave component $(e^{ikz} + e^{-ikz})/\sqrt{2\mathcal{V}}$ contains one particle. Swapping the labels of the indices α' and β' in the last sum yields

$$\begin{aligned} \psi(\mathbf{r}) \quad &\overset{r\to\infty}{=} \quad \frac{1}{\sqrt{\mathcal{V}}}\left(\frac{e^{izk_{\alpha\beta}}\,|\alpha\beta\rangle + e^{-izk_{\beta\alpha}}\,|\beta\alpha\rangle}{\sqrt{2}}\right) \\ &+ \quad \frac{1}{\sqrt{\mathcal{V}}}\sum_{\alpha'\beta'}\frac{e^{irk_{\alpha'\beta'}}}{r}\frac{f_{\alpha'\beta',\alpha\beta}(\vartheta) + f_{\alpha'\beta',\beta\alpha}(\pi-\vartheta)}{\sqrt{2}}\,|\alpha'\beta'\rangle\ . \end{aligned} \tag{A.2}$$

For $f(\vartheta)$ and $f(\pi-\vartheta)$ the outgoing spins $\alpha,'\,\beta'$ are the same, but the incoming spins α, β differ. The cross section becomes

$$\sigma = \sum_{\alpha'\beta'}\frac{k_{\alpha'\beta'}}{k_{\alpha\beta}}\int d\Omega\left|\frac{f_{\alpha'\beta',\alpha\beta}(\vartheta) + f_{\alpha'\beta',\beta\alpha}(\pi-\vartheta)}{\sqrt{2}}\right|^2 . \tag{A.3}$$

A particle scattered at an angle ϑ could stem from either incoming plane wave and thus could be scattered by an angle ϑ or $\pi - \vartheta$. Since the two possibilities cannot be distinguished, the corresponding amplitudes $f(\vartheta)$ and $f(\pi-\vartheta)$ interfere. For $\alpha \neq \beta$ there is no simple relationship between the two amplitudes because the incoming spins differ.

This is different for $\alpha = \beta$. When expanding $f(\vartheta)$ in partial waves Eq. (2.24), the symmetry of the spherical harmonics under parity is important $Y_{lm}(\pi - \vartheta, \pi + \phi) = (-1)^l Y_{lm}(\vartheta, \phi)$. As a result, for identical bosons only partial waves with even l' contribute to the total cross section Eq. (2.27).

For $\alpha \neq \beta$ there are two terms in the sum over $\alpha'\beta'$ of Eq. (A.3) which describe elastic scattering: $|\alpha'\beta'\rangle = |\alpha\beta\rangle$ or $|\alpha'\beta'\rangle = |\beta\alpha\rangle$. For $\alpha = \beta$ there is only one term in the sum. The elastic cross section is therefore

$$\sigma_{\mathrm{el}}^{\mathrm{boson}} = \frac{2}{1+\delta_{\alpha\beta}} \int d\Omega \left| \frac{f_{\alpha'\beta',\alpha\beta}(\vartheta) + f_{\alpha'\beta',\beta\alpha}(\pi - \vartheta)}{\sqrt{2}} \right|^2 . \tag{A.4}$$

Near threshold one obtains the two scattering lengths

$$f_{\alpha\beta,\alpha\beta}(\vartheta) \overset{k_{\alpha\beta}\to 0}{=} -a_{\alpha\beta,\alpha\beta} , \tag{A.5}$$

$$f_{\alpha\beta,\beta\alpha}(\vartheta) \overset{k_{\alpha\beta}\to 0}{=} -a_{\alpha\beta,\beta\alpha} , \tag{A.6}$$

and we define the bosonically symmetrized scattering length

$$a_{\alpha\beta}^{\mathrm{sym}} = \frac{a_{\alpha\beta,\alpha\beta} + a_{\alpha\beta,\beta\alpha}}{1+\delta_{\alpha\beta}} , \tag{A.7}$$

in accordance with Ref. [Sto88]. The elastic s-wave cattering cross section for bosons with spin becomes [Bur99]

$$\sigma_{\mathrm{el}}^{\mathrm{boson}} \overset{k_{\alpha\beta}\to 0}{=} (1+\delta_{\alpha\beta})\, 4\pi \left| a_{\alpha\beta}^{\mathrm{sym}} \right|^2 . \tag{A.8}$$

The inelastic cross section can be calculated in a similar way and one obtains [Bur99]

$$\sigma_{\mathrm{inel}}^{\mathrm{boson}} \overset{k_{\alpha\beta}\to 0}{=} (1+\delta_{\alpha\beta})\, \frac{4\pi}{k_{\alpha\beta}} \mathrm{Im}\left(-a_{\alpha\beta}^{\mathrm{sym}}\right) . \tag{A.9}$$

We conclude this appendix with a short remark on detector count rates. In a traditional scattering experiment, the number of particles counted by a detector at angle ϑ is proportional to the differential scattering cross section

$$\frac{d\sigma}{d\Omega} = |f(\vartheta, \varphi)|^2 . \tag{A.10}$$

When comparing the situation where a particle scatters off a potential to the situation where two particles scatter off another, the detector count rate depends on whether one or two particles are counted. If one particle is counted, the detector count rate equals the scattering event rate Γ in Eq. (2.21). If both particles are counted, then the detector count rate will be 2Γ. The latter case is inevitable for identical bosons. The factor of 2 in the detector count rate has no effect on the total scattering cross section σ because its definition is based on the scattering event rate Γ. When dealing with detector count rates, it is customary to include a factor of 2 in the definition of $d\sigma/d\Omega$ when identical particles are scattered. In this case, $d\sigma/d\Omega$ must be integrated over half the solid angle to obtain σ. In the field of ultracold gases detector count rates are usually irrelevant.

B Matrix Element for Atom-Molecule Coupling

Here, we derive the matrix element H_{am} for atom-molecule coupling in a harmonic oscillator. For a more detailed derivation see Ref. [Die07].

In order to relate H_{am} to parameters of the scattering problem, we first summarize some results of scattering theory. The asymptotic form of the scattering state in the absence of the molecular state is given by Eq. (2.20) and reads

$$\psi_{\mathbf{k}}(\mathbf{r}) = C\left(e^{i\mathbf{k}\cdot\mathbf{r}} + f_{\mathrm{bg}}\frac{e^{ikr}}{r}\right) , \tag{B.1}$$

where $\mathbf{r}$ is the relative coordinate, $\mathbf{k}$ is the wave vector in the relative coordinate, $f_{\mathrm{bg}} = (e^{-2ika_{\mathrm{bg}}} - 1)/2ik$ is the background scattering amplitude and C is a constant determined by normalization of the wave function. Obviously $\psi_{\mathbf{k}}(\mathbf{r})$ is proportional to C, so that

$$\langle\psi_m|\, H\, |\psi_{\mathbf{k}}\rangle \;=\; C\alpha\; . \tag{B.2}$$

For small enough k, the parameter α becomes independent of $\mathbf{k}$ [Tim99b]. For the scattering state Eq. (B.1), we use a large quantization volume V and obtain $|C|^2 = 1/V$. We thus recover Eq. (23) of Ref. [Tim99b]. A combination of Eqs. (25) and (42) of that reference yields

$$|\alpha|^2 \;=\; \frac{4\pi\hbar^2 a_{\mathrm{bg}}}{m}\Delta\mu\Delta B\; . \tag{B.3}$$

This relates α to known parameters of the Feshbach resonance.

We now turn to the problem of two identical bosons in a harmonic oscillator. Our following treatment rests on the central assumption that there is a separation of length scales: the typical range of the interatomic interaction is much smaller than the harmonic oscillator length $a_{\mathrm{ho}} = \sqrt{\hbar/m\omega}$ determined by the angular trap frequency ω. Hence, H_{am} can only be sensitive to the properties of the entrance-channel wave function at short radius. For the ground state of two elastically interacting particles in the harmonic oscillator, the short-range behavior is [Bus98]

$$\psi_a(r) = -\sqrt{\frac{1}{4\pi a_{\mathrm{ho}}^2\hbar\omega}\frac{\partial E}{\partial a}}\left(-\frac{a_{\mathrm{bg}}}{r} + 1 + \mathcal{O}\left(\frac{r}{a_{\mathrm{ho}}}\right)\right) , \tag{B.4}$$

with the energy $E(a)$ given by the implicit equation [Bus98]

$$\frac{a_{\rm ho}}{a} = \sqrt{2}\frac{\Gamma\left(\frac{3}{4}-\frac{E}{2\hbar\omega}\right)}{\Gamma\left(\frac{1}{4}-\frac{E}{2\hbar\omega}\right)}\,, \tag{B.5}$$

where Γ is the Euler gamma function. A series expansion yields for the ground state [Die07]

$$\frac{\partial E}{\partial a_{bg}}\frac{a_{ho}}{\hbar\omega} = \sqrt{\frac{2}{\pi}}\left(1+\underbrace{2\sqrt{\frac{2}{\pi}}(1-\ln 2)}_{=0.490}\frac{a_{bg}}{a_{ho}}+\mathcal{O}\left(\frac{a_{bg}}{a_{ho}}\right)^2\right)\,. \tag{B.6}$$

To connect these results to the scattering problem, we consider Eq. (B.1) in the limit $k \to 0$

$$\psi_{\mathbf{k}}(r) = Ce^{-ika_{\rm bg}}\left(1+O(ka_{\rm bg})^2\right)\times\left(-\frac{a_{\rm bg}}{r}+1+O(kr)+O(ka_{\rm bg})^2\right)\,, \tag{B.7}$$

We note that the typical wave vector in the harmonic oscillator ground state is $k \sim 1/a_{ho}$ so that neglecting terms of order $O(ka_{bg})^2$ is consistent with our above series expansion in Eq. (B.6) that neglects terms of order $O(a_{bg}/a_{ho})^2$. Evidently, Eq. (B.7) becomes identical to Eq. (B.4) if we choose

$$|C|^2 = \left(\frac{1}{\sqrt{2\pi}a_{ho}}\right)^3\left(1+0.490\,\frac{a_{bg}}{a_{ho}}+O\left(\frac{a_{\rm bg}}{a_{\rm ho}}\right)^2\right)\,. \tag{B.8}$$

As the coupling of an entrance-channel state to the molecular state is only sensitive to the wave function at short radius, and as the two wave functions at short radius Eqs. (B.4) and (B.7) are identical, the coupling for the two states is identical. Hence, Eq. (B.2) is again applicable and we obtain

$$|H_{\rm am}|^2 = \frac{4\pi\hbar^2 a_{bg}\Delta\mu\Delta B}{m\left(\sqrt{2\pi}\,a_{\rm ho}\right)^3}\left(1+0.490\frac{a_{\rm bg}}{a_{\rm ho}}+\mathcal{O}\left(\frac{a_{\rm bg}}{a_{\rm ho}}\right)^2\right)\,. \tag{B.9}$$

This result for $H_{\rm am}$ is a factor of $(\pi/3)^{1/4} \approx 1.01$ larger than Eq. (22) in Ref. [Jul04] where a different approximation is used, and also terms of order $\mathcal{O}(a_{\rm bg}/a_{\rm ho})$ are neglected.

Bibliography

[And95] M. H. Anderson, J. R. Ensher, M. R. Matthews, C. E. Wieman, and E. A. Cornell. Observation of Bose-Einstein condensation in a dilute atomic vapor. *Science* **269**, 198 (1995).

[And06] A. Andre, D. DeMille, J. M. Doyle, M. D. Lukin, S. E. Maxwell, P. Rabl, R. J. Schoelkopf, and P. Zoller. A coherent all-electrical interface between polar molecules and mesoscopic superconducting resonators. *Nature Phys.* **2**, 636 (2006).

[AS05] J. R. Abo-Shaeer, D. E. Miller, J. K. Chin, K. Xu, T. Mukaiyama, and W. Ketterle. Coherent molecular optics using ultracold sodium dimers. *Phys. Rev. Lett.* **94**, 040405 (2005).

[Ash76] N. W. Ashcroft and N. D. Mermin. Solid State Physics. Brooks/Cole, Pacific Grove (1976).

[Ast05] G. E. Astrakharchik, J. Boronat, J. Casulleras, and S. Giorgini. Beyond the Tonks-Girardeau gas: Strongly correlated regime in quasi-one-dimensional Bose gases. *Phys. Rev. Lett.* **95**, 190407 (2005).

[Bal97] N. Balakrishnan, V. Kharchenko, R. C. Forrey, and A. Dalgarno. Complex scattering lengths in multi-channel atom-molecule collisions. *Chem. Phys. Lett.* **280**, 5 (1997).

[Bar04] M. Bartenstein, A. Altmeyer, S. Riedl, S. Jochim, C. Chin, J. Hecker-Denschlag, and R. Grimm. Crossover from a molecular Bose-Einstein condensate to a degenerate Fermi gas. *Phys. Rev. Lett.* **92**, 120401 (2004).

[Bar06] R. Barnett, D. Petrov, M. Lukin, and E. Demler. Quantum magnetism with multicomponent dipolar molecules in an optical lattice. *Phys. Rev. Lett.* **96**, 190401 (2006).

[Ber91] W. Bernreuther and M. Suzuki. The electric dipole moment of the electron. *Rev. Mod. Phys.* **63**, 313 (1991).

[Blo05] I. Bloch. Ultracold quantum gases in optical lattices. *Nature Phys.* **1**, 23 (2005).

[Blo07] I. Bloch, J. Dalibard, and W. Zwerger, Many-Body Physics with Ultracold Gases, arXiv.org:0704.3011 (2007).

[Bos24] S. N. Bose. Plancks Gesetz und Lichtquantenhypothese. *Z. Phys.* **26**, 178 (1924).

[Bra95] C. C. Bradley, C. A. Sackett, J. J. Tollett, and R. G. Hulet. Evidence of Bose-Einstein condensation in an atomic gas with attractive interactions. *Phys. Rev. Lett.* **75**, 1687 (1995). Erratum *ibid.* **79**, 1170 (1997).

[Bra01] E. Braaten and H. Hammer. Three-body recombination into deep bound states in a Bose gas with large scattering length. *Phys. Rev. Lett.* **87**, 160407 (2001).

[Bra04] E. Braaten and H.-W. Hammer. Enhanced dimer relaxation in an atomic and molecular Bose-Einstein condensate. *Phys. Rev. A* **70**, 042706 (2004).

[Bra06] E. Braaten and H.-W. Hammer. Universality in few-body systems with large scattering length. *Phys. Rep.* **428**, 259 (2006).

[Bre02] H.-P. Breuer and F. Petruccione. The Theory of Open Quantum Systems. University Press, Oxford (2002).

[Brü05] R. Brühl, A. Kalinin, O. Kornilov, J. P. Toennies, G. C. Hegerfeldt, and M. Stoll. Matter wave diffraction from an inclined transmission grating: Searching for the elusive ^{4}He trimer Efimov state. *Phys. Rev. Lett.* **95**, 063002 (2005).

[Büc07] H. P. Büchler, A. Micheli, and P. Zoller. Three-body interactions with cold polar molecules. *Nat Phys* **3**, 726 (2007).

[Bur97] E. A. Burt, R. W. Ghrist, C. J. Myatt, M. J. Holland, E. A. Cornell, and C. E. Wieman. Coherence, correlations, and collisions: what one learns about Bose-Einstein condensates from their decay. *Phys. Rev. Lett.* **79**, 337 (1997).

[Bur99] J. P. Burke, Jr., Theoretical Investigation of Cold Alkali Atom Collisions, Ph.D. thesis, University of Colorado, Boulder (1999).

[Bus98] T. Busch, B. G. Englert, K. Rzazewski, and M. Wilkens. Two cold atoms in a harmonic trap. *Found. Phys.* **28**, 549 (1998).

[Cam06] G. K. Campbell, J. Mun, M. Boyd, P. Medley, A. E. Leanhardt, L. G. Marcassa, D. E. Pritchard, and W. Ketterle. Imaging the Mott insulator shells by using atomic clock shifts. *Science* **313**, 649 (2006).

[Chi05] C. Chin, T. Kraemer, M. Mark, J. Herbig, P. Waldburger, H. Nägerl, and R. Grimm. Observation of Feshbach-like resonances in collisions between ultracold molecules. *Phys. Rev. Lett.* **94**, 123201 (2005).

[Chi06a] C. Chin and V. V. Flambaum. Enhanced sensitivity to fundamental constants in ultracold atomic and molecular systems near Feshbach resonances. *Phys. Rev. Lett.* **96**, 230801 (2006).

[Chi06b] J. K. Chin, D. E. Miller, Y. Liu, C. Stan, W. Setiawan, C. Sanner, K. Xu, and W. Ketterle. Evidence for superfluidity of ultracold fermions in an optical lattice. *Nature* **443**, 961 (2006).

[Cor00] S. L. Cornish, N. R. Claussen, J. L. Roberts, C. E. Cornell, and C. E. Wieman. Stable ^{85}Rb Bose-Einstein condensates with widely tunable interactions. *Phys. Rev. Lett.* **85**, 1795 (2000).

[Cou98] P. Courteille, R. S. Freeland, D. J. Heinzen, F. A. van Abeelen, and B. J. Verhaar. Observation of a Feshbach resonance in cold atom scattering. *Phys. Rev. Lett.* **81**, 69 (1998).

[CS07] B. Capogrosso-Sansone, N. V. Prokof'ev, and B. V. Svistunov. Phase diagram and thermodynamics of the three-dimensional Bose-Hubbard model. *Phys. Rev. B* **75**, 134302 (2007).

[CT92] C. Cohen-Tannoudji, J. Dupont-Roc, and G. Grynberg, Atom-Photon Interactions, pp. 49–59, Wiley, New York (1992).

[Cub03] J. Cubizolles, T. Bourdel, S. J. J. M. F. Kokkelmans, G. V. Shlyapnikov, and C. Salomon. Production of long-lived ultracold Li_2 molecules from a Fermi gas. *Phys. Rev. Lett.* **91**, 240401 (2003).

[Dan] A. Danilova and J. H. Thywissen, Ultracold atom news, http://ucan.physics.utoronto.ca.

[Dav95] K. B. Davis, M. O. Mewes, M. R. Andrews, N. J. van Druten, D. S. Durfee, D. M. Kurn, and W. Ketterle. Bose-Einstein condensation in a gas of sodium atoms. *Phys. Rev. Lett.* **75**, 3969 (1995).

[DeM99] B. DeMarco and D. S. Jin. Onset of Fermi degeneracy in a trapped atomic gas. *Science* **285**, 1703 (1999).

[DeM02] D. DeMille. Quantum computation with trapped polar molecules. *Phys. Rev. Lett.* **88**, 067901 (2002).

[Die02] K. Dieckmann, C. A. Stan, S. Gupta, Z. Hadzibabic, C. H. Schunck, and W. Ketterle. Decay of an ultracold fermionic lithium gas near a Feshbach resonance. *Phys. Rev. Lett.* **89**, 203201 (2002).

[Die07] D. Dietze, Atom-Molekül Oszillationen in ^{87}Rb, Diplomarbeit, Max-Planck-Institut für Quantenoptik, Garching, and Technische Universität München (2007), unpublished.

[Don01] E. A. Donley, N. R. Claussen, S. L. Cornish, J. L. Roberts, E. A. Cornell, and C. E. Wieman. Dynamics of collapsing and exploding Bose-Einstein condensates. *Nature* **412**, 295 (2001).

[Don02] E. A. Donley, N. R. Claussen, S. T. Thompson, and C. E. Wieman. Atom-molecule coherence in a Bose-Einstein condensate. *Nature* **417**, 529 (2002).

[Dür04a] S. Dürr, T. Volz, A. Marte, and G. Rempe. Observation of molecules produced from a Bose-Einstein condensate. *Phys. Rev. Lett.* **92**, 020406 (2004).

[Dür04b] S. Dürr, T. Volz, and G. Rempe. Dissociation of ultracold molecules with Feshbach resonances. *Phys. Rev. A* **70**, 031601 (2004).

[Dür05] S. Dürr, T. Volz, N. Syassen, G. Rempe, E. van Kempen, S. Kokkelmans, B. Verhaar, and H. Friedrich. Dissociation of Feshbach molecules into different partial waves. *Phys. Rev. A* **72**, 052707 (2005).

[Dür06] S. Dürr, T. Volz, N. Syassen, D. M. Bauer, E. Hansis, and G. Rempe, A Mott-like state of molecules, in AIP Conf. Proc., volume 869, editors C. Roos, H. Häffner, and R. Blatt, pp. 278–283, AIP (2006).

[Efi70] V. Efimov. Energy levels arising from resonant two-body forces in a three-body system. *Phys. Lett. B* **33**, 563 (1970).

[Efi71] V. Efimov. Weakly-bound states of three resonantly-interacting particles. *Sov. J. Nucl. Phys.* **12**, 589 (1971).

[Ein24] A. Einstein. Quantentheorie des idealen einatomigen Gases. *Sitzber. Kgl. Preuss. Akad. Wiss.* **1924**, 261 (1924).

[Ein25] A. Einstein. Quantentheorie des idealen einatomigen Gases. *Sitzber. Kgl. Preuss. Akad. Wiss.* **1925**, 3 (1925).

[Esr99] B. D. Esry, C. H. Greene, and J. P. Burke. Recombination of three atoms in the ultracold limit. *Phys. Rev. Lett.* **83**, 1751 (1999).

[Fat00] F. K. Fatemi, K. M. Jones, and P. D. Lett. Observation of optically induced Feshbach resonances in collisions of cold atoms. *Phys. Rev. Lett.* **85**, 4462 (2000).

[Fed96a] P. O. Fedichev, Y. Kagan, G. V. Shlyapnikov, and J. T. M. Walraven. Influence of nearly resonant light on the scattering length in low-temperature atomic gases. *Phys. Rev. Lett.* **77**, 2913 (1996).

[Fed96b] P. O. Fedichev, M. W. Reynolds, and G. V. Shlyapnikov. Three-body recombination of ultracold atoms to a weakly bound s level. *Phys. Rev. Lett.* **77**, 2921 (1996).

[Fes58] H. Feshbach. Unified theory of nuclear reactions. *Ann. Phys.* **5**, 357 (1958).

[Fes62] H. Feshbach. A unified theory of nuclear reactions 2. *Ann. Phys.* **19**, 287 (1962).

[Fis89] M. P. A. Fisher, P. B. Weichmann, G. Grinstein, and D. S. Fisher. Boson localization and the superfluid-insulator transition. *Phys. Rev. B* **40**, 546 (1989).

[Föl06] S. Fölling, A. Widera, T. Müller, F. Gerbier, and I. Bloch. Formation of spatial shell structure in the superfluid to Mott insulator transition. *Phys. Rev. Lett.* **97**, 060403 (2006).

[Gan03] D. M. Gangardt and G. V. Shlyapnikov. Stability and phase coherence of trapped 1D Bose gases. *Phys. Rev. Lett.* **90**, 010401 (2003).

[Gir60] M. Girardeau. Relationship between systems of impenetrable bosons and fermions in one dimension. *J. Math. Phys.* **1**, 516 (1960).

[Gór02] K. Góral, L. Santos, and M. Lewenstein. Quantum phases of dipolar bosons in optical lattices. *Phys. Rev. Lett.* **88**, 170406 (2002).

[Gór04] K. Góral, T. Köhler, S. A. Gardiner, E. Tiesinga, and P. Julienne. Adiabatic association of ultracold molecules via magnetic-field tunable interactions. *J. Phys. B* **37**, 3457 (2004).

[GR08] J. J. García-Ripoll et al., No title yet (2008), in preparation.

[Gre02] M. Greiner, O. Mandel, T. Esslinger, T. W. Hänsch, and I. Bloch. Quantum phase transition from a superfluid to a Mott insulator in a gas of ultracold atoms. *Nature* **415**, 39 (2002).

[Gre03] M. Greiner, Ultracold Quantum Gases in Three-Dimensional Optical Lattice Potentials, Ph.D. thesis, Ludwig-Maximilians-Universität, München (2003).

[Gri00] R. Grimm, M. Weidemüller, and Y. B. Ovchinnikov, Optical dipole traps for neutral atoms, in Advances in Atomic, Molecular and Optical Physics, volume 42, editors B. Bederson and H. Walther, pp. 95–170, Academic Press, San Diego (2000).

[Han56] R. Hanbury-Brown and R. Q. Twiss. Correlation between photons in two coherent beams of light. *Nature* **177**, 27 (1956).

[Han06] E. Hansis, Ultracold Molecules in an Optical Lattice, Diplomarbeit, Max-Planck-Institut für Quantenoptik, Garching, and Technische Universität München (2006), unpublished.

[Hec02] J. Hecker-Denschlag, J. E. Simsarian, H. Häffner, C. McKenzie, A. Browaeys, D. Cho, K. Helmerson, S. L. Rolston, and W. D. Phillips. A Bose-Einstein condensate in an optical lattice. *J. Phys. B* **35**, 3095 (2002).

[Her03] J. Herbig, T. Kraemer, M. Mark, T. Weber, C. Chin, H.-C. Nägerl, and R. Grimm. Preparation of a pure molecular quantum gas. *Science* **301**, 1510 (2003).

[Hod05] E. Hodby, S. T. Thompson, C. A. Regal, M. Greiner, A. C. Wilson, D. S. Jin, E. A. Cornell, and C. E. Wieman. Production efficiency of ultracold Feshbach molecules in bosonic and fermionic systems. *Phys. Rev. Lett.* **94**, 120402 (2005).

[Hol01] M. Holland, S. J. J. M. F. Kokkelmans, M. L. Chiofalo, and R. Walser. Resonance superfluidity in a quantum degenerate Fermi gas. *Phys. Rev. Lett.* **87**, 120406 (2001).

[Hua87] K. Huang. Statistical Mechanics. Wiley, New York, second edition (1987).

[Hud05] J. J. Hudson, H. T. A. P. C. Condylis, M. R. Tarbutt, B. E. Sauer, and E. A. Hinds, Towards a new measurement of the electrons's dipole moment, in Proceedings of the 17th International Conference on Laser Spectroscopy, editors E. A. Hinds, E. Ferguson, and E. Riis, pp. 129–136, World Scientific Publ., Singapore (2005).

[Hut07] J. M. Hutson. Feshbach resonances in ultracold atomic and molecular collisions: threshold behaviour and suppression of poles in scattering lengths. *New J. Phys.* **9**, 152 (2007).

[Ino98] S. Inouye, M. R. Andrews, J. Stenger, H.-J. Miesner, D. M. Stamper-Kurn, and W. Ketterle. Observation of Feshbach resonances in a Bose-Einstein condensate. *Nature* **392**, 151 (1998).

[Jak98] D. Jaksch, C. Bruder, J. I. Cirac, C. W. Gardiner, and P. Zoller. Cold bosonic atoms in optical lattices. *Phys. Rev. Lett.* **81**, 3108 (1998).

[Jak02] D. Jaksch, V. Venturi, J. I. Cirac, C. J. Williams, and P. Zoller. Creation of a molecular condensate by dynamically melting a Mott insulator. *Phys. Rev. Lett.* **89**, 040402 (2002).

[Jen04] A. S. Jensen, K. Riisager, D. V. Fedorov, and E. Garrido. Structure and reactions of quantum halos. *Rev. Mod. Phys.* **76**, 215 (2004).

[Jes96] P. S. Jessen and I. H. Deutsch, Optical lattices, in Advances in Atomic, Molecular and Optical Physics, volume 37, editors B. Bederson and H. Walther, pp. 95–138, Academic Press, San Diego (1996).

[Joa75] C. J. Joachain. Quantum Collision Theory. North-Holland, Amsterdam (1975).

[Joc02] S. Jochim, M. Bartenstein, G. Hendl, J. Hecker Denschlag, R. Grimm, A. Mosk, and M. Weidemüller. Magnetic field control of elastic scattering in a cold gas of fermionic lithium atoms. *Phys. Rev. Lett.* **89**, 273202 (2002).

[Joc03] S. Jochim, M. Bartenstein, A. Altmeyer, G. Hendl, S. Riedl, C. Chin, J. Hecker-Denschlag, and R. Grimm. Bose-Einstein condensation of molecules. *Science* **302**, 2101 (2003).

[Jul04] P. S. Julienne, E. Tiesinga, and T. Köhler. Making cold molecules by time-dependent Feshbach resonances. *J. Mod. Opt.* **51**, 1787 (2004).

[Kag85] Y. Kagan, B. V. Svistunov, and G. V. Shlyapnikov. Effect of Bose condensation on inelastic processes in gases. *Sov. Phys. JETP Lett.* **42**, 209 (1985).

[Ket96] W. Ketterle and N. J. van Druten, Evaporative cooling of trapped atoms, in Advances in Atomic, Molecular, and Optical Physics, volume 37, pp. 181–236, Academic Press, San Diego (1996).

[Kha02] L. Khaykovich, F. Schreck, G. Ferrari, T. Bourdel, J. Cubizolles, L. D. Carr, Y. Castin, and C. Salomon. Formation of a matter-wave bright soliton. *Science* **296**, 1290 (2002).

[Kin04] T. Kinoshita, T. Wenger, and D. S. Weiss. Observation of a one-dimensional Tonks-Girardeau gas. *Science* **305**, 1125 (2004).

[Kin05] T. Kinoshita, T. Wenger, and D. S. Weiss. Local pair correlations in one-dimensional Bose gases. *Phys. Rev. Lett.* **95**, 190406 (2005).

[Köh05] M. Köhl, H. Moritz, T. Stöferle, K. Günter, and T. Esslinger. Fermionic atoms in a three dimensional optical lattice: Observing Fermi surfaces, dynamics, and interactions. *Phys. Rev. Lett.* **94**, 080403 (2005).

[Köh06] T. Köhler, K. Góral, and P. S. Julienne. Production of cold molecules via magnetically tunable Feshbach resonances. *Rev. Mod. Phys.* **78**, 1311 (2006).

[Kok] S. J. J. M. F. Kokkelmans, Personal communication.

[Kra04] T. Kraemer, J. Herbig, M. Mark, T. Weber, C. Chin, H.-C. Nägerl, and R. Grimm. Optimized production of a cesium Bose-Einstein condensate. *Appl. Phys. B* **79**, 1013 (2004).

[Kra06] T. Kraemer, M. Mark, P. Waldburger, J. G. Danzl, C. Chin, B. Engeser, A. D. Lange, K. Pilch, A. Jaakkola, H.-C. Nägerl, and R. Grimm. Evidence for Efimov quantum states in an ultracold gas of caesium atoms. *Nature* **440**, 315 (2006).

[Lab04] B. Laburthe Tolra, K. M. O'Hara, J. H. Huckans, W. D. Phillips, S. L. Rolston, and J. V. Porto. Observation of reduced three-body recombination in a correlated 1D degenerate Bose gas. *Phys. Rev. Lett.* **92**, 190401 (2004).

[Lan08] F. Lang, P. Straten, B. Brandstätter, G. Thalhammer, K. Winkler, P. Julienne, R. Grimm, and J. H. Denschlag. Cruising through molecular bound state manifolds with radio frequency. *Nat Phys* **4**, 223 (2008).

[Lee05] C. Lee and E. A. Ostrovskaya. Quantum computation with diatomic bits in optical lattices. *Phys. Rev. A* **72**, 062321 (2005).

[Lie63] E. H. Lieb and W. Liniger. Exact analysis of an interacting Bose gas. I. the general solution and the ground state. *Phys. Rev.* **130**, 1605 (1963).

[Lin76] G. Lindblad. On the generators of quantum dynamical semigroups. *Commun. Math. Phys.* **48**, 119 (1976).

[Lof02] T. Loftus, C. A. Regal, C. Ticknor, J. L. Bohn, and D. S. Jin. Resonant control of elastic scattering in an optically trapped Fermi gas of atoms. *Phys. Rev. Lett.* **88**, 173201 (2002).

[Lui96] O. J. Luiten, M. W. Reynolds, and J. T. M. Walraven. Kinetic theory of the evaporative cooling of a trapped gas. *Phys. Rev. A* **53**, 381 (1996).

[Man04] M. W. Mancini, G. D. Telles, A. R. L. Caires, V. S. Bagnato, and L. G. Marcassa. Observation of ultracold ground-state heteronuclear molecules. *Phys. Rev. Lett.* **92**, 133203 (2004).

[Mar98] M. Marinescu and L. You. Controlling atom-atom interaction at ultralow temperatures by dc electric fields. *Phys. Rev. Lett.* **81**, 4596 (1998).

[Mar02] A. Marte, T. Volz, J. Schuster, S. Dürr, G. Rempe, E. G. M. van Kempen, and B. J. Verhaar. Feshbach resonances in rubidium 87: Precision measurement and analysis. *Phys. Rev. Lett.* **89**, 283202 (2002).

[Mar03] A. Marte, Feshbach-Resonanzen bei Stößen ultrakalter Rubidiumatome, Ph.D. thesis, Max-Planck-Institut für Quantenoptik, Garching, and Technische Universität München (2003).

[Mar05] M. Mark, T. Kraemer, J. Herbig, C. Chin, H.-C. Nägerl, and R. Grimm. Efficient creation of molecules from a cesium Bose-Einstein condensate. *Europhys. Lett.* **69**, 706 (2005).

[Mar07] M. Mark, T. Kraemer, P. Waldburger, J. Herbig, C. Chin, H.-C. Nägerl, and R. Grimm. "Stückelberg interferometry" with ultracold molecules. *Phys. Rev. Lett.* **99**, 113201 (2007).

[Met99] H. Metcalf and P. van der Straten. Laser Cooling and Trapping. Springer, Heidelberg (1999).

[Mic06] A. Micheli, G. K. Brennen, and P. Zoller. A toolbox for lattice-spin models with polar molecules. *Nature Phys.* **2**, 341 (2006).

[Mie00] F. H. Mies, E. Tiesinga, and P. S. Julienne. Manipulation of Feshbach resonances in ultracold atomic collisions using time-dependent magnetic fields. *Phys. Rev. A* **61**, 022721 (2000).

[Mig85] A. L. Migdall, J. V. Prodan, W. D. Phillips, T. H. Bergeman, and H. J. Metcalf. First observation of magnetically trapped neutral atoms. *Phys. Rev. Lett.* **54**, 2596 (1985).

[Mis77] B. Misra and E. Sudarshan. The zeno's paradox in quantum theory. *J. Math. Phys.* **18**, 756 (1977).

[Moe95] A. Moerdijk, B. J. Verhaar, and A. Axelsson. Resonances in ultracold collisions of ^{6}Li, ^{7}Li, and ^{23}Na. *Phys. Rev. A* **51**, 4852 (1995).

[Mor05] H. Moritz, T. Stöferle, K. Günter, M. Köhl, and T. Esslinger. Confinement induced molecules in a 1D Fermi gas. *Phys. Rev. Lett.* **94**, 210401 (2005).

[Mot37] N. F. Mott and R. Peierls. Discussion of the paper by de Boer and Verwey. *Proc. Phys. Soc.* **49**, 72 (1937).

[Mot65] N. F. Mott and H. S. W. Massey. The Theory of Atomic Collisions. Clarendon, Oxford (1965).

[Muk04] T. Mukaiyama, J. R. Abo-Shaeer, K. Xu, J. K. Chin, and W. Ketterle. Dissociation and decay of ultracold Feshbach molecules. *Phys. Rev. Lett.* **92**, 180402 (2004).

[Nyg08] N. Nygaard, R. Piil, and K. Mølmer. Feshbach molecules in a one-dimensional optical lattice. *Phys. Rev. A* **77**, 021601 (2008).

[O'H02] K. M. O'Hara, S. L. Hemmer, S. R. Granade, M. E. Gehm, J. E. Thomas, V. Venturi, E. Tiesinga, and C. J. Williams. Measurement of the zero crossing in a Feshbach resonance of fermionic ^{6}Li. *Phys. Rev. A* **66**, 041401 (2002).

[Ols98] M. Olshanii. Atomic scattering in the presence of an external confinement and a gas of impenetrable bosons. *Phys. Rev. Lett.* **81**, 938 (1998).

[Osp06] C. Ospelkaus, S. Ospelkaus, L. Humbert, P. Ernst, K. Sengstock, and K. Bongs. Ultracold heteronuclear molecules in a 3D optical lattice. *Phys. Rev. Lett.* **97**, 120402 (2006).

[Ött05] A. Öttl, S. Ritter, M. Köhl, and T. Esslinger. Correlations and counting statistics of an atom laser. *Phys. Rev. Lett.* **95**, 090404 (2005).

[Pap06] S. B. Papp and C. E. Wieman. Observation of heteronuclear Feshbach molecules from a ^{85}Rb -^{87}Rb gas. *Phys. Rev. Lett.* **97**, 180404 (2006).

[Par04] B. Paredes, A. Widera, V. Murg, O. Mandel, S. Fölling, I. Cirac, G. V. Shlyapnikov, T. W. Hänsch, and I. Bloch. Tonks-Girardeau gas of ultracold atoms in an optical lattice. *Nature* **429**, 277 (2004).

[Pet02] C. J. Pethick and H. Smith. Bose-Einstein Condensation in Dilute Gases. Cambridge University Press, Cambridge (2002).

[Pet04a] D. S. Petrov. Three-boson problem near a narrow Feshbach resonance. *Phys. Rev. Lett.* **93**, 143201 (2004).

[Pet04b] D. S. Petrov, C. Salomon, and G. V. Shlyapnikov. Weakly bound dimers of fermionic atoms. *Phys. Rev. Lett.* **93**, 090404 (2004).

[Pit03] L. Pitaevskii and S. Stringari. Bose-Einstein Condensation. Clarendon Press, Oxford (2003).

[Pri83] D. E. Pritchard. Cooling neutral atoms in a magnetic trap for precision spectroscopy. *Phys. Rev. Lett.* **51**, 1336 (1983).

[Ram56] N. F. Ramsey. Molecular Beams. Oxford University Press, Oxford (1956).

[Reg03] C. A. Regal, C. Ticknor, J. L. Bohn, and D. S. Jin. Creation of ultracold molecules from a Fermi gas of atoms. *Nature* **424**, 47 (2003).

[Reg04a] C. A. Regal, M. Greiner, and D. S. Jin. Lifetime of molecule-atom mixtures near a Feshbach resonance in ^{40}K. *Phys. Rev. Lett.* **92**, 083201 (2004).

[Reg04b] C. A. Regal, M. Greiner, and D. S. Jin. Observation of resonance condensation of fermionic atom pairs. *Phys. Rev. Lett.* **92**, 040403 (2004).

[Rob98] J. L. Roberts, N. R. Claussen, J. P. Burke, C. H. Green, E. A. Cornell, and C. E. Wieman. Resonant magnetic field control of elastic scattering in cold ^{85}Rb. *Phys. Rev. Lett.* **81**, 5109 (1998).

[Rom04] T. Rom, T. Best, O. Mandel, A. Widera, M. Greiner, T. W. Hänsch, and I. Bloch. State selective production of molecules in optical lattices. *Phys. Rev. Lett.* **93**, 073002 (2004).

[Ryu05] C. Ryu, X. Du, E. Yesilada, A. M. Dudarev, S. Wan, Q. Niu, and D. J. Heinzen, Raman-induced oscillation between an atomic and a molecular quantum gas, arXiv.org:cond-mat/0508201 (2005).

[Sac99] S. Sachdev. Quantum Phase Transitions. Cambridge University Press, Cambridge (1999).

[Sag05] J. M. Sage, S. Sainis, T. Bergeman, and D. DeMille. Optical production of ultracold polar molecules. *Phys. Rev. Lett.* **94**, 203001 (2005).

[San01] B. Sang, Magnetische Speicherung eines ultrakalten atomaren Gases für die Bose-Einstein-Kondensation, Diplomarbeit, Max-Planck-Institut für Quantenoptik, Garching, and Universität Konstanz (2001), unpublished.

[Sav97] T. A. Savard, K. M. O'Hara, and J. E. Thomas. Laser-noise-induced heating in far-off resonance optical traps. *Phys. Rev. A* **56**, R1095 (1997).

[Sch01] J. Schuster, A. Marte, S. Amtage, B. Sang, G. Rempe, and H. C. Beijerinck. Avalanches in a Bose-Einstein condensate. *Phys. Rev. Lett.* **87**, 170404 (2001).

[Sch02] J. Schuster, Stoßlawinen in einem Bose-Einstein-Kondensat, Ph.D. thesis, Max-Planck-Institut für Quantenoptik, Garching, and Universität Konstanz (2002).

[Sch05] M. Schellekens, R. Hoppeler, A. Perrin, J. V. Gomes, D. Boiron, A. Aspect, and C. I. Westbrook. Hanbury-Brown Twiss effect for ultracold quantum gases. *Science* **310**, 648 (2005).

[Smi07] G. Smirne, R. M. Godun, D. Cassettari, V. Boyer, C. J. Foot, T. Volz, N. Syassen, S. Dürr, G. Rempe, M. D. Lee, K. Góral, and T. Köhler. Collisional relaxation of Feshbach molecules and three-body recombination in ^{87}Rb Bose-Einstein condensates. *Phys. Rev. A* **75**, 020702 (2007).

[Söd99] J. Söding, D. Guéry-Odelin, P. Desbiolles, F. Chevy, H. Inamori, and J. Dalibard. Three-body decay of a rubidium Bose-Einstein condensate. *Appl. Phys. B* **69**, 257 (1999).

[Sto88] H. T. C. Stoof, J. M. V. A. Koelman, and B. J. Verhaar. Spin-exchange and dipole relaxation rates in atomic hydrogen: Rigorous and simplified calculations. *Phys. Rev. B* **38**, 4688 (1988).

[Sto89] H. T. C. Stoof, A. M. L. Janssen, J. M. V. A. Koelman, and B. J. Verhaar. Decay of spin-polarized atomic hydrogen in the presence of a Bose condensate. *Phys. Rev. A* **39**, 3157 (1989).

[Stö04] T. Stöferle, H. Moritz, C. Schori, M. Köhl, and T. Esslinger. Transition from a strongly interacting 1D superfluid to a Mott insulator. *Phys. Rev. Lett.* **92**, 130403 (2004).

[Str02] K. E. Strecker, G. B. Partridge, A. G. Truscott, and R. G. Hulet. Formation and propagation of matter-wave soliton trains. *Nature* **417**, 150 (2002).

[Str03] K. E. Strecker, G. B. Partridge, and R. G. Hulet. Conversion of an atomic Fermi gas to a long-lived molecular Bose gas. *Phys. Rev. Lett.* **91**, 080406 (2003).

[Stw76] W. C. Stwalley. Stability of spin-aligned hydrogen at low temperatures and high magnetic fields: new field-dependent scattering resonances and predissociations. *Phys. Rev. Lett.* **37**, 1628 (1976).

[Sya06] N. Syassen, T. Volz, S. Teichmann, S. Dürr, and G. Rempe. Collisional decay of ^{87}Rb Feshbach molecules at 1005.8 G. *Phys. Rev. A* **74**, 062706 (2006).

[Sya07] N. Syassen, D. M. Bauer, M. Lettner, D. Dietze, T. Volz, S. Dürr, and G. Rempe. Atom-molecule Rabi oscillations in a Mott insulator. *Phys. Rev. Lett.* **99**, 033201 (2007).

[Sya08] N. Syassen, D. M. Bauer, M. Lettner, T. Volz, D. Dietze, J. J. García-Ripoll, J. I. Cirac, G. Rempe, and S. Dürr, Dissipation fermionizes a one-dimensional gas of bosonic molecules (2008), in preparation.

[Tay72] J. R. Taylor. Scattering Theory. Wiley, New York (1972).

[Tha06] G. Thalhammer, K. Winkler, F. Lang, S. Schmid, R. Grimm, and J. Hecker-Denschlag. Long-lived Feshbach molecules in a three-dimensional optical lattice. *Phys. Rev. Lett.* **96**, 050402 (2006).

[The04] M. Theis, G. Thalhammer, K. Winkler, M. Hellwig, G. Ruff, R. Grimm, and J. H. Denschlag. Tuning the scattering length with an optically induced Feshbach resonance. *Phys. Rev. Lett.* **93**, 123001 (2004).

[Tho05a] S. T. Thompson, E. Hodby, and C. E. Wieman. Spontaneous dissociation of ^{85}Rb Feshbach molecules. *Phys. Rev. Lett.* **94**, 020401 (2005).

[Tho05b] S. T. Thompson, E. Hodby, and C. E. Wieman. Ultracold molecule production via a resonant oscillating magnetic field. *Phys. Rev. Lett.* **95**, 190404 (2005).

[Tie92] E. Tiesinga, A. J. Moerdijk, B. J. Verhaar, and H. T. C. Stoof. Conditions for Bose-Einstein condensation in magnetically trapped atomic cesium. *Phys. Rev. A* **46**, 1167 (1992).

[Tie93] E. Tiesinga, B. J. Verhaar, and H. T. C. Stoof. Threshold and resonance phenomena in ultracold ground-state collisions. *Phys. Rev. A* **47**, 4114 (1993).

[Tim99a] E. Timmermans, P. Tommasini, R. Côté, M. Hussein, and A. Kerman. Rarified liquid properties of hybrid atomic-molecular Bose-Einstein condensates. *Phys. Rev. Lett.* **83**, 2691 (1999).

[Tim99b] E. Timmermans, P. Tommasini, M. Hussein, and A. Kerman. Feshbach resonances in atomic Bose-Einstein condensates. *Phys. Rep.* **315**, 199 (1999).

[Tim01] E. Timmermans, K. Furuya, P. W. Milonni, and A. K. Kerman. Prospect of creating a composite Fermi-Bose fluid. *Phys. Lett. A* **285**, 228 (2001).

[Ton36] L. Tonks. The complete equation of state of one, two and three-dimensional gases of hard elastic spheres. *Phys. Rev.* **50**, 955 (1936).

[Vol96] U. Volz and H. Schmoranzer. Precision lifetime measurements on alkali atoms and on helium by beam-gas-laser spectroscopy. *Phys. Scr.* **T65**, 48 (1996).

[Vol03] T. Volz, S. Dürr, S. Ernst, A. Marte, and G. Rempe. Characterization of elastic scattering near a Feshbach resonance in ^{87}Rb. *Phys. Rev. A* **68**, 010702 (2003).

[Vol05] T. Volz, S. Dürr, N. Syassen, G. Rempe, E. van Kempen, and S. Kokkelmans. Feshbach spectroscopy of a shape resonance. *Phys. Rev. A* **72**, 010704 (2005).

[Vol06] T. Volz, N. Syassen, D. M. Bauer, E. Hansis, S. Dürr, and G. Rempe. Preparation of a quantum state with one molecule at each site of an optical lattice. *Nature Phys.* **2**, 692 (2006).

[Vol07] T. Volz, Ultracold Rubidium Molecules, Ph.D. thesis, Max-Planck-Institut für Quantenoptik, Garching, and Technische Universität München (2007).

[Vul99] V. Vuletić, A. J. Kerman, C. Chin, and S. Chu. Observation of low-field Feshbach resonances in collisions of cesium atoms. *Phys. Rev. Lett.* **82**, 1406 (1999).

[Web03] T. Weber, J. Herbig, M. Mark, H.-C. Nägerl, and R. Grimm. Three-body recombination at large scattering lengths in an ultracold atomic gas. *Phys. Rev. Lett.* **91**, 123201 (2003).

[Wen04] X.-G. Wen. Quantum Field Theory of Many-Body Systems. Oxford University Press, Oxford (2004).

[Wid04] A. Widera, O. Mandel, M. Greiner, S. Kreim, T. W. Hänsch, and I. Bloch. Entanglement interferometry for precision measurement of atomic scattering properties. *Phys. Rev. Lett.* **92**, 160406 (2004).

[Wid07] A. Widera, S. Trotzky, P. Cheinet, S. Folling, F. Gerbier, I. Bloch, V. Gritsev, M. D. Lukin, and E. Demler, Quantum spin dynamics of squeezed Luttinger liquids in two-component atomic gases, arXiv.org:0709.2094 (2007).

[Win06] K. Winkler, G. Thalhammer, F. Lang, R. Grimm, J. Hecker-Denschlag, A. J. Daley, A. Kantian, H. P. Büchler, and P. Zoller. Repulsively bound atom pairs in an optical lattice. *Nature* **441**, 853 (2006).

[Win07] K. Winkler, F. Lang, G. Thalhammer, P. v. d. Straten, R. Grimm, and J. Hecker-Denschlag. Coherent optical transfer of Feshbach molecules to a lower vibrational state. *Phys. Rev. Lett.* **98**, 043201 (2007).

[Wyn00] R. Wynar, R. S. Freeland, D. J. Han, and D. J. Heinzen. Molecules in a Bose-Einstein condensate. *Science* **287**, 1016 (2000).

[Xu03] K. Xu, T. Mukaiyama, J. R. Abo-Shaeer, J. K. Chin, D. E. Miller, and W. Ketterle. Formation of quantum-degenerate sodium molecules. *Phys. Rev. Lett.* **91**, 210402 (2003).

[Yas96] M. Yasuda and F. Shimizu. Observation of two-atom correlation of an ultracold neon atomic beam. *Phys. Rev. Lett.* **77**, 3090 (1996).

[Zwi03] M. W. Zwierlein, C. A. Stan, C. H. Schunck, S. M. F. Raupach, S. Gupta, Z. Hadzibabic, and W. Ketterle. Observation of Bose-Einstein condensation of molecules. *Phys. Rev. Lett.* **91**, 250401 (2003).

[Zwi04] M. W. Zwierlein, C. A. Stan, C. H. Schunck, S. M. F. Raupach, A. J. Kerman, and W. Ketterle. Condensation of pairs of fermionic atoms near a Feshbach resonance. *Phys. Rev. Lett.* **92**, 120403 (2004).

[Zwi05] M. W. Zwierlein, J. R. Abo-Shaeer, A. Schirotzek, C. H. Schunck, and W. Ketterle. Vortices and superfluidity in a strongly interacting Fermi gas. *Nature* **435**, 1047 (2005).

List of Publications

- **Dissipation fermionizes a one-dimensional gas of bosonic molecules**.
  N. Syassen, D.M. Bauer, M. Lettner, T. Volz, D. Dietze, J.-J. García-Ripoll, J.I. Cirac, G. Rempe, and S. Dürr. *In preparation* (2008).

- **Atom-molecule Rabi oscillations in a Mott insulator**.
  N. Syassen, D. M. Bauer, M. Lettner, D. Dietze, T. Volz, S. Dürr, and G. Rempe. *Phys. Rev. Lett.* **99**, 033201 (2007).

- **Collisional relaxation of Feshbach molecules and three-body recombination in ^{87}Rb Bose-Einstein condensates**.
  G. Smirne, R. M. Godun, D. Cassettari, V. Boyer, C. J. Foot, T. Volz, N. Syassen, S. Dürr, G. Rempe, M. D. Lee, K. Góral, and T. Köhler. *Phys. Rev. A* **75**, 020702 (2007).

- **Collisional decay of ^{87}Rb Feshbach molecules at 1005.8 G**.
  N. Syassen, T. Volz, S. Teichmann, S. Dürr, and G. Rempe. *Phys. Rev. A* **74**, 062706 (2006).

- **A Mott-like state of molecules**.
  S. Dürr, T. Volz, N. Syassen, D.M. Bauer, E. Hansis, and G. Rempe. in Atomic Physics 20: XXth International Conference on Atomic Physics, edited by Christian Roos, Hartmut Häffner, and Rainer Blatt, *AIP Conf. Proc. No. 869*, pp. 278-283 (AIP, New York, 2006).

- **Preparation of a quantum state with one molecule at each site of an optical lattice**.
  T. Volz, N. Syassen, D. M. Bauer, E. Hansis, S. Dürr, and G. Rempe. *Nature Phys.* **2**, 692–695 (2006).

- **Dissociation of Feshbach molecules into different partial waves**.
  S. Dürr, T. Volz, N. Syassen, G. Rempe, E. van Kempen, S. Kokkelmans, B. Verhaar, and H. Friedrich. *Phys. Rev. A* **72**, 052707 (2005).

- **Feshbach spectroscopy of a shape resonance**.
  T. Volz, S. Dürr, N. Syassen, G. Rempe, E. van Kempen, and S. Kokkelmans. *Phys. Rev. A* **72**, 010704(R) (2005).

Danksagung

Zum Schluss möchte ich die Gelegenheit nutzen, all denjenigen meinen Dank auszusprechen, die zum Gelingen dieser Arbeit beigetragen haben.

An erster Stelle ist hier mein Doktorvater Prof. Dr. Gerhard Rempe zu nennen, der mir die Möglichkeit gab, die faszinierende Welt der ultrakalten Moleküle zu erforschen. Dabei hat er mir stets großes Vertrauen entgegengebracht und mich jederzeit großzügig unterstützt. Die Diskussionen, besonders während der nächtlichen Messungen, waren sehr motivierend.

Stephan Dürr, unser Habilitand, beantwortete alle meine Fragen immer ausführlich und sorgte dafür, dass der Lerneffekt dabei maximal war. Er hatte stets wunderbar anschauliche Erklärungen, wenn es um komplizierte Sachverhalte ging. In atemberaubendem Tempo entwickelte er ausgefeilte theoretische Modelle zur Beschreibung der experimentellen Daten und rechnete auch dann noch analytisch, wenn andere bereits numerische Methoden benutzen. Ein besonderer Dank gilt ihm für das kritische Korrekturlesen dieser Arbeit und die produktiven Verbesserungsvorschläge.

Ganz besonders möchte ich mich bei meinen Mitdoktoranden Thomas Volz, Dominik Bauer und Matthias Lettner bedanken. Die "Jungs" tragen einen großen Anteil am Gelingen der Experimente. Thomas beeindruckte im Labor durch das Finden kleinster Signale und deren liebevoller Optimierung. Bevor ein Experiment abgeschlossen war, hatte er meist schon eine brilliante Idee für das nächste Experiment im Kopf. Dominik, der "Gittermeista", sorgte mit stabilen optischen Aufbauten für das Gitter und die Dipolfalle dafür, dass das Experiment in den langen Messnächten ohne großes "Driften, Wackeln, Fluktuieren" äußerst zuverlässig lief. Gemeinsame Touren auf verschiedenste Berggipfel waren "top", und die Kicker-Zweikämpfe ein großer Spass. Matthias, unser "Junior" hat sich in rasantem Tempo in das komplizierte Experiment eingearbeitet und sorgte mit vollem Einsatz für nächtlichen Messsupport. Jungs, Danke für die tolle Teamarbeit.

Vielen Dank an unsere Diplomanden Daniel Dietze, Eberhard Hansis und Sven Teichmann. Eberhard hat ein exzellentes Programm zur Experimentsteuerung geschrieben, ohne das die Experimente nicht hätten durchgeführt werden können. Daniel hat die Software weiterentwickelt und hervorragende "Features" implementiert. Die beiden haben eindeutig mehr Bugs gedebugged als Debugs gebugged und nebenher sehr gute Arbeit im "Lab" geleistet.

Die erstklassige Unterstützung durch unsere "Techniker" beschleunigte die Arbeit im Labor erheblich. Ein Dankeschön an Franz Denk, Helmuth Stehbeck, und Josef Bayerl, die dafür sorgten, dass die Mechanik perfekt funktionierte. Vielen Dank an Tom Wiesmaier für die ausgeklügelten elektronischen Schal-

tungen. Unserer Sekretärin Odette Gori sei für Ihre große Hilfsbereitschaft bei Problemen aller Art gedankt.

Die Unterstützung von theoretischer Seite durch Juan Jose García-Ripoll und Ignacio Cirac führte zu einer Menge neuer Erkenntnisse, mit deren Hilfe wir viele unserer Daten verstehen konnten. Vielen Dank auch an Servaas Kokkelmans für die Parameter der Feshbach-Resonanz und an Thorsten Köhler für die Theorie zu den Dreikörper-Verlusten.

Bedanken möchte ich mich auch bei unseren Werkstudenten Stephan Albert, Florian Huber, Johannes Lenz und Christoph Skrobol für die Unterstützung bei Bau und Entwicklung elektronischer Komponenten.

Auch allen anderen Mitgliedern der Rempe-Gruppe ein herzliches Dankeschön für die sehr angenehme Arbeitsatmosphäre und den intensiven Austausch von Wissen und Material aller Art. Besonderer Dank gilt Jörg Bochmann für das Überlassen seines Faserlasers und Thomas Rieger für die äußerst hilfreichen Vakuumtipps.

Für das Korrekturlesen meiner Arbeit möchte ich mich ganz herzlich bei Thomas Volz, Dominik Bauer und Karim Murr bedanken.

Ein schöner Ausgleich (hoffentlich für alle Beteiligten) waren die verschiedensten sportlichen Aktivitäten auf dem Weg zum Institut und zurück, in der Mittagspause oder während der Gruppenklausur in Ringberg und Rechtegg. Ein Dankeschön dafür an Markus Hijlkema, Eberhard Hansis, Markus Hennrich, Thomas Puppe, Simon Webster, Tobias Schätz, Martin Mücke, Laurens van Buuren und Tobias Müller. Für Ausgleich besonders während der Zeiten, wenn das optische Gitter mal wieder justiert werden musste, half der Tischkicker, der von Tatjana Wilk freundlicherweise zur Verfügung gestellt wurde. Dankeschön.

Einen ganz besonderen Dank möchte ich meinen Eltern Viktoria Syassen-Klausa und Karl Syassen für ihre immer bedingungslose Unterstützung während meiner gesamten Ausbildung aussprechen.

Schließlich ein riesig großes Dankeschön an meine Freundin Katja Wilms, die mich in schwierigen Situationen immer wieder aufzumuntern wusste und dafür gesorgt hat, dass ich die Physik innerhalb kürzester Zeit auch mal komplett vergessen konnte.